Technical University of Denmark

DTU

Z-phase in 9-12% Cr Steels

Danielsen, Hilmar Kjartansson; Somers, Marcel A. J.; Hald, John

Link back to DTU Orbit

DTU Library
Technical Information Center of Denmark

Z-phase in

9-12%Cr Steels

Ph.D. thesis

February 2007

by

Hilmar Kjartansson Danielsen

Department of Manufacturing
Engineering and Management
Technical University of Denmark
DK-2800 Kgs. Lyngby, Denmark

To the loving memory of Freida

Preface

This thesis is submitted in candidacy for a Ph.D. degree from the Technical University of Denmark (DTU).

The work presented in this thesis has been carried out at the Department of Manufacturing Engineering and Management (IPL) under the supervision of Professor Marcel A.J. Somers and affiliated Professor John Hald from 1.february 2004 to 31.january 2007

The following four papers are included in the thesis:

Paper I

H.K. Danielsen, J. Hald: *"Behaviour of the Z-phase in 9-12%Cr steels"* Energy Materials, 1, 2006, pp. 49-57.

I performed the experimental work and wrote the first draft. Comments and suggestions from co-authors were incorporated in to a final version by me.

Paper II

H.K. Danielsen, J. Hald, F. B. Grumsen, M. A. J. Somers: *"On the Crystal Structure of Z-phase, Cr(V,Nb)N"* Metallurgical and Materials Transactions A, 37A, 2006, pp. 2633-2640.

I performed the experimental work (together with F.B. Grumsen) and wrote the first draft. Comments and suggestions from co-authors were incorporated in to a final version by me.

Paper III

H.K. Danielsen, J. Hald: *"A Thermodynamic model of the Z-phase, Cr(V,Nb)N"* CALPHAD, in press

I performed the modelling work and wrote the first draft. Comments and suggestions from co-authors were incorporated in to a final version by me.

Paper IV

H.K. Danielsen, J. Hald: *"On the Dissolution and Nucleation of Z-phase, Cr(V,Nb)N"* in manuscript.

I performed the experimental work and wrote the first draft. Comments and suggestions from co-authors were incorporated in to a final version by me.

Contributions to the following work were also produced during the same period, but have not been included because of partial overlap with the work presented in the abovementioned manuscripts.

H.K. Danielsen, J. Hald: "*Z-phase in 9-12%Cr steels*" Proc. Conf. on 'Advances in Material Technology for Fossil Power Plants' (ed. R. Viswanathan et al) 999-1012, 2005, Hilton Head, USA, ASM international.

H.K. Danielsen, J. Hald: "*Z-phase in 9-12%Cr steels – observations and thermodynamic modelling*" Proc. Conf. on 'Materials for Advanced Power Engineering' (ed. J. Lecomte-Beckers et al) 1275-1284, 2006, Liege, Belgium, Forschungszentrum Julich GmbH.

V. Vodarek, H.K. Danielsen, F.B. Grumsen, J. Hald, A. Strang: "Electron *Diffraction Studies on (Nb,V)CrN Particles in 12CrMoVNbN steels*" Proc. Conf. on 'Materials for Advanced Power Engineering' (ed. J. Lecomte-Beckers et al) 1251-1266, 2006, Liege, Belgium, Forschungszentrum Julich GmbH.

A. Golpayegani, H.O. Andren, H.K. Danielsen, J. Hald: "*A study on Z-phase nucleation in martensitic chromium steels*", in manuscript.

Abstract

The 9-12%Cr martensitic creep resistant steels investigated in this work are applied for steam power plant applications at steam conditions up to 600°C/300bar. Several new steels with 11-12%Cr have been under development and are intended for operations at 650°C steam temperature. These steels have suffered dramatic failures during long term creep testing. Several hypotheses have been put forward to explain these abrupt breakdowns. One of these proposes that Z-phase, Cr(V,Nb)N, grows at the expense of MX precipitates, which provide creep strength. The aim of the work presented in this thesis is to investigate the Z-phase with focus on its behaviour in 9-12%Cr martensitic creep resistant steel. Experimental microstructure characterisation, using mainly transmission electron microscopy, was performed and combined with thermodynamic and kinetic numerical modelling.

The microstructure of several 9-12%Cr steels was investigated. Z-phase was identified in all of these steels, but only after they had received prolonged exposure to temperatures close to service conditions. The largest quantities of Z-phase were observed in the 11-12%Cr steels, which show a clear tendency between high quantity of Z-phase and early failure during creep testing.

Heat treatment investigations determined the dissolution temperature of Z-phase in 9-12%Cr steels to 800°C, providing vital information for the modelling efforts.
A new Nb-free version of Z-phase was found experimentally, after modelling predicted its existence.
Electron diffraction of Z-phase showed inconsistencies in the traditional description of the crystal structure, giving a hybrid cubic/tetragonal lattice instead of only tetragonal.
Investigations of the nucleation of Z-phase through unconventional heat treatments revealed a correlation with the presence of MX precipitates.

Using the thermodynamic modelling software ThermoCalc, a model of the Z-phase in austenitic and martensitic steels was developed based on input data obtained from literature and own investigations. It predicts that Z-phase is thermodynamically stable in all 9-12%Cr steels containing its constituents. This effectively means that the occurrence of Z-phase is kinetic phenomenon. Using driving force calculations, the model shows that the precipitation rate is accelerated by a high Cr content. Driving force calculations may appear useful for alloy design, for example developing steel compositions where Z-phase precipitation is retarded.

Kinetic modelling of Z-phase was commenced, using the developed thermodynamic model in conjuncture with the kinetic modelling software MatCalc, in order to give more specific predictions on the Z-phase precipitation rate at different temperatures and steel compositions. Experimental work on the nucleation of Z-phase indicated that an alternative approach is required for implementing the kinetics of Z-phase development in MatCalc.

<u>Resumé</u>

De 9-12%Cr martensitiske krybefaste stål som er blevet undersøgt i dette arbejde bliver anvendt i dampkraftværker ved damptilstande op til 600°C/300bar. Adskillige nye stål med 11-12%Cr har været under udvikling og er tilsigtet brug ved 650°C damptemperatur. Disse stål er alle blevet ramt af dramatiske nedbrud ved langtids krybeforsøg. Flere hypoteser er blevet foreslået for at forklare disse pludselige sammenbrud. En af disse foreslår at Z-fase, $Cr(V,Nb)N$, vokser på bekostning af MX precipitater, hvilke giver krybestyrke. Formålet med arbejdet præsenteret i denne afhandling er at undersøge Z-fasen med fokus på dens opførsel i 9-12%Cr martensitiske krybefaste stål. Eksperimentelt mikrostruktur karakterisering, hovedsageligt ved brug af Transmissions elektronmikroskopi, blev udført sammen med termodynamisk og kinetisk computer modellering.

Mikrostrukturen af flere 9-12%Cr stål blev undersøgt. Z-fase blev identificeret i alle disse stål, men kun efter at de igennem længere til var blevet udsat for temperaturer tæt på driftsbetingelser. De største mængder af Z-fasen er blevet observeret i 11-12%Cr stål, hvilket viser en klar tendens imellem høj mængde af Z-fase og tidlige nedbrud i krybeforsøg.

Varmebehandlings forsøg har fastlagt Z-fasens opløsnings temperatur i 9-12%Cr stål til 800°C, hvilket har bidraget med afgørende information til modellerings arbejdet.
En ny Nb-fri version af Z-fasen blev fundet eksperimentelt, efter at modellering havde forudsagt dens eksistens.
Elektron diffraktion af Z-fasen viste uoverensstemmelser i den traditionelle beskrivelse af krystal strukturen, hvilke gav et hybrid kubisk/tetragonalt gitter i stedet for kun tetragonalt.

Undersøgelser af kimdannelsen af Z-fasen igennem ukonventionel varmebehandling viste en tæt forbindelse med tilstedeværelsen af MX precipitater.

Med brug af, det termodynamisk modelleringsprogram ThermoCalc, blev en model af Z-fasen i austenitiske og martensitiske stål udviklet baseret på data fremskaffet fra litteratur og egne undersøgelser. Den forudsiger at Z-fasen er termodynamisk stabil i alle 9-12%Cr stål indeholdende dens bestanddele. Dette betyder at tilstedeværelsen af Z-fase er et kinetisk fænomen. Ved udregninger af den termodynamiske drivkraft for Z-fase dannelse, viser modellen at udskillelseshastigheden øges med forøget Cr indhold. Drivkraftsberegninger kan måske være nyttige for legeringsudvikling, for eksempel til bestemmelse af stålsammensætninger hvor udskillelsen af Z-fase hæmmes.

Kinetisk modellering af Z-fase udskillelse er blevet påbegyndt ved brug af den udviklede termodynamiske model og med, det kinetiske modelleringsprogram, MatCalc, med henblik på at give mere specifikke forudsigelser af Z-fase udskillelseshastigheden ved forskellige temperaturer og stålsammensætninger. Eksperimentelt arbejde med kimdannelsen af Z-fasen indikerede at der var brug for en alternativ fremgangsmåde til at implementere kinetikken af Z-fase udskillelse i MatCalc.

<u>Acknowledgements</u>

There are several people who have helped me during this work, which I owe my gratitude:

First I would like to thank my supervisor John Hald for introducing me to the complex world of 9-12%Cr steels in the first place and actually talking me into doing a Ph.D. on the subject. It has been three great years with lots of challenges, which I hope we can continue facing together in the future.

Also thanks to my supervisor Marcel Somers, who taught me the proper way of writing a paper, from the delicate subtleties of layouts to the crucial importance of references.

Many thanks to Flemming Grumsen for helping me with all things experimental, from sample preparation to advanced TEM operations, and not least for the cheerful company during those many long days at Risø.

Thanks to Vlastimil Vodarek without whose help I would not have been able to delve so deeply into the dark arts of diffraction.

To Ernst Kozeschnik, Bernard Sondernegger, Ivan Holzer, Peter Mayr and all the others at TU Graz, thanks for the thorough introduction into the intricate ways of MatCalc modelling, and of course the unforgettable "steak nights".

I would also like to thank my fellow colleagues Thomas Christiansen, Kristian V. Dahl, Wen-Chi Chiang and all the other at MTU, for the support and great atmosphere, both inside and outside work.

Table of contents

1 Introduction

Coal fired steam power plants constitute about 40% of the total electricity produced worldwide. There has been an increasing demand over the past decades to increase the efficiency of these power plants, because of lower production costs and partly because of demands to reduce the emission of greenhouse gasses as CO_2.

The prime solution for increasing the efficiency of the power plants is to increase the steam temperature and pressure. Currently, the upper limits are around 600°C/300bar, while demands for an increase of these parameters to 650°C/350bar have been made for over a decade now. This would allow for an increase in efficiency of 10%, but so far little progress has been achieved.

The main bottleneck for operating at higher temperatures is the availability of suitable materials for steam pipes and turbines. 9-12%Cr martensitic steels have traditionally been the material of choice for such components, as they combine high creep strength and good oxidation resistance in order to keep degradation to a minimum. In addition these steels also must have good ductility, good thermal cycling properties, including acceptable room temperature properties, especially good toughness, and the inevitable microstructure degradation must not result in embrittlement. All of these conditions must be met without impairing the forgeability or weldability of the material.

Recently, many of the newly developed alloys intended for operations at 650°C experienced sudden drops in strength during creep tests. These steels get their good creep strength from precipitate strengthening, most notably MX particles, (V,Nb)(N,C). Recent attempts to increase operating temperature to 650°C have resulted in the precipitation of Z-phase, Cr(V,Nb)N. This complex nitride is blamed for dissolving the beneficial MX particles during service life, and thus decreasing the creep strength. As the Z-phase could be responsible for the

recent failures to improve the 9-12%Cr steels, it has recently attracted a lot of attention.

The purpose of the present project was to investigate the Z-phase in 9-12%Cr steels, as very little knowledge on this subject was available. This study includes microstructure investigations as well as computational modelling.

2 9-12%Cr steels

9-12% steels consisting of tempered martensite have long been considered as the most suitable material for fossil fired power plant steam pipes and turbines, and have formed the basis for the improvements of efficiency made the past decades [1]. The 9-12%Cr martensitic steels combine creep strength with oxidation resistance at a low price, and have widely been used for power plant applications since the 1960´s [2]. There are other candidate materials which have the necessary creep strength and oxidation resistance, but none of which fulfils all of the requirements. For example austenitic steels have poor thermal cycling capabilities, making them unsuitable for thick section components, while nickel based superalloys, which can be used for up to 700°C, are 10 times more expensive [3].
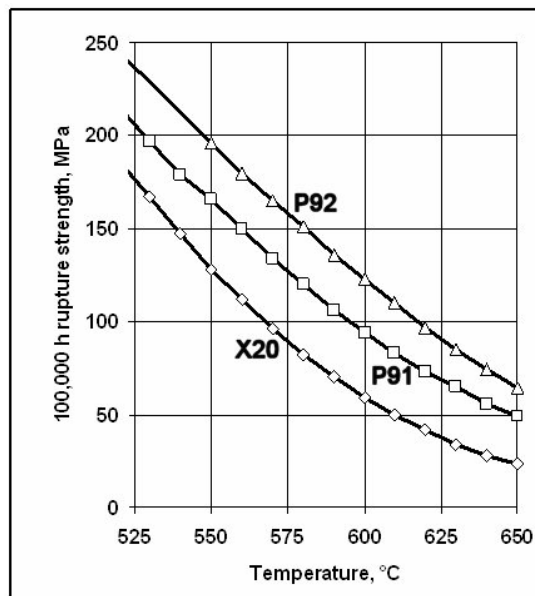

Figure 1: *The development of 9-12%Cr steels for the past decades has led to a significant increase in creep strength. [4]*

2.1 Historical development
Over the past decades the development of 9-12%Cr steels has resulted in doubling of their creep strength at 600°, see figure 1. Hence the allowable steam

parameters under which they can operate has increased greatly. The increase in creep strength is mainly due to the introduction of new precipitate types, which are vital to the creep strength. Table 1 shows the development in compositions of 9-12%Cr steels over the past decades, each steel becoming substantially stronger than the previous, except for the long term creep strength of TAF650, which suffered from Z-phase precipitation.

	C	N	Cr	Mo	W	V	Nb	Co	B	Ni
X20	0.20	-	11.5	1.0	-	0.25	-	-	-	0.7
P91	0.10	0.05	9.0	1.0	-	0.20	0.06	-	-	0.1
P92	0.10	0.05	9.0	0.5	2.0	0.20	0.06	-	0.002	0.1
TAF650	0.10	0.025	11.0	0.2	2.5	0.2	0.1	3.0	0.013	0.5

Table 1: *Typical composition of various generations of 9-12%Cr steels (in wt %).*

2.1.1 Accomplishments of the past

The 12CrMoV steel X20 was developed during the 1950's in Germany and represented a significant increase in creep strength over materials existing at that time [2]. The precipitates present in X20 are mainly $M_{23}C_6$, but some VN is also present.

During the 1970's, the modified 9CrMoVNbN steel P91 was developed in USA with the introduction of small amounts of Nb and controlled addition of N. This led to the precipitation of (V,Nb)(C,N) type MX particles, that these steels rely on to the present day. As compared to X20 the creep strength in P91 is significantly enhanced [2].

The creep strength of P91 was at its turn exceeded by P92 which was developed in Japan during the 1980's. The Japanese used a composition similar to P91, but added W and B. W contributed to solution strengthening and precipitated as Fe_2W Laves phase, while B stabilised the $M_{23}C_6$ particles. Both factors had a significant effect on the creep strength. Today, P92 remains the premier commercial steam pipe steel in the 9-12%Cr range for power plant applications, as its creep strength is still unsurpassed [2].
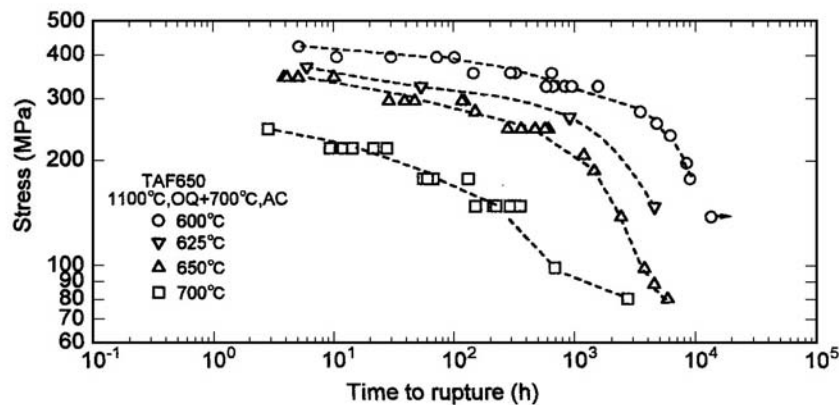
Figure 2: *Steels where large amounts of Z-phase have been found all suffer a sudden drop in creep strength, in this case only after a few thousand hours [5].*

2.1.2 Recent failures

The 9-12%Cr steels intended for power plant application should normally have a lifetime of 30+ years. Validation of the long-term creep strength of the material by testing for such a timescale is unpractical, and shorter tests are carried out under several different higher loads. By putting the data into a double logarithmic plot, strength at longer test times can be predicted by extrapolating the resulting (almost) straight line. In the tests of some steels this relatively straight line breaks down after a certain exposure time, only after a few thousand hours in figure 2.

Over the last decade several new alloys, like the TAF650, have been produced which, in short term tests, have properties superior to P92 [5]. However, all of these materials suffered from mysterious breakdowns during long-term creep tests (see figure 2). Initially the Laves phase was held responsible for these failures, as it precipitated during service exposure. It was reasoned that the W-containing Laves phase did not contribute to precipitate strengthening, because of its relatively large size, and that precipitation of Laves phase removed W from solid solution and thereby solid solution strengthening Consequently the development of Laves phase would lower the creep strength. As many of these steels had been alloyed with up to 3% W, this argumentation was widely accepted, in spite of P92 (heavily W alloyed) did not show a dramatic drop in

creep strength. As a consequence, European steel manufacturer developments would largely avoid W alloyed steels. However, in the end this remedy was unable to prevent new failures [6].

In the middle of the 1990's the V containing Z-phase, Cr(V,Nb)N also called modified Z-phase, was associated with microstructure instabilities in some heavily alloyed 11%Cr steels [7]. As the Z-phase precipitated, it dissolved the MX particles, which are crucial for the creep strength. These steels had a much higher Nb content compared to modern 9-12%Cr steels, so the Z-phase was not considered a serious threat for future development.

At the start of the millennium the Z-phase was found in TAF650, and it was speculated whether it could have the observed detrimental effect in combination with the development of Laves phase. The full realisation of the consequences of Z-phase precipitation did not become apparent until recently, after large amounts of Z-phase were identified in several steels which had suffered failures similar to TAF650.

2.2 Physical metallurgy

As the development of the 9-12%Cr steels have made them increasingly more complex, an understanding of the fundamental principles of their creep strength is important. The improvements made in the 9-12%Cr steels have been accomplished by small but important changes in composition. These changes include the addition of relatively small amounts of elements like V, Nb, N, W and B. The main effects of these elements concern the precipitates they form. Development of 9-12%Cr steels with the required properties is a long and complex process. The aim of the end product would be to obtain a tempered martensite microstructure with a fine distribution of precipitates.

2.2.1 Heat treatment

The standard heat treatment of 9-12%Cr steels consists of normalising and tempering. The normalising is usually carried out at around 1050°C (inside the

austenitic loop, see figure 3), typically for about 1-2 hours[1-2]. This should be sufficient to dissolve most carbides and nitrides, and obtain a fully austenitic microstructure. If ferrite is still present at this time it is usually designated as δ ferrite. After cooling to room temperature by air cooling, the steel should become fully martensitic (provided no δ ferrite was present at the normalising temperature), with a high dislocation density. As the steel is hard and brittle at this point, it is necessary to soften it by tempering.
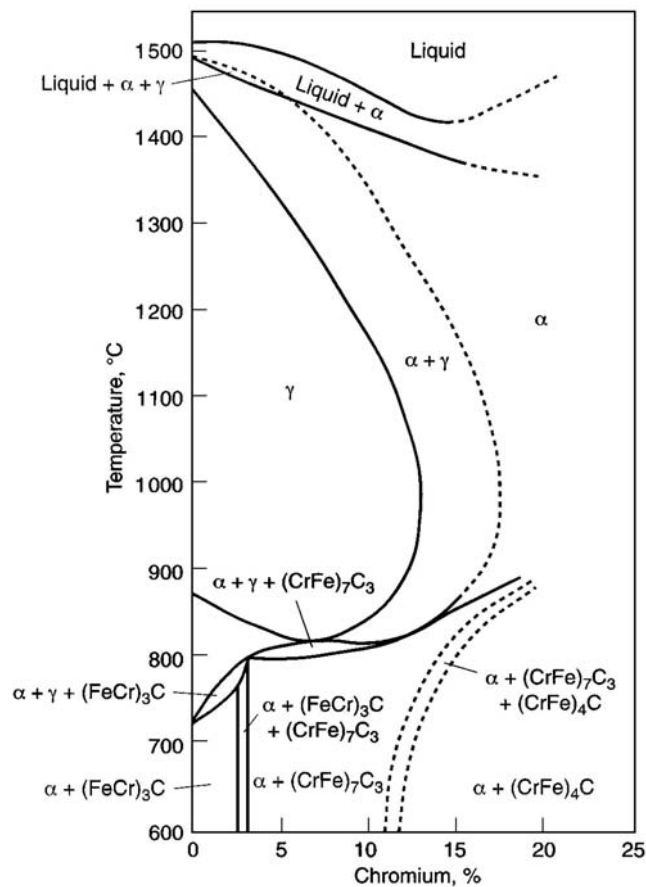

Figure 3: *The austenitic loop in a 0.1%C steel, α being ferrite, γ being austenite and (CrFe)$_4$C is the M$_{23}$C$_6$ carbide. [8]*

2.2.2 Austenite

During normalising most precipitates dissolve, but some Nb-containing carbo-nitride particles remain undissolved and prevent grain growth, thus contributing positively to the toughness.

7

Because of oxidation problems at operating temperatures, it is necessary to have a minimum content of 9% Cr. In order to stay within the austenitic loop (figure 3), the maximally allowed Cr content is about 12%Cr, because ferrite does not transform to austenite above this level. Many of the alloying elements have an effect on the austenite loop, some extend it (austenite formers), others restrict it (ferrite formers). Unfortunately it is necessary to alloy with predominately ferrite formers for creep and oxidation properties. Large amounts Cr, and more recently also Si, are needed for oxidation resistance. V and Nb are added for precipitation of MX, while Mo and W provide solid solution strengthening (in solid solution) and precipitation hardening (as Laves phase). This makes the addition of austenite formers necessary in order to prevent the presence of δ ferrite. Some steels do however contain a small amount of δ ferrite.
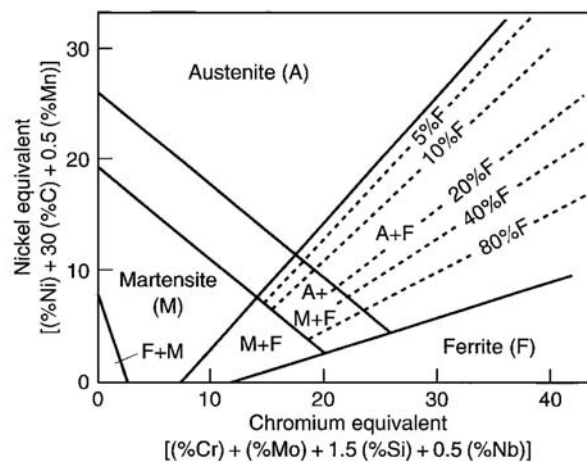
Figure 4: *A Schaeffler-Schneider diagram. [8]*

Ni is the traditional austenite former, as it can be added in moderate amounts (1%), but excessive additions can lower the A_1 temperature, below which ferrite is stable. In principle the A_1 temperature is the highest possible tempering temperature. The effectiveness of other austenite formers is usually evaluated by the equivalent content of Ni, while ferrite formers are evaluated by the equivalent content of Cr. Using these equivalents, a diagram of the steel matrix can be approximated, see figure 4. C is the cheapest austenite former, but only small

amounts can be added, as it lowers the toughness and weldability. Also N can be used as an austenite former, but excessive amounts may be required, leading to a risk for developing N_2 filled pores. Other elements, like Mn and Cu, have been used as austenite formers, but they may also lower the A_1 temperature. Co has recently been shown an excellent austenite former as it does not have any technical drawbacks, but it is rather expensive.

The simplified Cr and Ni equivalents are given by the following equations (mass%) [8]:

Cr equivalent = Cr + 2Si + 1.5Mo + 5V + 5.5Al + 1.75Nb + 1.5Ti + 0.75W   [1]

Ni equivalent = Ni + Co + 0.5Mn + 0.3Cu + 25N + 30C   [2]

These equations only count as long as the elements are in solid solution. As Nb carbo-nitrides remain undissolved at normalising temperatures, the effective Nb, C and N contents in the matrix are lower.
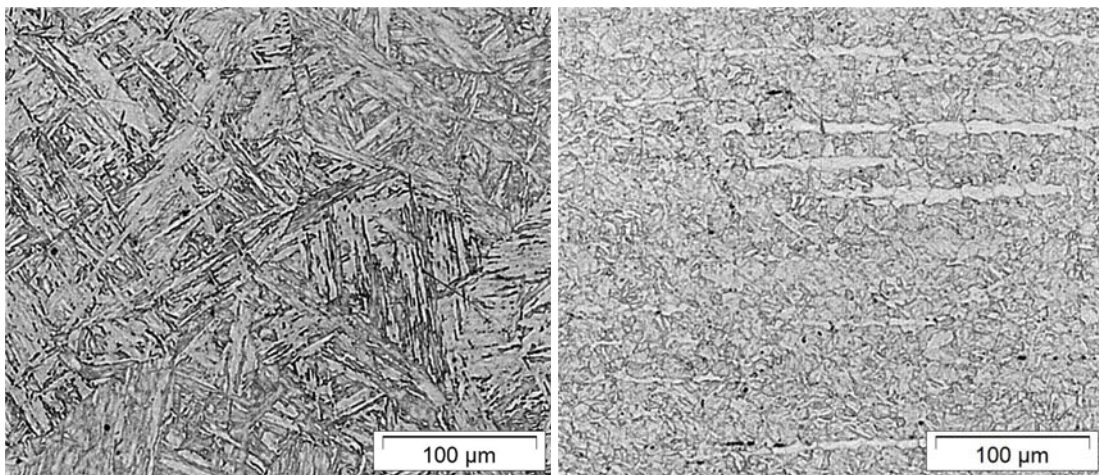
Figure 5: *Left: Tempered martensite seen in light optical microscope. Right: Fine grained tempered martensite with inclusions of δ ferrite (white phase).*

2.2.3 Martensite

Martensite is a slightly distorted tetragonal version of the ferritic bcc crystal structure. When austenite is rapidly cooled, a direct (diffusionless) transformation

into martensite takes place by a shear process. In order to achieve optimum strength, it is important that most of the austenite is transformed into martensite (figure 5a) on cooling to room temperature. This depends on the temperature were austenite is fully transformed into martensite, the M_f temperature. M_f should be above room temperature or else retained austenite is present after cooling. This can lower the strength prior to tempering, and lead to untempered brittle martensite after tempering (because a lowering of the C content in the matrix due to carbide precipitation may raise M_f). Normally air cooling of 9-12 % Cr steels is sufficient for a martensitic transformation, because the high level of Cr retards diffusion of C, thus preventing the formation of ferrite, figure 6.
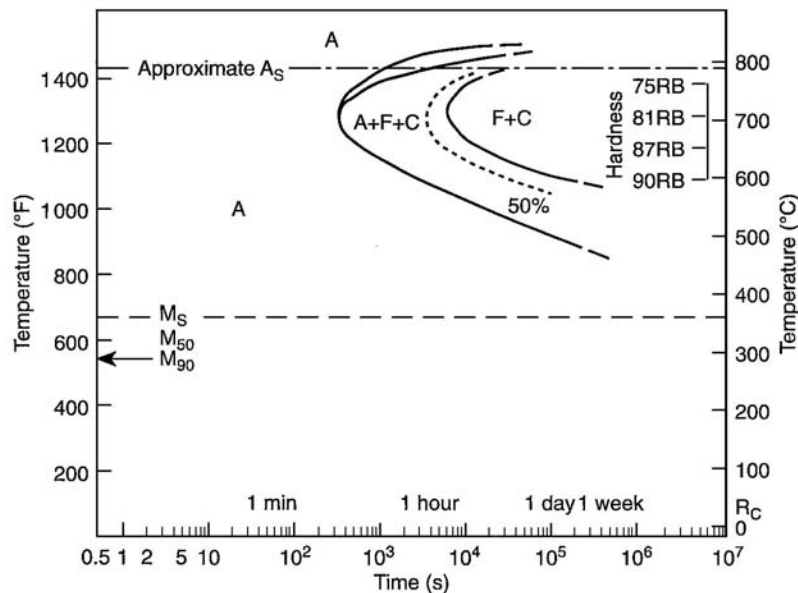
Figure 6: *A CCT diagram showing the effect of the cooling rate for 0.1%C, 12%Cr. [8]*

For a 0.1%C 12%Cr steel the M_s (the temperature where the martensitic transformation starts) is around 300°C and the M_f temperature lies in the 100-150°C range [8]. Most of the alloying elements lower M_s and M_f temperatures, but small grain sizes may also lower the M_f temperature. The following equation gives a rough estimate of the effect of alloying elements (mass%) on M_s temperature [8]:

10

$$M_s = 550°C - 450C - 33Mn - 20Cr - 17Ni$$
$$- 10W - 20V - 10Cu - 11Nb - 11Si + 15Co \qquad [3]$$

The only element that raises the M_s temperature is Co, which also is an austenite former, making it important in heavily alloyed steels. Again some elements might precipitate and not be present in the matrix.

2.2.4 Tempering

Tempering is done in order to recover ductility from the hard and brittle martensite. The temperature for tempering is usually in the 680-780°C range, depending on the properties required [1-2]. Components which require high ductility and tempering resistance for post weld treatments, like steam pipes, are tempered in the higher range. When high tensile strength is required, e.g. for large components like turbine rotors, the tempering temperatures are lower, sometimes requiring a two step process in order to relieve stresses, with the first tempering being below 600°C [6].

The higher tempering temperature limit is the A_1 temperature, where austenite becomes stable. Some elements, especially Ni and Mn, can lower the A_1 temperature substantially. If austenite forms during tempering, it could transform into brittle untempered martensite upon cooling. Some of the alloying elements will affect the A_1 temperature (mass%) [8]:

$$A_1 \ (°C) = - 30Ni - 25Mn - 5Co + 25Si + 30Al + 25Mo + 50V \qquad [4]$$

Again, some elements might vanish from the matrix due to precipitation during the heat treatments, especially Vanadium.
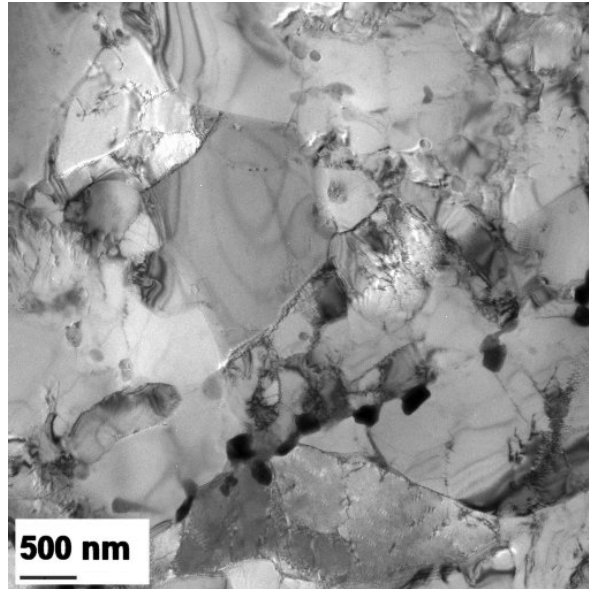
Figure 7: *Tempered martensite seen in transmission electron microscope.*

2.2.5 Tempered martensite

The final state of the 9-12%Cr steels before service consists of tempered martensite. This microstructure contains a great deal of inhomogeneities in addition to prior austenite grain boundaries, including martensitic lath boundaries and a high dislocation density, see figure 7. The carbides and nitrides precipitating during the heat treatment should be densely distributed as fine particles along these inhomogeneities, providing the steels with excellent creep properties. During service exposure, this microstructure will slowly evolve towards an equilibrium ferritic matrix.

3 Precipitation in 9-12%Cr steels

Precipitation of a secondary phase from a supersaturated solid solution is usually subdivided in three stages: nucleation, growth and coarsening. As 9-12%Cr steels rely mainly on precipitates for their creep strength, understanding the precipitation process is vital.

3.1 Creep and precipitates

Slow, time-dependent deformation under a continuous load at high temperature, i.e. creep, is the main concern for the application of 9-12%Cr steels. Various creep mechanisms include the movement of dislocations. Creep strength can be obtained by introducing obstacles to hinder the movement of these dislocations. Precipitation strengthening and solid solution strengthening are the most common ways of increasing the creep strength. Solid solution strengthening occurs by alloying with differently sized atoms (usually Mo and W in 9-12%Cr steels), creating strain fields in the lattice, while precipitation strengthening introduces secondary phases in the structure. The 9-12%Cr steels rely mainly on precipitation strengthening, and the general principle is that the more finely distributed a secondary phase is, the better the strengthening effect. If such precipitates dissolve during service, a breakdown in the creep strength would follow. The Orowan stress from particles on dislocations can be used to estimate the effects on creep strength. The following equation shows the relationship between Orowan stress and the precipitate volume fraction f_p, and precipitate diameter d_p:

$$\sigma_{Orowan} = 3.32 \frac{Gb\sqrt{f_p}}{d_p}$$

[5]

G is the shear modulus and b is the Burgers vector. As follows from equation 5, larger volume fractions and smaller diameters enhance the Orowan stress. Thus, if finely dispersed precipitates would be replaced by coarse precipitates, the creep strength should fall.

3.1.1 Nucleation

The nucleation process of precipitates is very important for their effect on the creep strength. The nucleation rate is primarily controlled by the thermodynamic driving force and the interfacial energy of the nuclei, but also by the availability of its necessary elements in the matrix. If a precipitate has a fast nucleation rate, many small particles will form, benefiting the creep strength, see equation 5. If the nucleation rate is slow, the precipitates that nucleate early will have time to grow, depleting the area in their vicinity of the necessary elements, thus preventing other precipitates from nucleating, resulting in the presence of only a few relatively coarse particles.

Precipitates usually nucleate at defects in the crystal structure, like grain boundaries, dislocations or other precipitates. The distribution of the precipitates depends on the preferred sites of nucleation, but also on the time of nucleation. If NbC nucleates during normalising, it must nucleate on austenite grain boundaries, while VN, which nucleates during tempering, can nucleate on martensitic lath boundaries and dislocations introduced during cooling. As Laves phase precipitates last, they might have to nucleate on other precipitates.

3.1.2 Growth

When nuclei have reached a certain critical size, the growth phase will start. The precipitates will be thermodynamically stable and continue to grow until they reach the same chemical potential as the elements dissolved in the matrix. In the growth period both volume fraction and precipitate size grow with time. The growth of precipitates is mainly controlled by their thermodynamic driving force coupled with the diffusion rate and concentration of their necessary elements in the matrix.

In 9-12%Cr steels growth is mainly diffusion controlled and varies greatly for the various types of particles. For some precipitates the growth phase is completed after the tempering ($M_{23}C_6$, MX), while for others growth continues during service exposure (Laves phase, Z-phase).

3.1.3 Coarsening

Coarsening of precipitates, also called Ostwald ripening, is the last stage of precipitation, and is very important for the long term creep strength. When the coarsening sets in, no new particles nucleate, but the largest particles grow at the expense of the smaller ones. This process results in fewer but larger particles and the volume fraction remains constant. It is apparent that this will affect precipitate strengthening (equation 5), and the creep strength of the steel. Ostwald ripening is driven by the total decrease in the interfacial energy, as a few coarse particles have a smaller surface area compared to a corresponding amount (in volume) of small particles. The coarsening rate can be described as:

$$r_t^3 - r_0^3 = K_p t \qquad\qquad [6]$$

where t is time, r_0 and r_t are radius of the particles at time 0 and t respectively. K_p is the coarsening constant, which itself is dependent on the temperature, diffusion constants, interfacial energies and composition of the precipitates.

3.2 Precipitates in 9-12%Cr steels

As a plethora of precipitates can appear in 9-12% Cr steels, see figure 8, only the most common ones will be described here.

3.2.1 Metastable precipitates

Many of the precipitates which are formed in the 9-12%Cr steels are metastable, and will disappear with time. Some of them have a very short lifespan, and are already dissolved in the tempering process, and replaced by more stable precipitates. The thermodynamic driving force for the metastable precipitates is lower than for the stable precipitates. Their occurrence is kinetically favoured, either because the elements necessary for their formation are more readily available in the matrix or the interfacial and/or strain energy terms involved in their development are lower.

An example of a precipitation sequence in 9-12%Cr steels could be:

$M_3C \rightarrow M_7C_3 + M_2X \rightarrow M_{23}C_6 + MX \rightarrow M_{23}C_6 + Z\text{-phase}$
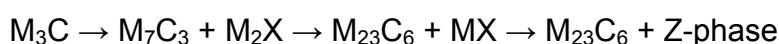
Here, there is a great difference in lifetime, as the early carbides may only exist for a few hours, while it can take decades for Z-phase to develop and dissolve MX. MX may be present during the entire lifetime of certain steels.
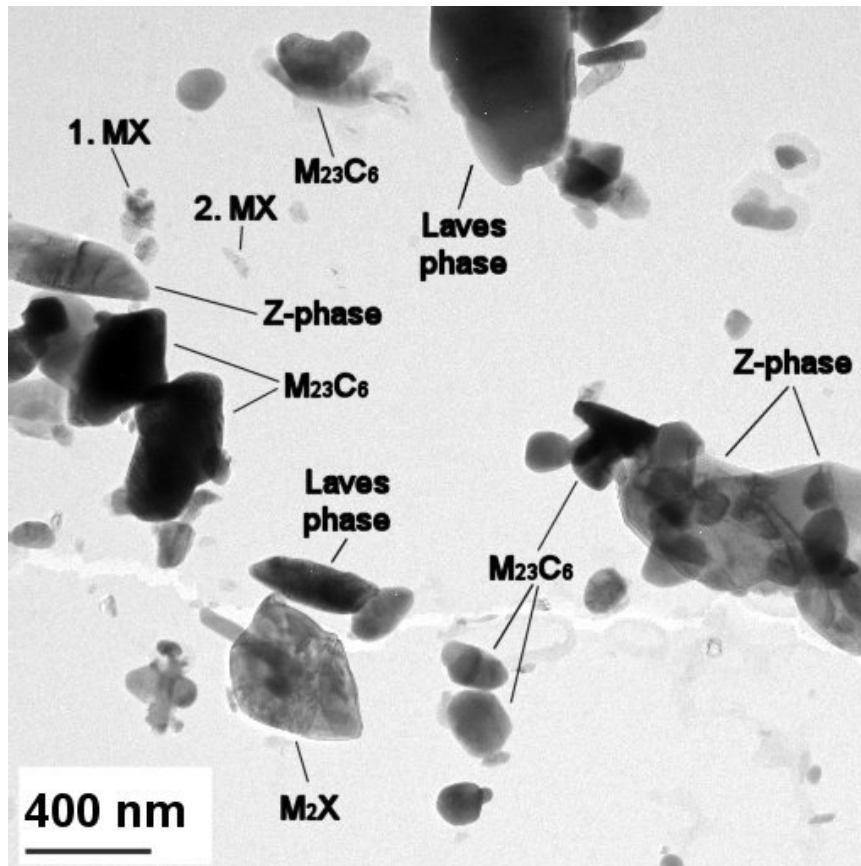
Figure 8: *An illustration of the most common precipitates in 9-12%Cr steels.*

3.2.2 $M_{23}C_6$

$M_{23}C_6$ is the most stable carbide, and will be present in all 9-12%Cr steels with a carbon content. It is often the most abundant precipitate and dissolves nearly all other carbides (except NbC) during tempering. It precipitates mainly on prior austenite grain boundaries and martensite lath boundaries. After tempering, the average size of the carbides is about 100 nm [9], but the coarsening rate is comparatively high, decreasing their influence on creep strength with time[10].

The $M_{23}C_6$ has a cubic crystal structure and consists mainly of Cr and C, but has also minor contents of Fe, Mo, W and B. In steels with B, the coarsening rate of

$M_{23}C_6$ is considerably lowered, but the mechanism of this effect is not entirely clear.

3.2.3 M_2X

In steels with high N contents, M_2X is thermodynamically stable, and even in steels with lower N contents they are relatively stable and can still be present after several thousands of hours. With low tempering temperatures they usually precipitate on grain boundaries and dislocations, i.e. sites where MX usually precipitates. It is therefore believed that they interfere with fine MX precipitation [2]. In contrast to the MX precipitates, M_2X particles usually get quite large, and are thus often undesired.

The M_2X have a hexagonal crystal structure, and are basically Cr_2N precipitates, but as up to 30% of the Cr can be replaced with V, they might be confused with Z-phase. The M_2X also appear as faceted plate like particles; in this sense they are morphologically similar to Z-phase.

3.2.4 MX

The MX precipitates in 9-12%Cr steels are V and Nb rich carbonitrides. In most 9-12%Cr steels they can be divided into two groups, NbC and VN. As the NbC remain undissolved throughout the heat treatment, they are also called primary MX, while the VN are called secondary MX. They have the same cubic NaCl type crystal structure (not the same lattice parameters though), but behave differently otherwise.

The primary MX, NbC, precipitates at high temperatures on austenite grain boundaries. Here they will prevent grain growth during normalising, and increase the toughness of the steel. NbC can be replaced by Z-phase, but in low N steels they may be thermodynamically stable. Z-phase has been observed to precipitate near NbC [11], probably because of their affinity to Nb. NbC particles usually appear as spheres of various sizes, and have a comparatively pure composition.

17

The secondary MX, VN, precipitates during tempering. They nucleate on imperfections within the grains, where they can pin down the movement of dislocations. As they also precipitate very fast as homogenously distributed fine particles, this will greatly increase the creep strength. The MX particles in general coarsen only very slowly [10], giving the steels their long term creep strength. The VN particles can usually be found as the smallest particles in 9-12%Cr steels, and are known to have minor Nb, Cr and C contents.

3.2.5 Laves phase

In Mo or W containing steels Laves Phase, $Fe_2(W,Mo)$, may precipitate. Laves Phase also contains minor amounts of Cr and Si, and has a hexagonal crystal structure. Usually the Laves phase does not nucleate during tempering as it is not stable at high temperatures, and it has a long nucleation and growth phase [12]. It forms during service exposure, and during the growth phase it becomes larger than most other particles, but the coarsening rate is slower than $M_{23}Cr_6$ [10]. W-containing Laves phase usually nucleates faster, thus becoming smaller and more finely distributed as compared to the Mo Laves phase [12].

The W Laves phase has in the past been blamed for breakdowns in creep strength of several 9-12%Cr steels, as it removes W from the matrix, which would imply a loss of solid solution strengthening by W. However, this explanation seems unlikely, as the precipitation strengthening contribution of Laves Phase should more than compensate for this. Additionally the breakdowns have been observed in steels without W [6], and some steels containing W (like P92) have not suffered any breakdowns.

3.3 Z-phase

The Z-phase is probably the most stable nitride in 9-12%Cr steels. It has an empiric formula of CrXN, were X can be Nb, V or Ta. The historical perception of the effects of Z-phase has varied greatly, from beneficial to insignificant to disastrous, and it is still under debate.

3.3.1 Original Z-phase, CrNbN

The first observation of Z-phase was made in 1950 by Binder [13] in Nb alloyed creep resistant austenitic steels. Since then it has frequently been observed and credited with beneficial strengthening effects in austenitic steels. The Z-phase precipitates very quickly and as small finely distributed rod-like particles in these high alloyed steels, and it was often the first precipitate to appear. Many attempts have been made to determine its crystal structure [14-15], but in 1972 Jack & Jack identified it as tetragonal CrNbN [16], see figure 9, which is now widely accepted. In addition to the main elements, minor concentrations of Fe, Mo and traces of other elements have also been identified in Z-phase. In austenitic steels the empirical formula has been found to be approximately $(Cr_{0.8}Fe_{0.2})(Nb_{0.9}Mo_{0.1})N$, although the composition varies with the composition of the steel. The dissolution temperature of CrNbN in austenitic steels has been observed to be as high as 1250°C [17], again dependent on the steel composition. Sourmail [18] has given a thorough review on the CrNbN Z-phase in austenitic steels.

In 1971 Ettmayer [15] investigated the stability of Z-phase in the ternary systems normally associated with Z-phase: CrTaN, CrNbN and CrVN. The Z-phase was observed in the CrNbN and CrTaN systems, but no Z-phase was found in the vanadium system. Phase stability investigations by Gridnev et al [19] in 1983 on the CrVN systems at 800°C and above showed no presence of a vanadium Z-phase.

In 1981 Kurosawa et al [20] found CrNbN Z-phase particles in a ferritic 19Cr-2Mo-NbN steel. The precipitation in the 700-1000°C range was very fast, and the Z-phase appeared as large (>1µm) faceted particles, in contrast to the small particles usually found in austenitic steels.
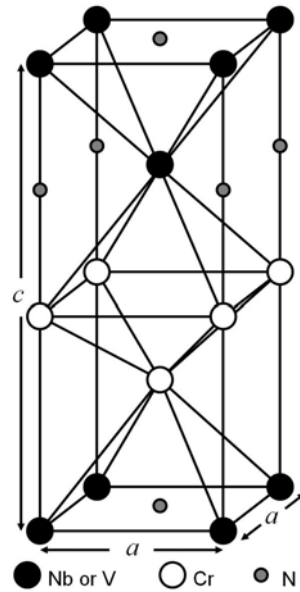
Figure 9: *The crystal structure of the Z-phase[11]. The lattice parameters of the original Z-phase, CrNbN, are a=0.304 nm and c=0.739 nm, while the modified version, Cr(V,Nb)N, has a slightly smaller unit cell, with a=0.286 nm and c=0.739 nm.*

3.3.2 Modified Z-phase, Cr(V,Nb)N

Particles with Z-phase composition were observed in 1985 by Andren et al [21] in an 18Cr-12Ni-VNbN austenitic steel after isothermal annealing at 750°C up to 1170 h. Half of the Nb content in these particles had been replaced by V, the chemical composition being Cr(V,Nb)N. They were not positively identified as Z-phase since they had an fcc NaCl crystal structure. It was speculated that they could be a metastable precursory phase to the Z-phase. Ishitsuka [22] has recently investigated the possibility of using the modified V containing Z-phase as a strengthening agent in vanadium containing austenitic creep resistant steels to supplement to CrNbN original Z-phase.

In 1986 Schnabel et al [23] identified a vanadium containing Z-phase in a martensitic 11Cr-1Mo-VNbN steel (X19 CrMoVNbN 11 1) which showed a very dramatic drop in creep strength. However, no connection was made between the appearance of the Z-phase and this drop in strength. It was first in 1996 that Strang and Vodarek [7,24] drew the connection between Z-phase precipitation

and creep strength degradation, as they were investigating creep specimens of 11-12%CrMoVNbN steels, which had experienced breakdowns in long-term creep strength. They found that the Z-phase precipitated as large particles simultaneously with the breakdown in strength and proposed that the Z-phase was dissolving the beneficial MX particles, which contain the same elements as Z-phase. With the dissolution of fine MX particles, the creep strength of the steel would drop sharply. The crystal structure of this V containing Z-phase was found to have slightly smaller lattice parameters compared to that of CrNbN. It was thus dubbed the modified Z-phase, Cr(V,Nb)N. This modified Z-phase behaved differently compared to the original one, only precipitating after long exposure times, and then only as very few and coarse particles. The modified Z-phase can contain small amounts of Fe and has an empirical formula of $(Cr_{0.9}Fe_{0.1})(V_{0.8}Nb_{0.2})N$ in martensitic steels, although the V/Nb ratio can vary significantly. Strang and Vodarek concluded that the Ni content had a large effect on the precipitation rate of Z-phase, based on the varying nickel content in their investigated steels.

The investigations by Strang and Vodarek were performed on older steels with approximately five times higher niobium content compared to the modern 9-12%Cr steels, so there was only little concern of the Z-phase affecting the stability of newly developed steels. However, a number of experimental 10-12%Cr steels under development for application up to 650°C steam temperature showed promising creep behaviour in short term tests, but after prolonged exposure times the strength dropped dramatically. In 2001 Svoboda et al [25] investigated the 11Cr-3W-3Co-VNbN experimental steel TAF650, which suffered a severe drop in creep strength after 10,000h of creep testing at 650°C. They observed Laves phase (Fe_2W), Z-phase and only few of the smaller MX particles and concluded that the Z-phase was responsible for the dissolution of the MX particles, and that the combined effect of Laves phase and Z-phase precipitation was responsible for the breakdown of the steel. More recent observations of steels with and without W suggest that the Laves phase is not responsible for

21

such breakdowns in creep strength, whereas there are strong indications that Z-phase could be responsible.

There have been several other observations of Z-phase in 9-12%Cr steels [22-25], but little is known how to affect its precipitation or how to avoid it. The Z-phase is often observed in steels which have been exposed at high temperatures for prolonged times, but it is not always accompanied by a dramatic decrease in creep strength. For more detailed information on Z-phase see appendix A.

4 Experimental methods

Most of the experimental work was carried out using transmission electron microscopy, supplemented by X-ray powder diffraction, primarily for quantitative investigations of the precipitates.

4.1 Electron microscopy

The advantage offered by electron microscopy over light microscopy lies in the improved image resolution obtained by the lower wavelength of the radiation (electrons as compared to visible light). This allows magnification beyond the restrictions posed by the wavelength of visible light. Modern electron microscopes enable us to observe features down to less than 1 nm (exceptionally below 1 Å), and are thus a valuable tool in microstructure characterisation of materials. The experimental investigations of this work focused on precipitates in mainly 9-12% Cr steels. As these precipitates are small (<1µm), electron microscopy is the only viable choice for investigating and identifying them.

Electron microscopes are mainly divided into two types, Scanning Electron Microscopes (SEM) and Transmission Electron Microscopes (TEM). The images in the SEM consist of electrons which are back-scattered from the surface (or near the surface) or generated in the surface (secondary electrons) of the specimens, and thus allow investigations of the external morphology and topography. TEM uses electrons which are transmitted through the investigated material, giving much better resolution and yielding information on the internal microstructure of the material such as precipitates, grain boundaries, dislocations and lattice defects. As this work concentrates on precipitates, TEM is the ideal choice of microscopy, and nearly all experimental work in the present thesis was performed on it.
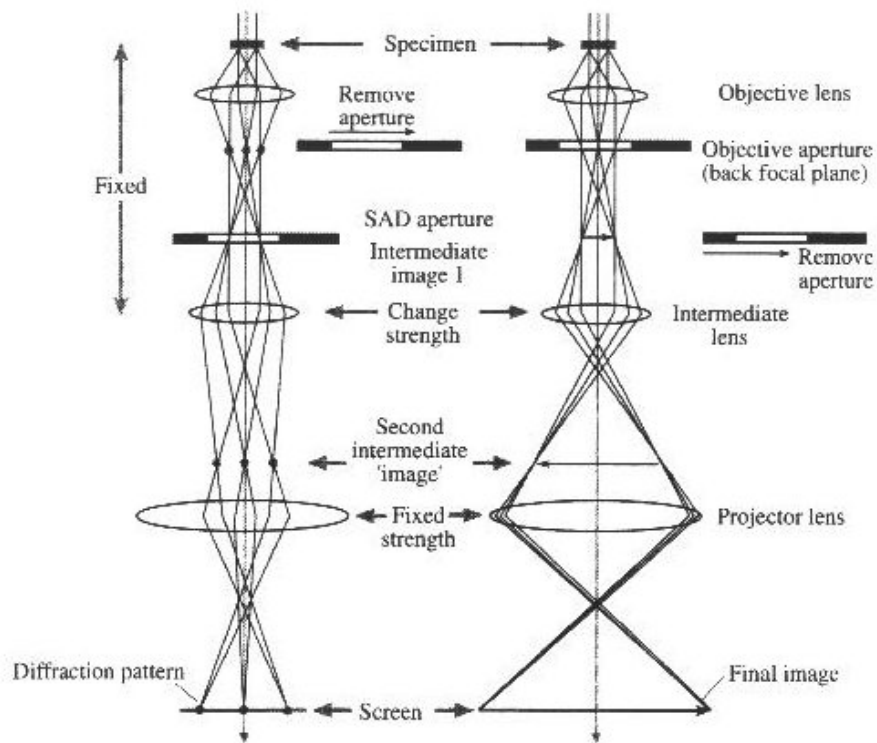
Figure 10: *Illustration of the TEM in diffraction mode (left) and image mode (right).[26]*

4.1.1 TEM

A TEM consists of an electron gun (illumination), an assembly of electromagnetic lenses (focus and magnification) and a fluorescent screen + camera (imaging) all enclosed in vacuum.

The electrons emitted by the electron gun are usually accelerated using a voltage of 200-300 keV. Since the wavelength of these electrons is very small, it allows a high resolution below 1 nm. In the lens system, the electrons are focused on the specimen by condenser lenses and apertures. After passing through the specimen the electrons are focused again by the objective lens, creating an intermediate image and a diffraction pattern. An intermediate lens (diffraction lens) is used for focusing on either the image plane or on the diffraction plane, usually called image mode and diffraction mode, see figure 10. Finally the image or diffraction pattern is magnified and visualized on the screen, using the projector lenses.

4.1.2 Sample preparation

Two sample preparation methods were used for TEM investigations, thin-foils and carbon extraction replicas. Thin-foils are basically slices of bulk material, which are thin enough for electrons to pass through. They are cut as thin slices, then electropolished until a small hole appears in the middle of the slice, see figure 11a. The area in the vicinity of the hole is thin enough for electrons to pass through. This is useful for a variety of investigation of microstructure features like grain boundaries and dislocations in the matrix.

Carbon extraction replicas are very thin carbon films with precipitates caught on them. First the carbon is evaporated on an etched sample, thereafter the rest of the matrix is etched away, leaving the carbon film with the precipitates stuck on it. Studying precipitates is made much easier with the removal of bulk material, but some information is lost, like the positioning of the precipitates in the microstructure.
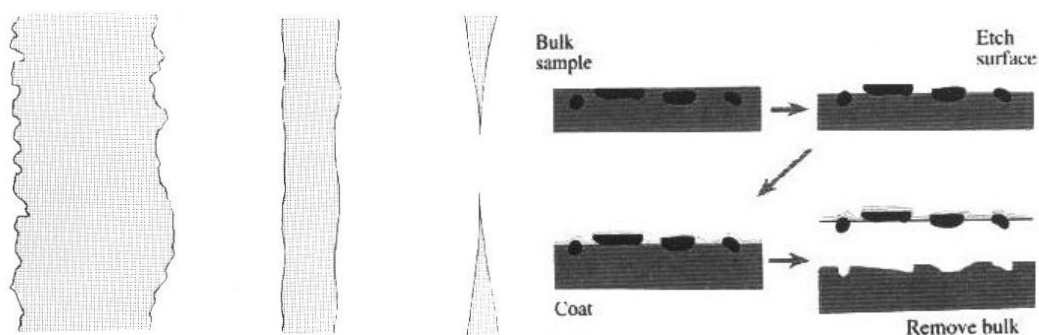
Figure 11: *Left: Preparation of thin-foil [27]. Right: Preparation of carbon replica [26].*

When particles are present in the matrix, it may be difficult to distinguish them from the matrix, especially when looking at small particles. The transparent area suitable for TEM on a thin-foil can be rather limited when compared to an extraction replica. The precipitates in a thin-foil must also be located on a thin plane, while the extraction replica can contain precipitates from a much larger thickness, dependent on the dept of the etching. Thus there are far more precipitates present on a replica, they are much easier to spot, and furthermore

they are not magnetic (martensitic thin-foils are), making work with TEM much easier. As this work was focused on the precipitates, carbon extraction replicas were mostly used. In cases where information from the matrix or measurements concerning the carbon content was needed, thin-foils had to be used.
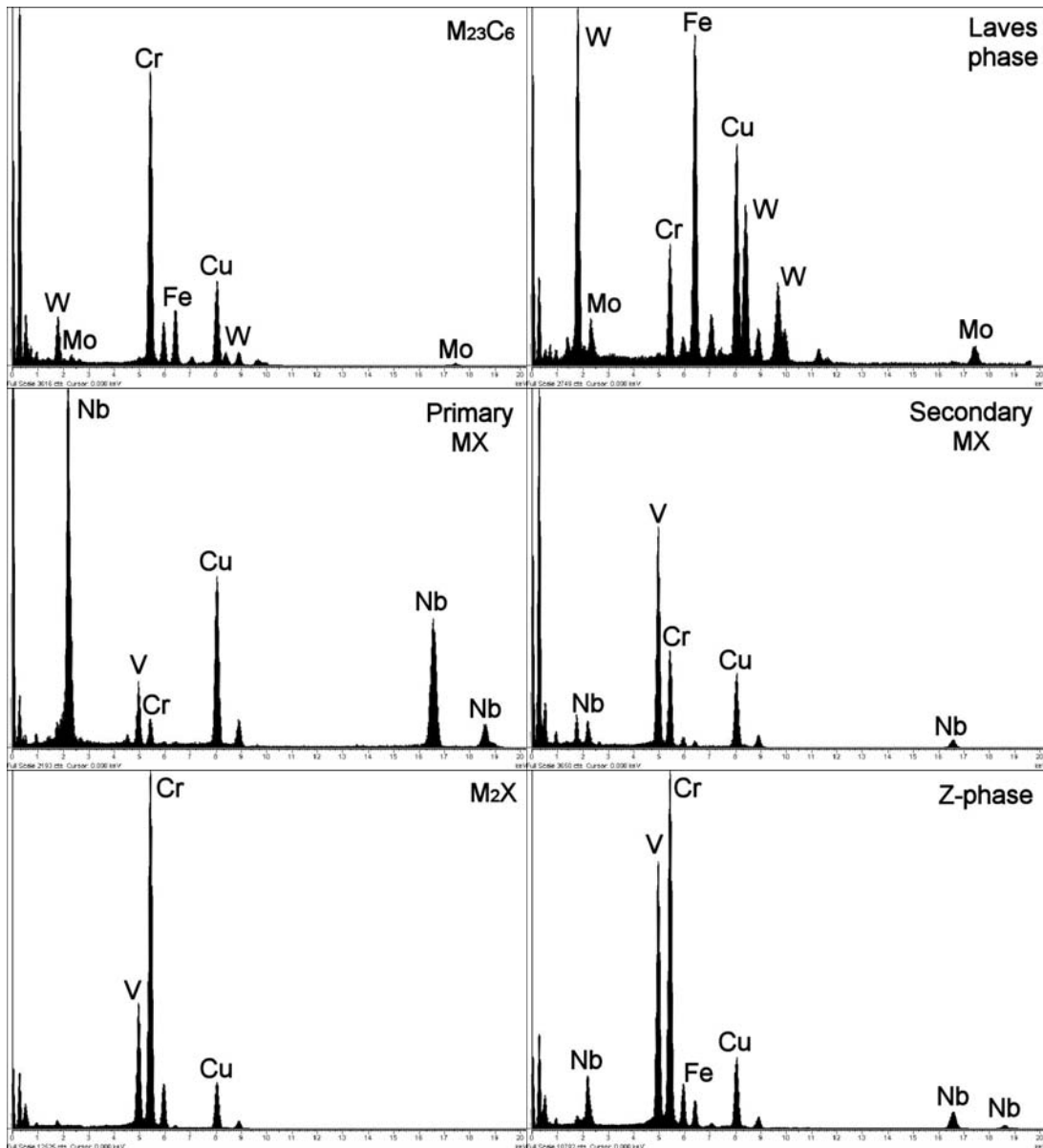
Figure 12: *EDS spectra of various precipitates found in 9-12%Cr steels.*

4.1.3 EDS

Energy Dispersive X-ray Spectrometry (EDS) utilises the fact that the interaction between the accelerated electrons and the specimen excites the involved atoms, which then generate X-ray photons. The energy of these X-rays is dependent on the atomic number Z of the atoms they originated from. By measuring the characteristic energy of the emitted X-rays, the composition of the investigated volume can be quantified, see figure 12. Each element has at least one characteristic peak, while higher Z elements have several. Unfortunately EDS has problems with detecting low energy (<1 keV) X-rays, which makes it difficult to quantify the contents of lighter elements like C or N. For this purpose EELS is better suited.

Figure 12 shows the EDS spectrum of the most common particles encountered in this work. Some of the spectra are distinct and easily recognisable, but those from the nitrides are quite similar, as they all contain V and Cr to some extent. They have to be identified by quantity, Cr(V,Nb)N having 50% Cr+Fe and 50% V+Nb, VN having >70% V and the rest being Nb+Cr, Cr_2N having >70% Cr and the rest being V.
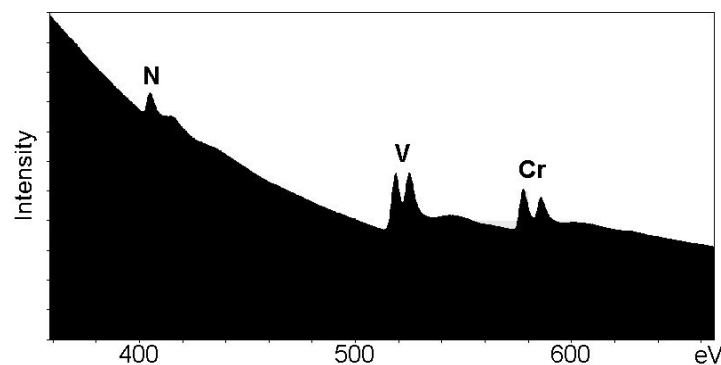
Figure 13: *An EEL spectrum of a Z-phase, showing the presence of its major elements.*

4.1.4 EELS

Electron Energy Loss Spectroscopy (EELS) is a relative new method of analysing the chemistry of the specimen. As the accelerated electrons pass

through the specimen, they will lose energy by interacting with the specimen. When an accelerated electron inelastically excites one of the inner shell electrons (usually generating X-rays or Auger electrons) of a specific element, it will lose a specific amount of energy dependent on the binding energy of the electron. As the binding energies of the electrons is dependent on the element in question and these energy losses can be measured, the quantitative composition of the specimen can be determined from the intensities of the loss peaks, see figure 13. There are many other interaction processes which cause inelastic scattering of electrons, creating a lot of background, and making the EEL spectrum harder to read compared to EDS, compare figure 12 to figure 13. However, EELS does not have the same limitations on light elements as EDS, so it was primarily used for measuring the C and N content of precipitates in this work.
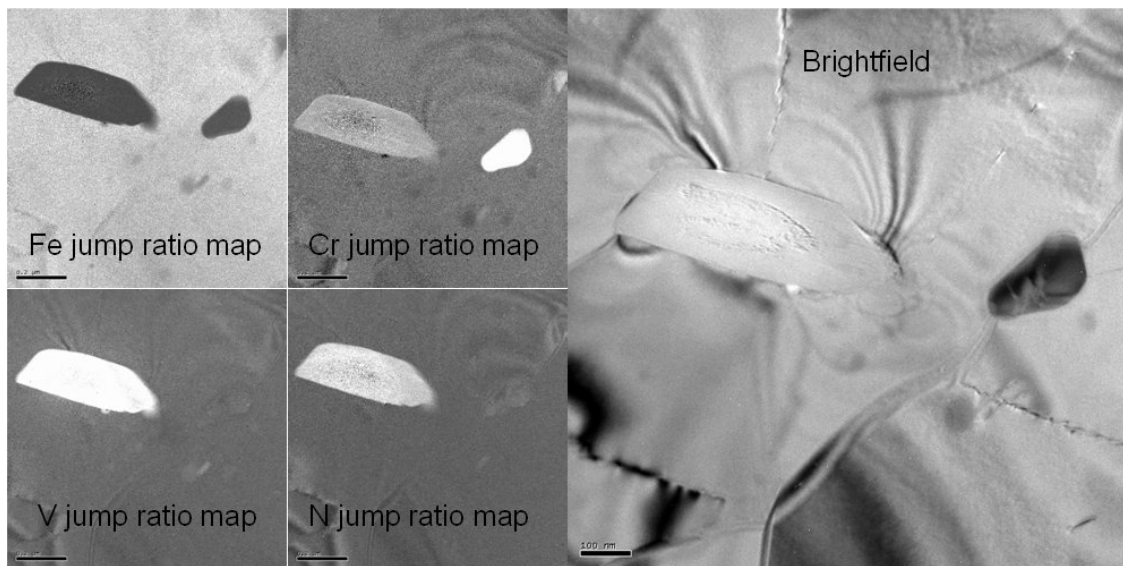
Figure 14: *Elemental mapping, showing a Z-phase (large) and a $M_{23}C_6$ (small) in a martensitic matrix.*

4.1.5 EFTEM

Energy Filtered TEM (EFTEM) works in principle the same way as EELS, measuring the loss of the electrons as they pass through the specimen. But as EELS focuses on a small area and measures the entire spectrum, EFTEM focuses on a larger area while only measuring a small part of the spectrum.

28

Hence EFTEM works like elemental mapping, showing the concentration profile of a single element on an area, see figure 14. This can be useful when investigating thin-foils, as certain particles can otherwise be difficult to distinguish from the matrix. As Z-phase is usually very difficult to observe on brightfield images, it can be advantageous to use V post edge images to search for them.

4.1.6 Electron diffraction

Electron diffraction is constructive interference of elastically scattered electrons in a crystalline material. These elastically scattered electrons cam form patterns which yield information on the crystal structure, and were used for investigations of precipitates in this work.
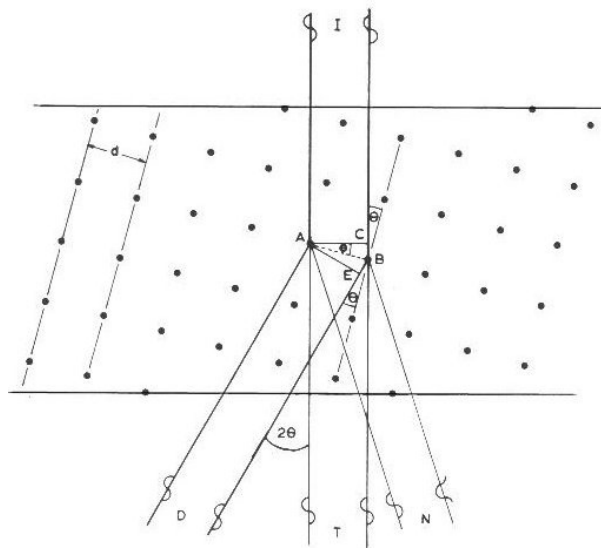
Figure 15: *Schematic overview of diffraction in a crystalline specimen. [27]*

In order to explain diffraction we have to consider the electron beam as a wave motion. Before the electron beam interacts with the crystal, it is coherent, i.e. the individual electron waves are in phase. Some electrons passing through the crystal will be scattered elastically by the atoms. As the electrons hit the atoms in the crystal they will scatter elastically. If the scattered electron waves are in phase with one another, they will reinforce each other and lead to a strong beam of electrons, but if they are not in phase they will not reinforce. The electron

waves are only in phase when leaving the crystal when the distance CB+BE in figure 15 is equal to an integral number of wavelengths. From trigonometry can be seen that CB=BE is equal to dsinθ, hence the condition for constructive interference, known as Braggs Law, is:

$$2d\sin\theta = n\lambda \hspace{4cm} [7]$$

where *d* is the interplanar spacing in the crystal, *λ* is the wavelength of the electrons and n is an integer.
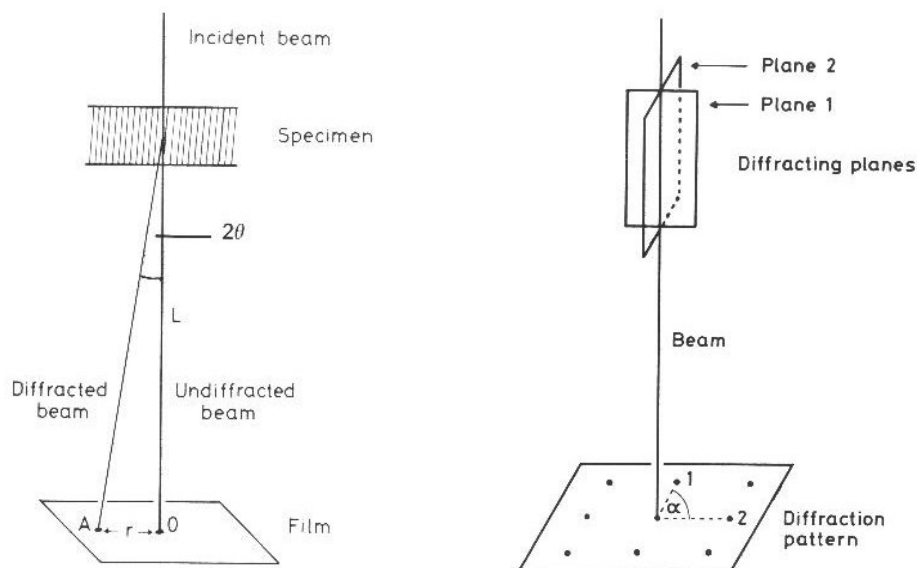
Figure 16: *Schematic overview over the scattered electrons (left) and the appearance of a diffraction pattern when in zone axis (right). [27]*

Constructive interference of the elastically scattered electrons will only occur at specific scattering angles from the incident beam, such as 2θ, see figure 15 and 16(left). The angles are exaggerated; an electron beam will only be strongly diffracted from planes of atoms which are almost parallel to the electron beam. When the beam is almost parallel to two planes of atoms (a zone axis), it will form a diffraction pattern, consisting of well ordered spots, see figure 16(right). By measuring the distance r between the spots, figure 16(left), and the angle α between these spots, figure 16(right), it is possible to obtain valuable information on the crystal structure of the investigated crystalline material. For a more detailed description, see appendix E.

4.1.7 SAED and CBED

The usual method of obtaining diffraction patterns is using Selected Area Electron Diffraction (SAED), where the incident electron beam is parallel, see figure 17a. The size of the area which contributes to the SAED pattern is determined by the SAED aperture, see figure 10. The minimum size of this aperture is usually around 200nm. Thus when investigating small particles in thin-foils or particles which are in close contact with each other, the diffraction pattern normally contains information from more than one phase, which may complicate the analysis of the pattern. When obtaining orientation relationships, using SAED is preferable, as information from a large area is obtained.
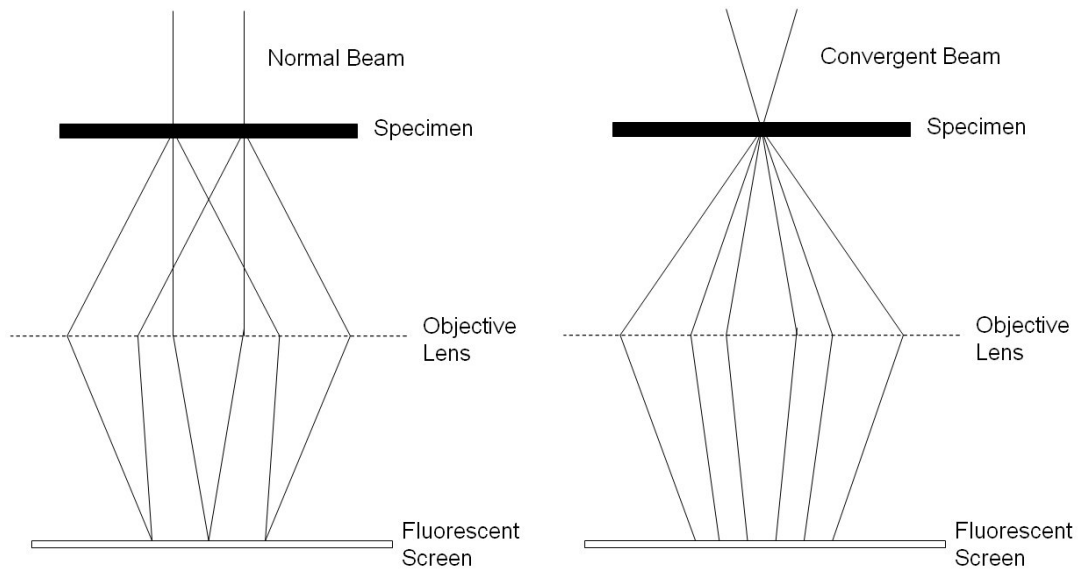
Figure 17: *Schematic overview of the difference between SAED (left) and CBED (right).*
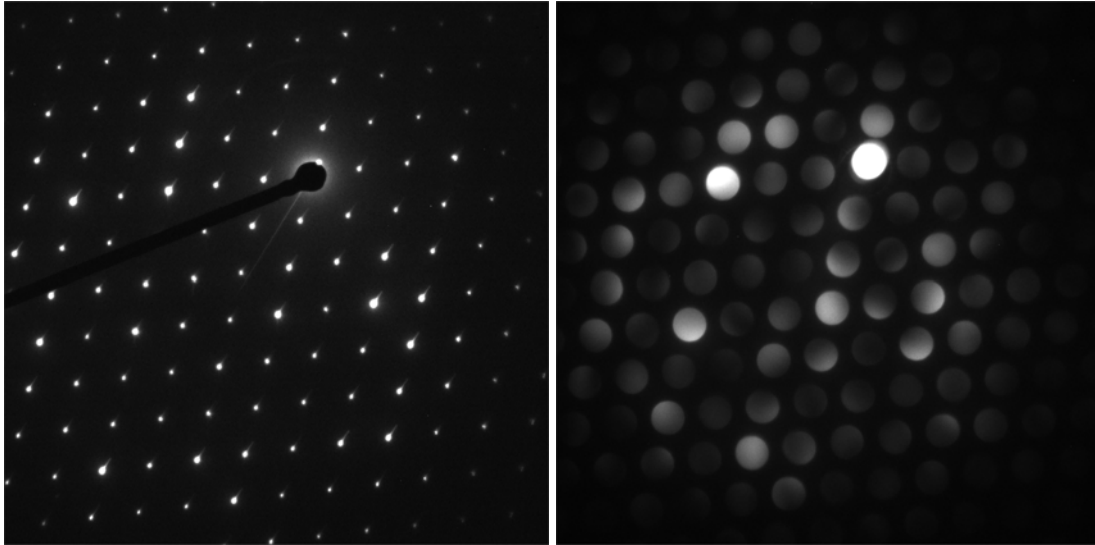
Figure 18: *The difference between SAED (left) and CBED (right) patterns. Patterns are a [101] zone axis of a $M_{23}C_6$.*

With Convergent Beam Electron Diffraction (CBED) the electron beam is focused on a very small area on the specimen, making sure the diffraction pattern only contains information from just that spot. This makes it possible to obtain information on structural changes even within precipitates. Since the electron beam is not parallel when entering the specimen, the diffraction spots will appear as discs, see figure 17b. The different appearances of SAED and CBED images are exemplified in figure 18.

4.1.8 Kikuchi lines

When dealing with crystalline materials, some of the inelastically scattered electrons might be scattered elastically (diffraction scattered), and this phenomena manifests itself as Kikuchi lines. In a diffraction pattern this will manifest itself as two parallel lines, one dark and one bright. The angular separation of the Kikuchi lines is 2θ, which is the same for the diffraction spots of the corresponding plane. The parallel lines will always follow the plane from where they can be elastically scattered, and will cross each other in zone axes. Maps from these lines can be drawn so they can be used to "navigate" in the

crystal, see figure 19. This was used to good effect when investigating the Z-phase.
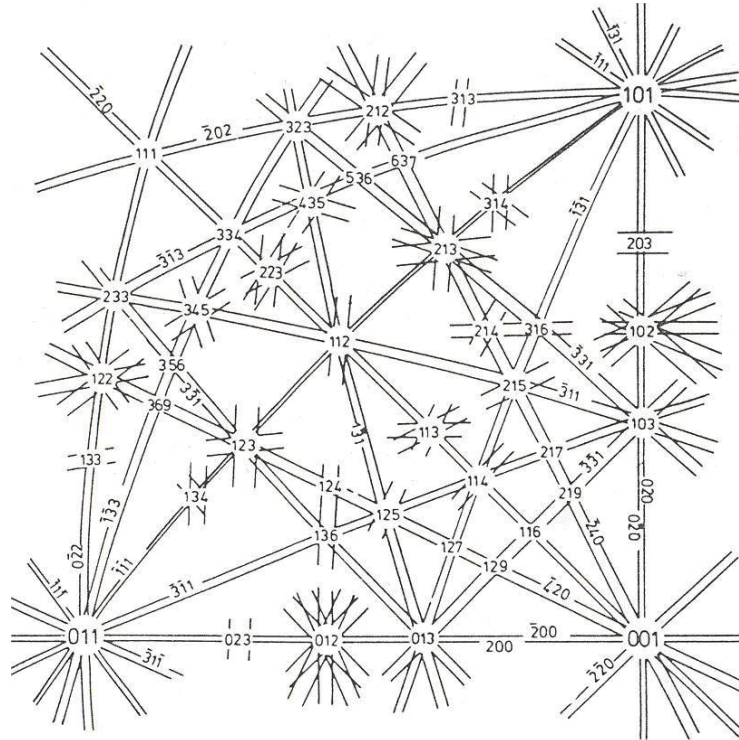
Figure 19: *A map of the Kikuchi lines of an fcc crystal structure. The lines represent the planes and the zones axes are located where the planes cross each other. [28]*

4.2 X-ray powder diffraction

X-ray diffraction has long been used for investigation of the crystal structure in crystalline materials. The principles involved are basically the same as in electron diffraction. In this work X-ray powder diffraction was used, were the powder consisted of precipitates from 9-12%Cr steels.

When obtaining X-ray powder diffraction spectrum, contribution is gained from many crystallites (precipitates), each which is randomly oriented. This gives a ring pattern as opposed to the spot patterns of electron diffraction. By measuring the radius and intensity of the rings, knowledge on the crystal structure of the precipitates can be gained. A typical result is given in figure 20, x-axis being the radius and y-axis the intensity.
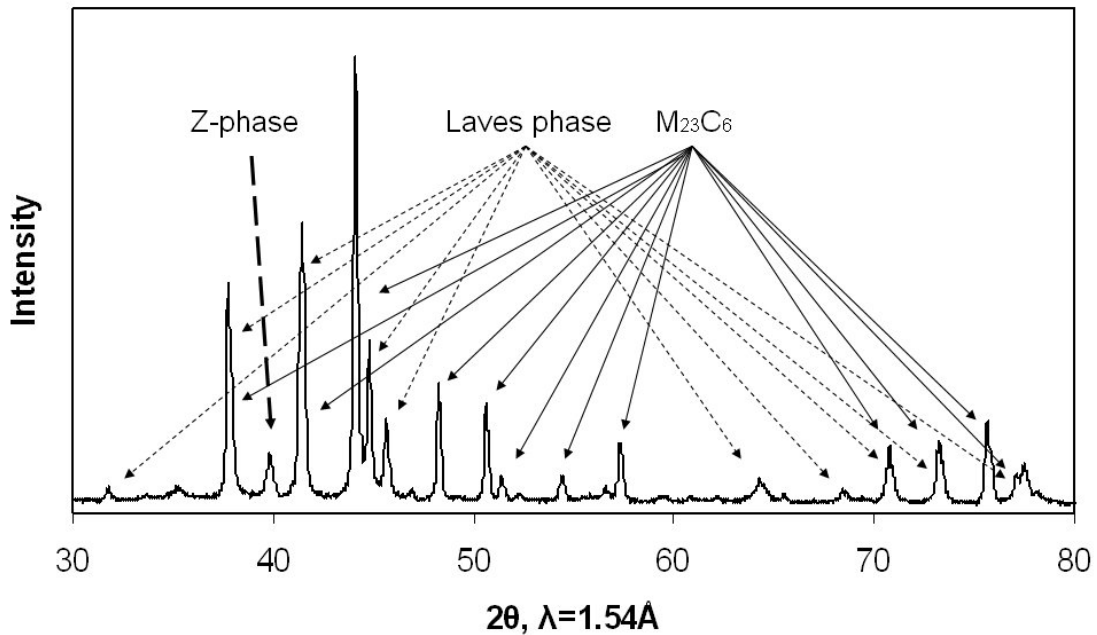
Figure 20: *An X-ray spectrum of a 12%Cr close to equilibrium. Most of the peaks are from $M_{23}C_6$ or Laves phase, only one peak is exclusively from Z-phase.*

The precipitate powder used for X-ray powder diffraction was extracted by electrolytically dissolving the steel matrix. This did not dissolve the precipitates, which remained in the electrolyte. As relatively many particles are needed, a certain amount of matrix needs to be dissolved, preferably a few grams. The precipitates were then fixed upon a glass surface or on a silicon single crystal for further analysis.

4.2.1 X-ray powder spectra

As shown in previous chapters, there are many different precipitates present in 9-12%Cr steels. $M_{23}C_6$ usually have the highest volume fraction, which give many peaks in the X-ray spectrum. This may (and often will) overshadow many of the peaks from other precipitates. Figure 20 shows a 12%Cr steel which has been exposed for prolonged time and is close to equilibrium. Most of the peaks are from $M_{23}C_6$ and Laves phase, with frequent overlaps. Unfortunately, only one peak for the Z-phase is visible, making qualitative measurements (crystal

structure, lattice parameters, etc.) of Z-phase difficult. However, it is possible to get quantitative information, by comparing it to the carbide peak, or more importantly the MX peaks, if present. In TEM it is possible to find some Z-phase in most 9-12%Cr steels which have been exposed for 10.000h/650°C, but it can be difficult to asses the quantity. With X-ray diffraction it is relatively simple, as the Z-phase peak will only appear if Z-phase is present in a certain quantity. Even though it is possible to find Z-phase in TEM, they will not necessarily show on the X-ray spectrum.

5 Thermodynamic and kinetic modelling

Thermodynamic and kinetic computer modelling has successfully established itself as an important tool for alloy design and predictions of precipitation behaviour. It has long been used for evaluation of phase stability for matrix and precipitates in 9-12%Cr steels, and has yielded valuable information on the effect of precipitates on creep strength.

Mainly two different computer programs have been used during this work, ThermoCalc and MatCalc. The ThermoCalc software has been used for thermodynamic modelling of Z-phase. The resulting model has been implemented in the MatCalc software for kinetic simulations of the Z-phase.

5.1 ThermoCalc

The ThermoCalc software [29] is primarily used for calculations on thermodynamic equilibria. It uses the CALPHAD approach, where thermodynamic functions expressed as polynomials are used to predict higher order systems by extrapolating from descriptions of lower order systems. It is based on the principle that at equilibrium the system Gibbs energy is at a minimum. ThermoCalc calculates the Gibbs energy contribution for every phase in a multi-component systems and sums them up, so for equilibrium:

$$G = \sum_{i=1}^{n} n_i G_i^m = \text{minimum} \tag{8}$$

where n_i is the moles of phase i and G_i^m is the molar Gibbs energy of phase i. Valuable information on phase fractions, compositions, driving forces etc. at this minimum can then be obtained.

ThermoCalc relies mostly on thermodynamic data like chemical composition and temperature. This does not include features such as crystal structure, interfacial energies or mechanical stresses.

For a general description of all phases, the sublattice model which was developed by Hillert and Staffanson [30] and extended by Ågren and Sundman [31] is used. This model considers phases with an arbitrary number of components and sublattices. In this model the site fraction y_c^l is introduced, which represent the mole fraction of components (including vacancies) in a sublattice. The site fractions may be represented as a l x c matrix, Y, where l are the sublattices and c the components:

$$Y = \begin{bmatrix} y_1^1 & y_2^1 & .... & y_{m-1}^1 & y_m^1 \\ y_1^2 & y_2^2 & .... & y_{m-1}^2 & y_m^2 \\ .... & .... & .... & .... & .... \\ y_1^{n-1} & y_2^{n-1} & .... & y_{m-1}^{n-1} & y_m^{n-1} \\ y_1^n & y_2^n & .... & y_{m-1}^n & y_m^n \end{bmatrix}$$ [9]

n is the number of sublattices and m is the number of components.

For the sublattice model the molar Gibbs free energy of the phases can be divided into the following contributions:

$$G^m = G^0 + G^{mix} + G^{xs}$$ [10]

where G^0 is the Gibbs energy of a stoichiometric compound, G^{mix} represents the contribution due to the entropy of mixing for an ideal solution and G^{xs} is the excess energy which represents the energy of a mechanical mixture of the elements.

The Gibbs energy of a stoichiometric compound, where each sublattice is occupied by only one component, can be defined as:

$$G^0 = \sum_i P_i[Y]G_i^0$$ [11]

where i denotes the components for the phase and $P_i[Y]$ is the corresponding product of site fractions from the Y matrix. As no absolute values of the Gibbs energy can be defined, G_i^0 is referred to the standard element reference (SER) enthalpy state. In addition there is usually a polynomial function which must be fitted using calculations or experimental data:

37

$$G_i^0 = H_i^{SER} + A + BT + ...$$ [12]

A would be the total energy of formation related to the SER states of the pure constituents at zero K, while the rest of the polynomial function describes the temperature dependence. Various forms of polynomials are used, and some may be contributed to a physical meaning, but they are essentially just fitting parameters.

The contribution of the entropy of mixing of an ideal solution, which does not consider interactions between the components, can be expressed as:

$$G^{mix} = RT \sum_l a^l \sum_c y_c^l \ln y_c^l$$ [13]

where a^l is the number of sites on the sublattice *l* per mole formula units of the phase.

For non-ideal solutions the excess Gibbs energy must be defined. The G^{xs} term represents the interaction between different types of atoms located on the same sublattice (non-stoichiometric compounds). A pragmatic, albeit empirical way of expressing the excess Gibbs energy is by using the Redlich-Kister equation:

$$G^{xs} = \sum_{Z>0} \sum_{iZ} P_{iZ}[Y] \sum_{v=0} L_{ij}^v (y_i - y_j)^v$$ [14]

where Z is the order of the system, 1 being one extra element introduced into the sublattice, 2 for two extra elements etc. *v* is an integer, usually not higher than 2. L_{ij}^v can be expressed as a polynomial:

$$L_{ij}^v = C + DT ....$$ [15]

The *C* and *D* constants in this polynomial must be fitted using calculations or experimental data.

5.1.1 Z-phase in ThermoCalc

In order to demonstrate how the above equations work for a phase with multiple sublattices, an example will be performed using the Z-phase. For this demonstration the Z-phase is assumed to consist of five elements: Cr, V, N, Nb

and Fe. The Z-phase is defined to consist of a ABC stoichiometry, the three sublattices aptly named 1, 2 and 3. The first sublattice is considered to be occupied by Cr and Fe atoms, the second to consist of Nb and V, and the third exclusively of N. If G^i_0 is fitted using a simple $A+BT$ polynomial, the G^0 term can be expressed as:

$$G^0 = x^1_{Cr}x^2_V x^3_N G^{Z-phase}_{Cr:V:N} + x^1_{Fe}x^2_V x^3_N G^{Z-phase}_{Fe:V:N} + x^1_{Cr}x^2_{Nb} x^3_N G^{Z-phase}_{Cr:Nb:N} + x^1_{Fe}x^2_{Nb} x^3_N G^{Z-phase}_{Fe:Nb:N} \qquad [16]$$

where

$$G^{Z-phase}_{Cr:V:N} = H^{SER}_{Cr} + H^{SER}_{V} + H^{SER}_{N} + A_1 + B_1 T \qquad [17]$$

$$G^{Z-phase}_{Fe:V:N} = H^{SER}_{Fe} + H^{SER}_{V} + H^{SER}_{N} + A_2 + B_2 T \qquad [18]$$

$$G^{Z-phase}_{Cr:Nb:N} = H^{SER}_{Cr} + H^{SER}_{Nb} + H^{SER}_{N} + A_3 + B_3 T \qquad [19]$$

$$G^{Z-phase}_{Fe:Nb:N} = H^{SER}_{Fe} + H^{SER}_{Nb} + H^{SER}_{N} + A_4 + B_4 T \qquad [20]$$

All of the A and B constants have to be fitted separately.

The ideal entropy of mixing can be expressed as:

$$G^{ideal} = RT\left(x^1_{Fe}\ln x^1_{Fe} + x^1_{Cr}\ln x^1_{Cr}\right) + RT(x^2_V \ln x^2_V + x^2_{Nb}\ln x^2_{Nb}) + RT\left(x^3_N \ln x^3_N\right) \qquad [21]$$

The excess Gibbs energy expression can be written as:

$$G^{xs} = x^1_{Cr}x^1_{Fe}x^2_V x^3_N L_{Cr,Fe:V:N} + x^1_{Cr}x^1_{Fe}x^2_{Nb}x^3_N L_{Cr,Fe:Nb:N}$$
$$+ x^1_{Cr}x^2_V x^2_{Nb}x^3_N L_{Cr:V,Nb:N} + x^1_{Fe}x^2_V x^2_{Nb}x^3_N L_{Fe:V,Nb:N} \qquad [22]$$

where the L parameters can be described using the Redlich-Kister polynomial (v=2):

$$L_{Cr,Fe:V:N} = {}^0L_{Cr,Fe:V:N} + {}^1L_{Cr,Fe:V:N}(x_{Cr} - x_{Fe}) + {}^2L_{Cr,Fe:V:N}(x_{Cr} - x_{Fe})^2 \qquad [23]$$

$$L_{Cr,Fe:Nb:N} = {}^0L_{Cr,Fe:Nb:N} + {}^1L_{Cr,Fe:Nb:N}(x_{Cr} - x_{Fe}) + {}^2L_{Cr,Fe:Nb:N}(x_{Cr} - x_{Fe})^2 \qquad [24]$$

$$L_{Cr:V,Nb:N} = {}^0L_{Cr:V,Nb:N} + {}^1L_{Cr:V,Nb:N}(x_V - x_{Nb}) + {}^2L_{Cr:V,Nb:N}(x_V - x_{Nb})^2 \qquad [25]$$

$$L_{Fe:V,Nb:N} = {}^0L_{Fe:V,Nb:N} + {}^1L_{Fe:V,Nb:N}(x_V - x_{Nb}) + {}^2L_{Fe:V,Nb:N}(x_V - x_{Nb})^2 \qquad [26]$$

The ^0L, ^1L and ^2L parameters can be described by a polynomial function, linear used in this case:

$${}^0L_{Cr,Fe:V:N} = C_1 + D_1 T \qquad [27]$$

$${}^0L_{Cr,Fe:Nb:N} = C_2 + D_2 T \qquad [28]$$

$${}^0L_{Cr:V,Nb:N} = C_3 + D_3 T \qquad \text{[29]}$$

$${}^0L_{Fe:V,Nb:N} = C_4 + D_4 T \qquad \text{[30]}$$

$${}^1L_{Cr,Fe:V:N} = C_5 + D_5 T \qquad \text{[31]}$$

$${}^1L_{Cr,Fe:Nb:N} = C_6 + D_6 T \qquad \text{[32]}$$

$${}^1L_{Cr:V,Nb:N} = C_7 + D_7 T \qquad \text{[33]}$$

$${}^1L_{Fe:V,Nb:N} = C_8 + D_8 T \qquad \text{[34]}$$

$${}^2L_{Cr,Fe:V:N} = C_9 + D_9 T \qquad \text{[35]}$$

$${}^2L_{Cr,Fe:Nb:N} = C_{10} + D_{10} T \qquad \text{[36]}$$

$${}^2L_{Cr:V,Nb:N} = C_{11} + D_{11} T \qquad \text{[37]}$$

$${}^2L_{Fe:V,Nb:N} = C_{12} + D_{12} T \qquad \text{[38]}$$

All *C* and *D* constants have to be fitted separately.

For a full description of the Z-phase (all elements observed included) there is a bewildering number of constants available for fitting. It may however not be necessary to use all of them, fitting the G parameters can often prove sufficient.

5.1.2 The Z-phase model

The thermodynamic model of Z-phase has been created using the newest iron based database from ThermoCalc, TCFE3. Figure 21 shows calculation performed on a 9%CrVNbN steel, using the TCFE3 database before and after being modified with the Z-phase model. All of the 9-12%CrVNbN steels show similar results, with Z-phase completely replacing VN below 800°C, although this process is observed to be very slow. The Z-phase model is mainly suitable for equilibrium circumstances and cannot calculate when the Z-phase will replace MX using ThermoCalc. However it can be used for calculating the thermodynamic driving force for Z-phase (difference in Gibbs energy for a system with and without Z-phase), giving some estimation of its kinetics. For more detailed information see appendix C.
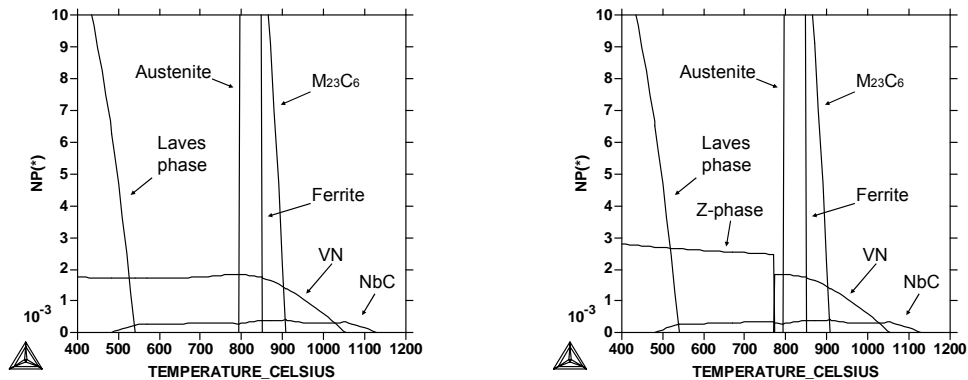
Figure 21: *A calculation made on a 9%CrVNbN steel with and without the Z-phase model implemented.*

5.2 MatCalc

MatCalc [32-33] is a relatively new software, which models the evolution of precipitates in multi-component, multi-particle and multi-phase systems. The program is based on the Onsager extremal thermodynamic principle, which postulates that a thermodynamic system evolves with a constraint maximum Gibbs energy dissipation [34-35]. The MatCalc software utilises CALPHAD type databases also used in ThermoCalc and DICTRA [36] to obtain basic thermodynamic and mobility data. Using these, it calculates the chemical potential and driving forces of all phases as well as the diffusivities of the elements in the matrix. Based on this data, the evolution of the numbers, radius, composition etc. of the precipitates can be calculated.

5.2.1 Basic equations

MatCalc has the capability to simulate precipitation behaviour during the entire lifetime of a material, from nucleation and growth to coarsening. The area of particular interest in this work is the nucleation and growth of the Z-phase. The governing equations in these fields are therefore given in detail here.

5.2.1.1 Nucleation

In MatCalc the classical nucleation theory for precipitate nucleation in solid state systems has been adapted to apply to the multi-component system and used to

41

calculate the number of newly formed precipitates in time steps. The number of new precipitates in a given time step, ΔN, can be calculated from the following equation [37]:

$$\Delta N = J \cdot \Delta t \qquad [39]$$

where J is the nucleation rate given by:

$$J = J_S \exp\left(\frac{-\tau}{t}\right) \qquad [40]$$

where J_s is steady state nucleation rate, and τ is the incubation time to form a critical nucleus. These factors are again given by the equations:

$$\tau = \frac{1}{2\beta^* Z^2} \qquad [41]$$

and

$$J_S = Z\beta^* N_C \exp\left(\frac{-\Delta G^*}{kT}\right) \qquad [42]$$

In these equations the β^* is the atomic attachment rate, Z is the Zeldovich factor, N_c the number of potential nucleation sites, G^* the energy barrier to form a critical nucleus, k the Boltzmann constant and T the absolute temperature. The Zeldovich factor can be calculated from:

$$Z = \left[\frac{-1}{2\pi kT}\frac{\partial^2 \Delta G}{\partial n^2}\Bigg|_{n^*}\right]^{\frac{1}{2}} \qquad [43]$$

where n is the number of atoms in the nucleus. The atomic attachment rate is given by:

$$\beta^* = \frac{4\pi \rho^{*2}}{a^4 \Omega}\left[\sum_{i=1}^{N}\frac{(c_{ki} - c_{0i})^2}{c_{0i} D_{0i}}\right]^{-1} \qquad [44]$$

where ρ^* is the critical radius of the nucleus, a is the atomic distance, Ω is the molar volume, D_{0i} is diffusivity in the matrix, c_{ki} and c_{0i} are the element concentration in the precipitate and matrix respectively. The energy barrier to form a critical nucleus is calculated by:

$$\Delta G^* \cong \Delta H^* = \frac{16\pi \gamma_k^3}{3F^2} \qquad [45]$$

where F is the effective thermodynamical driving force and γ is the interfacial energy. The critical radius can be calculated by:

$$\rho^* = \frac{2\gamma_k}{F} \tag{46}$$

MatCalc does not normally consider entropy in these equations, but during investigations of the nucleation it would prove necessary to take entropy into account.

5.2.1.2 Growth and coarsening

As the precipitates have nucleated they can start to grow. This process is described by the thermodynamic extremum principle, which states that a system evolves with a maximum rate of entropy production constrained by the balance law for the entropy production and dissipation. In solid state precipitation at a constant temperature, this principle is equivalent to a minimum of the rate of the Gibbs Energy G of a system with m precipitates and n components. The Gibbs energy can be expressed as [38]:

$$G = \sum_{i=1}^{n} N_{0i}\mu_{0i} + \sum_{k=1}^{m} \frac{4\pi\rho_k^3}{3}\left(\lambda_k + \sum_{i=1}^{n} c_{ki}\mu_{ki}\right) + \sum_{k=1}^{m} 4\pi\rho_k^2\gamma_k \tag{47}$$

The first term is the energy contribution from the matrix, the second is from the precipitates and the third from the interfaces. μ_{0i} and μ_{ki} are the chemical potentials of element i of the matrix and precipitate k respectively. λ_k denotes the stress introduced into the system by the precipitate k.

It is assumed that three different processes are active during the growth period: The movement of interfaces, diffusion in the precipitates and diffusion in the matrix. These processes are rate controlling, constraining the evolution of the system. They are denominated as Q_1, Q_2 and Q_3 respectively:

$$Q_1 = \sum_{k=1}^{m} \frac{4\pi\rho_k^2 \dot{\rho}_k^2}{M_k} \tag{48}$$

$$Q_2 = \sum_{k=1}^{m} \sum_{i=1}^{n} \frac{4\pi R T \rho_k^5 \dot{c}_{ki}^2}{15 c_{ki} D_{ki}} \tag{49}$$

$$Q_3 = \sum_{k=1}^{m} \sum_{i=1}^{n} \frac{4\pi R T \rho_k^3 (\dot{\rho}_k (c_{ki} - c_{0i}) + \rho_k \dot{c}_{ki}/3)^2}{c_{0i} D_{0i}} \tag{50}$$

The mobility of interfaces, M_k, is set very high in this work, as the precipitate growth is considered to be diffusion controlled. The coarsening process is governed by the same set of equations. The only factors that have any influence on the coarsening are the diffusivities and the interfacial energy.

Application of the extremum principle leads to evolution equations that describe the change of radius and the mean chemical composition of each precipitate class (VN, NbC etc.) on the basis of a linear system of equations. The development of the entire system is obtained by numerical integration of the evolution equations. For a further detailed analysis of these integrations see references [39-40].

5.2.2 Input factors

MatCalc needs a lot of input factors in order to calculate a precipitate system, f. ex. thermodynamic, diffusion and microstructure data. It gets much of the needed information from mobility and thermodynamic databases, also used in software such as ThermoCalc and DICTRA, but other factors must be entered by the users. Only input factors which are deemed important for understanding the fundamentals are dealt with here.

5.2.2.1 System

In MatCalc a system can be organised into different precipitation domains. This could for example be a separate domain for grain boundaries and grain interior, or two different matrix phases in a duplex material. Each precipitation domain consists of a matrix phase and can have a number of different precipitation phases. In this work calculations were made on steels. Only one precipitation

domain was considered to be present at a time, e.g. austenite during normalising and ferrite (martensite) during tempering and service. A precipitation domain must be defined to have a microstructure which will provide a number of nucleation sites for the precipitates. This microstructure can be defined by the grain and subgrain size, elongation factors for these grains and subgrains and dislocations density.

The composition of the system and the temperature must be defined. In this work, 9-12% Cr steels were used, some minor variations in composition were used in calculations in order to validate different steel grades. Specific heat treatments for these steels had to be simulated, so the temperature/time gradients also have to be specified in MatCalc.

The diffusivities in the matrix are calculated using mobility databases. However, the diffusion rates in precipitates are generally not known, but they are considered to be much slower compared to matrix diffusion. The diffusion rate in precipitates is approximated using the diffusion rate in the matrix multiplied with a certain factor, 0.01 used in this work.

In order to avoid nucleation of precipitates too close to other precipitates, an inactive radius factor is applied. This signifies that when a particle nucleates on f. ex. a grain boundary, further nucleation on a certain part of this grain boundary surrounding the newly formed precipitate will be much less likely. A radius factor of 5 is used in this work.

5.2.2.2 Matrix

The matrix phase of the precipitation domain is usually the phase which has the highest phase fraction (fcc or bcc iron in the case of steels). The matrix contains the elements which the precipitates need in order to nucleate and grow. When coarsening of the precipitates takes place, the elements have to be exchanged through the matrix. In contrast to many other models, which calculate

concentration gradients near precipitates (discrete models), MatCalc does not calculate any gradients in the composition of the matrix, assuming an average composition (mean-field approach). This is also the case for the precipitates. This simplification significantly decreases the calculation time needed, while the error in accuracy is only considered to be very small [40].

In this work, the system was defined as consisting of one matrix, although the matrix could change with time. The matrix was specified as being austenite when doing calculations above a certain calculated temperature (847°C in this work) and ferrite when below this temperature. The sudden change in matrix does not have any immediate effect on its composition, nor the precipitates in it, although a change with time is likely.

The role of the factors describing the microstructure is basically to provide nucleation sites for precipitates. The microstructure is defined by inserting grain and subgrain diameters (in this work 10^{-4} and 10^{-7}m respectively for martensite), their respective size elongation factors (1 for grains and 100 for subgrains), and the dislocation density (10^{14} m/m^3). The interfacial energy of the grains, subgrains and the dislocation energy can be calculated by MatCalc. When precipitates nucleate and grow on f. ex. the grain boundaries, MatCalc will subtract the energy of the surface area of the boundary covered by the precipitate from the formation energy of the precipitate.

5.2.2.3 Precipitates

Any number of precipitation phases may be introduced into a precipitate domain. It is also possible to define several phases of the same kind, for example primary and secondary MX precipitates. MatCalc assumes the precipitates to be spherical, even though this might not always be the case in 9-12%Cr steels. Each precipitate phase is divided up into one or more size classes (classes of precipitates with different radius). The precipitates in a given size class all have the same radius and the same composition. The number of precipitates in each
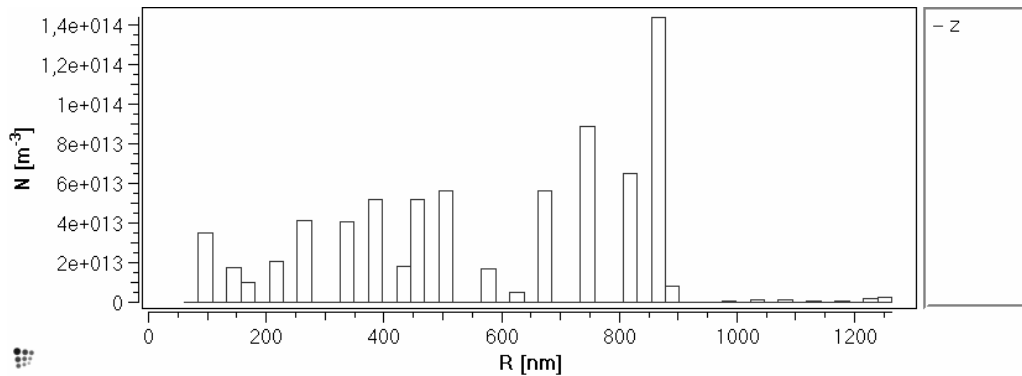
Figure 22: *An example of how size classes can be displayed, showing the number of particles in each size class.*

size class may be different, see figure 22, and so may the chemical composition. The number of size classes (10 usually used in this work) is important for the accuracy of the description of the precipitate size distribution. More size classes will give better accuracy, but will also slow down calculations. The number of size classes is kept constant, so whenever a size class nucleates, two size classes will merge, and when one dissolves another one will split up.
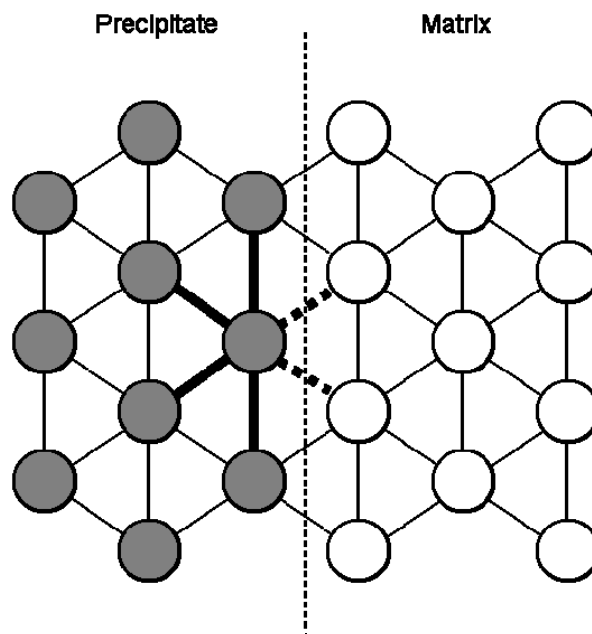
Figure 23: *An illustration of an interface, showing the broken bonds. In this example z_s is 2 and z_l is 6.*

The possible nucleation sites have to be defined of each precipitate phase. A precipitate can have several possible nucleation sites, f. ex. both on dislocation and grain boundaries. Precipitates can even precipitate on other precipitates. When precipitates nucleate, the available nucleation sites will decrease, and so will the nucleation rate. The specific positions of the precipitates are not taken into consideration, e.g. the distance between two precipitates or whether they are present on the same grain boundary etc. The precipitates are all isolated in the matrix under the same conditions, and they have to interact with each other through the matrix on equal terms.

The interfacial energy has a very large effect on the precipitation kinetics. The nucleation rate depends exponentially on the cube of the interfacial energy, see equation 42 and 45. It is difficult to obtain the value of the interfacial energy experimentally, but in MatCalc it can be calculated by using the "nearest-neighbour broken bond" model [41-42]:

$$\gamma = \frac{n_s z_s}{N z_l} \Delta E_{sol} \tag{51}$$

where n_s is the numbers of atoms per m^2 interface and N is Avogadros number. z_l is the number of nearest neighbours per atom and z_s the number of broken bonds across the interface per atom, see figure 23. ΔE_{sol} is the solution enthalpy and can be calculated from:

$$\Delta E_{sol} = \frac{\partial H}{\partial f_p} \tag{52}$$

where H is the system enthalpy and f_p the precipitate phase fraction. This equation only calculates the chemical interface, not the structural interface, i.e. it calculates coherent interfaces. It still seems to work well for most precipitates, even though some are semi-coherent. No information on the crystal structure has been included in this equation, but the calculated interfacial energy differences in most crystal structures (like bcc, fcc and hcp) are small,

5.2.3 Equilibrium calculations

MatCalc can perform similar operations as contemporary software for thermodynamic calculations. An example of equilibrium calculations is shown below, figure 24, compare with the results from ThermoCalc in figure 21. The calculations done by MatCalc are generally less time consuming compared to ThermoCalc, but when using the same databases, these two programs give the same results (as they should), in spite of slightly different approaches. Any openly available CALPHAD type database can be used for calculations, and in the end it is the quality of the databases which is the important factor in equilibrium calculations, not the algorithm.
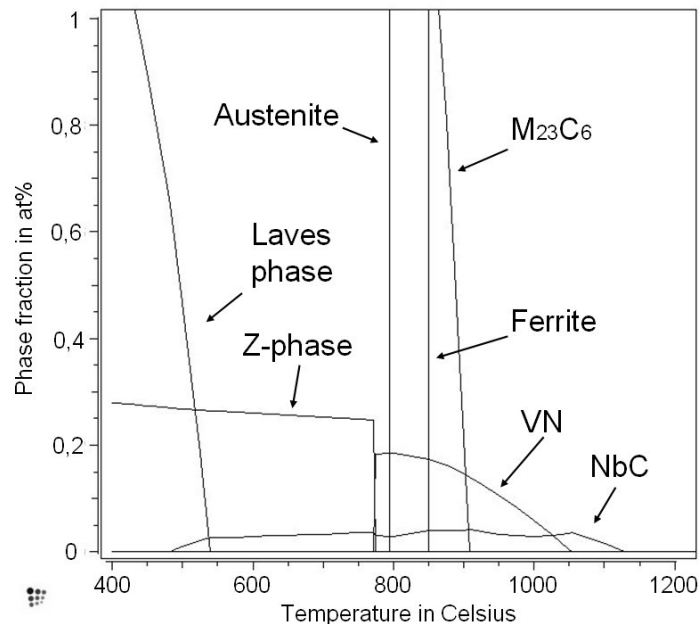
Figure 24: *A thermodynamic calculation made on the same 9CrVNbN steel as in figure 21 with the Z-phase model implemented. Results are identical.*

5.2.4 Kinetic calculations

It is with kinetic calculations that MatCalc stands out. Unlike other programs, such as DICTRA, it has been designed for calculations of systems with several precipitation classes. Instead of handling a few specific precipitates at a time, MatCalc does its calculations on systems with large numbers of precipitates which are averaged with respect to composition and size, see above. A lot of

assumptions are made in this process, but such assumptions are necessary in order to reduce calculation times to reasonable levels. This allows reasonable simulations of precipitate evolution in relatively complex systems.

5.2.5 MatCalc and Z-phase

The first simulations of Z-phase in MatCalc were carried out as if Z-phase was behaving like all other precipitates, i.e. using classical nucleation theory. In such a case, the Z-phase has to nucleate during heat treatment, before the VN precipitates are fully precipitated. If the VN first are fully precipitated, it would be impossible to nucleate the Z-phase, as the matrix would nearly be empty of the necessary elements (N, V or Nb). As the driving force of Z-phase is generally larger than that of VN, it would seem reasonable from a modelling point of view that they would nucleate during the tempering together with VN, as the only difference in composition is Cr which is abundant in the matrix.

Experimental observations of the Z-phase have shown that the Z-phase most likely nucleates during the service exposure, i.e. clearly after the VN precipitates are fully precipitated. Small Z-phases (<50nm) can be observed along with larger ones (>1µm) after prolonged exposure at service temperature, see appendix A. The nucleation seems to take place predominantly on VN precipitates, which might also be expected since there are some striking similarities in the crystal structures of Z and VN, see figure 25 (and appendix B). The nucleation mechanism seems to involve a physical transformation from VN to Z-phase by Cr diffusion (see appendix D). More recent MatCalc simulations were made with the assumption that Z-phase has to nucleate on VN with VN physically transforming into Z-phase. However, the nucleation descriptions in MatCalc are developed for the classical nucleation theories only. Much work has been focused on implementing a physical transformation mechanism into MatCalc, in order to simulate the experimental results.
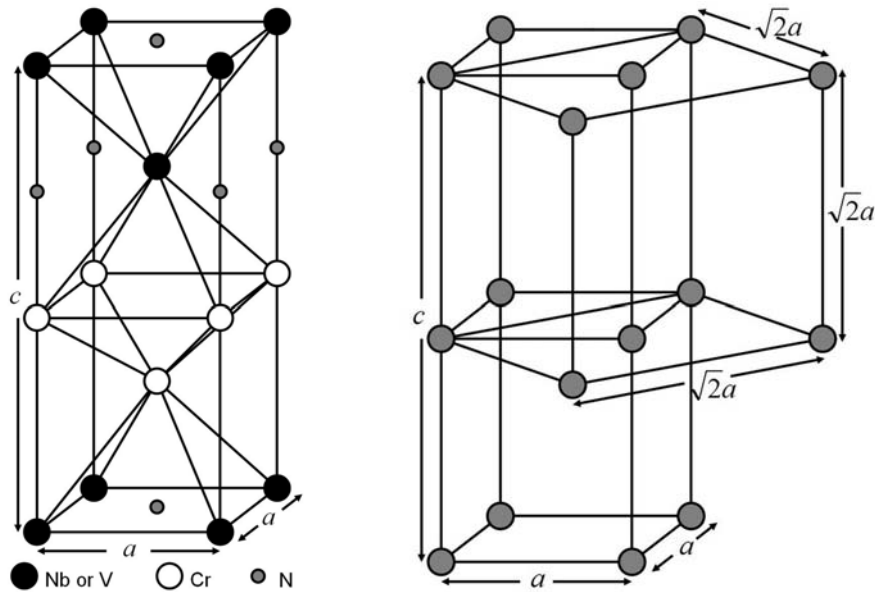
Figure 25: *Left: the tetragonal Z-phase structure, which is divided into VN and Cr layers. Right: The orientation relationship between the cubic VN and tetragonal Z-phase structures. Some atoms have been left out for clarity.*

5.2.6 Modifying MatCalc

The classical nucleation theory was scrutinised in order to see whether there could be a theoretical explanation as to why Z-phase appeared only after all VN had precipitated. After looking carefully at the crystal structure of the Z-phase, figure 25(left), it was concluded that in such a complicated crystal structure entropy could be of significance to the nucleation. Normally the entropy term in nucleation theory is disregarded, as the nucleus of most precipitate crystal structures can only form in a certain way, f. ex. VN. The investigations of Z-phase crystal structure have shown similarities between the Z-phase and normal fcc VN crystal structure. If the Cr and V atoms of the Z-phase do not split up into Cr and VN layers, a Cr rich VN precipitate would essentially emerge, see figure 25(right). The probability of all Z-phase atoms ordering themselves into Cr and VN layers in a nucleus of the size of 24 atoms (8 Cr, 8V, 8N) is are very small. The Cr and V atoms are on the substitutional sites, while N and vacancies (normally located in the Cr layers) are in the interstitial sites, so there are:

$$\frac{(16!)^2}{(8!)^4} = 1.65 \cdot 10^8 \tag{53}$$

51

ways of arranging the atoms. Only a handful of these will result in a Z-phase structure.

The classical nucleation theory, including the entropy term is as following:

$$J_S = Z\beta^* N_C \exp\left(\frac{-\Delta H^* + \Delta S^* T}{kT}\right)$$ [54]

and when

$$S = k \ln \omega$$ [55]

ω being the randomness factor the classical nucleation gives:

$$J_S = \omega Z \beta^* N_C \exp\left(\frac{-\Delta H^*}{kT}\right)$$ [56]

As the randomness factor is inversely dependent on the number of possible ways to arrange the atoms in the nucleus, equation 53, it would be in the size of 10^{-5} to 10^{-8}, depending on the size of the critical nucleus. Thus the entropy term makes a considerable difference. When using this entropy term in MatCalc, it will slow down Z-phase precipitation to a point, where another nucleation mechanism for the Z-phase would be more probable to dominate the precipitation process.

The possibility of a physical transformation of VN into Z-phase by Cr diffusion was implemented into MatCalc as an alternative to the classical nucleation process. In the classical nucleation process, the Z-phase would have to nucleate using elements still being dissolved in the matrix. As VN precipitates had consumed most of the V, Nb and N, the concentration of these elements in the matrix was low, giving a very low driving force for nucleation of Z-phase, hindering precipitation. In the implementation of physical transformation mechanism the concentrations of the matrix are not considered (not directly at least). Instead the difference between the stability (driving force) of Z-phase and VN is used as driving force for the nucleation process. The Z-phase was set to nucleate on VN precipitates, and when a Z-phase nucleated, the critical radius of this Z-phase was assumed to be the average radius of the existing VN precipitates. The elements for the Z-phase precipitation (Cr,V,Nb,N) are taken from the matrix. Furthermore, for every Z-phase nucleated, a VN precipitate was

removed, and dissolved into the matrix. The removed VN precipitates were taken from all size classes in relatively equal amounts. The forced dissolution of VN precipitates ensured a mass balance in the system. Unfortunately the processing time for each simulation was increased because of this, making calculations rather slow.

Even though a physical transformation was simulated, the classical nucleation theory (including the entropy term) was still used for this. It is questionable if a transformation process would depend on the classical nucleation theory, but it was used for a lack of alternatives. Factors which no longer made any physical sense, like β^*, were eliminated from the equation. The interfacial energy had no physical meaning either, so an equivalent factor, γ equivalent, was used instead. This γ equivalent was basically used as a fit parameter.

The composition of the matrix still has an influence on the nucleation rate of Z-phase, even though it is considered as a physical transformation. As the composition of the matrix changes, primarily because of coarsening of VN and precipitation of Z-phase, the stability (driving force) of both VN and Z-phase change. Even though the change in stability for VN and Z-phase is very similar, there is still a small difference, which can alter the (newly defined) driving force for Z-phase.

5.2.7 MatCalc results

Calculated results for a TAF650 type 11%CrCoWVNbN steel are shown in figure 26. This calculation is just for demonstration of a possible Z-phase precipitation, but represents a typical method of displaying the results, with a logarithmic time scale as an x-axis, from 1 to 100,000 hours in this case. The first graph in figure 26 shows the temperature, with the heat treatment at the start followed by a service temperature at 650°C. The second graph shows the phase fractions of the precipitates, and as can be seen the Z-phase completely replaces VN nitride after about 20,000h, which corresponds fairly well to experimental results.
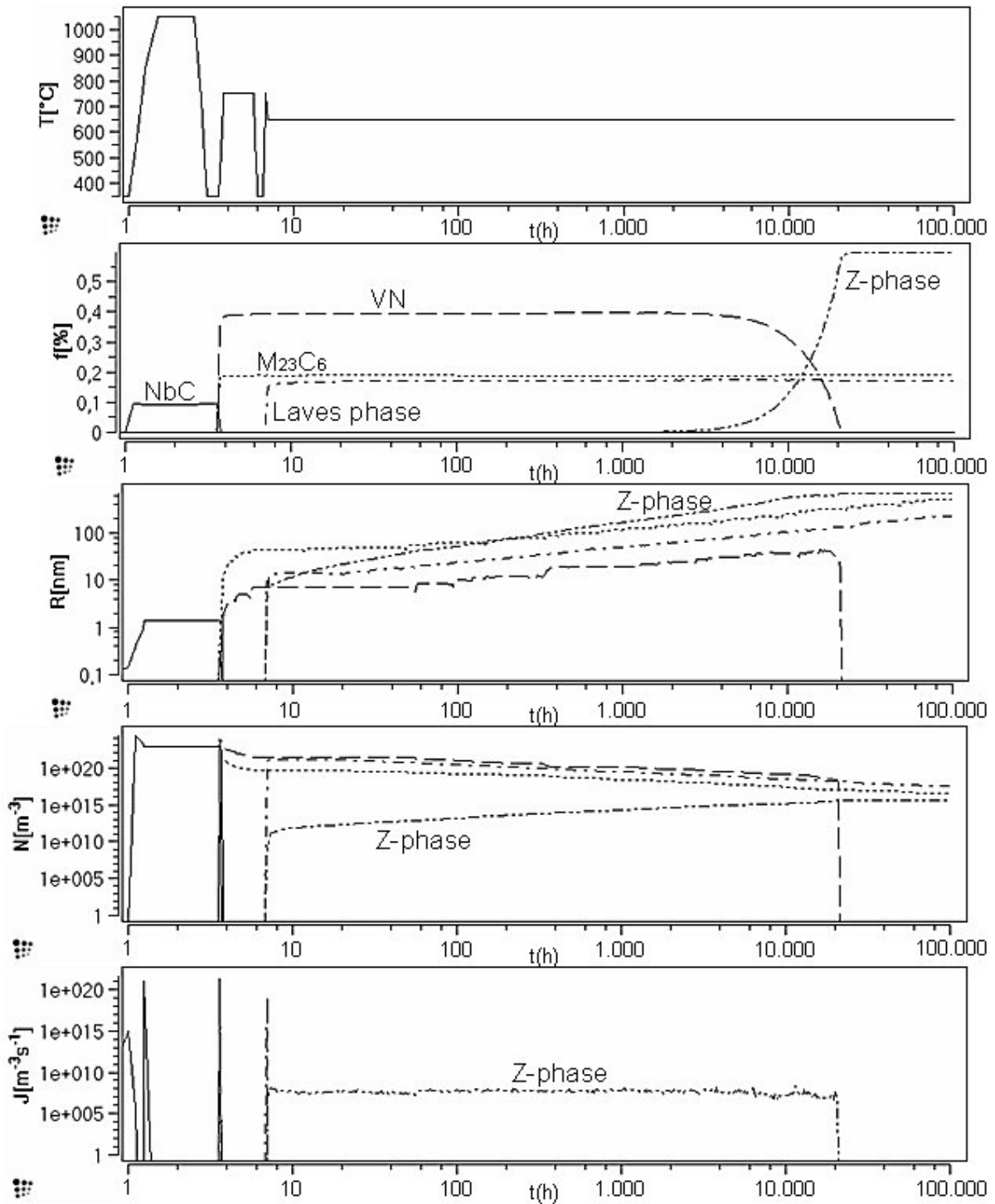
Figure 26: *Results of calculations using the new physical transformation nucleation mechanism. Along the X-axis time (h) is given, while the y-axes are temperature, phase fraction, radius of precipitates, number of precipitates and nucleation rate respectively. Note the two first y-scales are linear while the three last (and the x-axis) are logarithmic. The phase fraction of $M_{23}C_6$ and Laves phase has been divided with 10 as to better follow the behaviour of the nitrides.*

The third graph shows the radius of the precipitates and in the fourth the number of precipitates are displayed, both in logarithmic scales. These two graphs clearly show how the coarsening progresses, with increasing radius and decreasing numbers. The last graph is the nucleation rate, which is very interesting in this case. It was fitted to produce a flat curve for Z-phase, giving a steady increase in the numbers of Z-phase as indicated by experiments, see appendix A. In this case it works fairly well, but there are still instabilities in the calculations which need to be sorted out in order to create reliable simulations of the kinetic behaviour of Z-phase.

The initial MatCalc calculations have revealed a number of problems, both qualitative and numerical, and although many of these problems have been solved satisfactorily, some remain. Further work is needed in order to check for potential problems, and to compare calculated results with experimental results.

6 Summary

The performed work focuses on the Z-phase and the effect of its development in 9-12%Cr steels. Several aspects of the Z-phase were investigated, applying both transmission electron microscopy and computer modelling. The experiments carried out extended from identifying the crystal structure to investigating thermal stability and nucleation of the Z-phase. Modelling efforts focused on a thermodynamic description of the Z-phase; work on kinetic modelling was initiated, but further efforts are required.

Four papers were written on the basis of the present work, all of them focusing on the various aspects of the Z-phase. Three of them have been published or submitted to publishers, the fourth is included in manuscript. There are two conference papers which have not been included in this thesis, because of overlap, and two papers which are co-authored, but not initiated in the present Ph.D. project.

6.1 Behaviour of Z-phase in 9-12%Cr Steels

This paper gives a general overview of the Z-phase, mainly in 9-12%Cr steels, including literature data and own observations.

When the work described in this paper started, only little was known of the development of Z-phase in 9-12%Cr steels. Failures or strength breakdowns, which had occurred in several high Cr steels intended for operations at 650°C, were mainly attributed to the occurrence of Laves phase precipitation, which depletes the matrix from W and thereby reduces solid solution strengthening of the matrix. At the time, only very few sources had indicated that Z-phase might play a role in these steels.

Several steels were investigated for Z-phase formation during this project, using EDS on carbon extraction replicas. It soon became clear that there was a relationship between the amount of Z-phase observed and the long term creep strength. Steels which had dramatic drops in creep strength also had a significant Z-phase content. Furthermore it became clear that the observed Z-phase amount was closely connected to the Cr content of the steels, with the high Cr steels having far more Z-phase compared to the low Cr steels after similar exposure. As a consequence it will be a major challenge for the development of new steels for higher operating temperatures to combine oxidation resistance, which requires a high Cr content, and long term creep strength, which demands a relatively low Cr content because of Z-phase precipitation.

During this work, many important new observations concerning Z-phase were made. The dissolution temperature for modified Z-phase was experimentally established as being close to 800°C in 9-12%Cr steels, far lower compared to that of the original Z-phase. A pure Nb-free Z-phase, CrVN, was also observed for the first time, and observations show its precipitation rate to be slower compared to the normal Nb-containing modified Z-phase.

This work has shown a clear relationship between long term creep strength of modern 9-12%Cr steels and the presence of Z-phase. Furthermore it was experimentally established that the Cr content is a decisive factor of the precipitation rate of Z-phase. The amount of data collected for this paper formed the basis for all further investigation of Z-phase.

6.2 On the Crystal Structure of Z-phase, Cr(V,Nb)N

This paper describes discrepancies found in the crystal structure of modified Z-phase, using electron diffraction.

Electron diffraction investigations were carried out in order to verify that the Nb-free CrVN phase was indeed a Z-phase. Discrepancies were found in its crystal

structure, and soon turned out to be present in Nb containing modified Z-phases as well.

The crystal structure of several Z-phase versions (CrVN, Cr(V,Nb)N, CrNbN) were investigated, and a three fold symmetry not compatible with the normally accepted tetragonal lattice was observed in all V containing Z-phases, but not for CrNbN. While the tetragonal lattice was present in these Z-phases, experiments also showed a clear presence of fcc type diffraction patterns. These patterns where assumed to stem from a NaCl type lattice, not unlike those of the MX precipitates. The cubic and tetragonal lattice structures were both present in the Z-phase, forming a hybrid crystal structure. The orientation relationship between them was found, and the lattice parameters corresponded perfectly.

It is still unknown how the lattices coexist in the Z-phase hybrid structure. It can be assumed that the cubic structure is a metastable precursor to a thermodynamically stable tetragonal structure. Thus the particles observed in this work would be in a transition stage, where an ordering of the atoms into VN and Cr layers of the tetragonal structure takes place.

6.3 A Thermodynamic Model of the Z-phase, Cr(V,Nb)N

This paper describes in detail the development of and results obtained by a thermodynamic model of the Z-phase. The paper focuses on 9-12%Cr steels, but also yields information on austenitic steels.

Modelling of Z-phase was carried out in order to predict which steels would be vulnerable to Z-phase precipitation and how Z-phase can be avoided. The model was implemented into ThermoCalc´s newest iron based database using experimental data from own work and literature. The work on the model extended over a longer period, and it has been under continuous improvement as new data became available, like the dissolution temperature of modified Z-phase. It produced synergy with the experimental work in the project, as a prototype

version predicted the existence of CrVN Z-phase, which gave the impetus for a persistent search for its actual existence.

The model predicts the Z-phase to be stable in all 9-12%Cr steels containing its constituents. This is an important realisation, as it makes the development of Z-phase precipitation a kinetic rather than a thermodynamic problem. Experimental observations indicate that Z-phase is indeed present in most steels, but if the precipitation rate is slow enough, it should not affect the creep strength within the usual lifetime of the steel (as is the case for steels P91, P92 and X20). The model predicts the precipitation rate in terms of a driving force for Z-phase. The calculations show that Cr is the most influential element, corresponding well with experimental observations. The driving force calculations provide an important tool for future alloy design.

6.4 On the Dissolution and Nucleation of Z-phase, Cr(V,Nb)N

The purpose of this paper is to give a detailed description of the nucleation process of Z-phase.

Large Z-phase precipitates are present in most 9-12%Cr steels after exposure, but the number of Z-phase particles varies greatly. This indicates that the nucleation is a crucial factor in Z-phase precipitation. In this paper the nucleation of Z-phase is investigated using unconventional heat treatments.

The nucleation of Z-phase is very difficult to study as it happens slowly over a relatively long time span and as the nuclei are very small it is very hard to investigate them. The crystal structure investigations showed similarities between Z-phase and MX lattices. Exposing Z-phase containing steels above the Z-phase dissolution temperature led to a partial dissolution of the Z-phase, and Z-phase and MX particles were observed to be in direct contact, with a core/rim structure.

After a full dissolution treatment the MX precipitates became very large, and a prolonged heat treatment at 650°C made it possible to observe the re-appearance of Z-phase in direct contact with large MX particles during nucleation.

A clear orientation relationship between MX and Z-phase was found, with only a slight difference in lattice parameter. During dissolution of Z-phase, concentration profiles indicate that Cr diffuses out of Z-phase. The resulting core/rim structure develops large cracks in the rim, probably because of the mass reduction of the rim. As Z-phase re-emerges, it also forms a core/rim structure with MX. However, the transition between MX core and Z-phase rim is sharper.

Dissolution and nucleation of Z-phase appears to be closely related to MX. If this happens simply by nucleation of one precipitate type onto another or whether a physical transformation mechanism by Cr diffusion in the precipitates themselves is active in the nucleation is still under debate.

7 Conclusion

At the start of this project there was much debate as to the cause of many observed breakdowns or failures in high Cr creep resistant martensitic steels, and the development of Z-phase was a rather unknown phenomenon in 9-12%Cr steels. The results obtained during this work have helped shed some light on the behaviour of Z-phase, which is now considered as a highly detrimental precipitate in 9-12%Cr steels. Both modelling and experimental investigations performed in the present work point at Cr as the decisive constituent for the driving force for Z-phase precipitation. This fact may seem trivial, as the only difference between (V,Nb)N and Cr(V,Nb)N is Cr, but it is nevertheless an important new realisation. Z-phase has become a considerable obstacle for the development of 9-12%Cr steels, as a combination of high oxidation resistance and creep strength pose contradictory requirements to the Cr content.

Detailed conclusions on the experimental and modelling results can be found in appendices A-D.

8 Outlook

During this work, new observations, insights and awareness of the role of Z-phase have been revealed, but still many unresolved matters remain. Among these the nucleation process is considered the most crucial, as it probably is the governing factor of the rate of Z-phase precipitation. Although this work shows a clear connection with the MX precipitates, the details of the nucleation of Z-phase remain unresolved. The observed hybrid crystal structure of the Z-phase may also be closely related to the nucleation mechanism. It could thus be interesting to investigate exactly how the two crystal structures coexist and how the ordering process from the cubic to the tetragonal lattice occurs.

The thermodynamic model of Z-phase provides reasonable results, but it also has some room for improvement. A better description of the ternary systems and particularly a better MX model would greatly benefit future versions of the model. The Z-phase model does also have some potential as an alloy design tool, but unfortunately it gives little indication of how to retard Z-phase precipitation without impairing oxidation resistance.

Work on kinetic modelling of Z-phase precipitation applying MatCalc has been initiated, however much work is still needed on this. The ultimate goal would be a model capable of kinetic simulations of Z-phase at different temperatures and various steel compositions. To be able to reach this ambitious goal, the nucleation process of Z-phase needs to be determined.

There are still many unknown aspects of the Z-phase, one them being the Ta version of Z-phase. Little information is available on Ta in 9-12%Cr steels and the nitrides it may form. The existence of a Ta version of the Z-phase has been confirmed in ternary systems, but it has not been reported in 9-12%Cr steels.

9 References

[1] J. Hald, *VGB Powertech*, **12,** 2004, 74-79.

[2] J. Hald, *Steel Research*, 1996, **67**, pp. 369-374.

[3] J.P. Shingledecker, I.G. Wright, in Proc. Conf. "*Materials for Advanced power Engineering 2006*", Liege, Belgium, September 2006, J. Lecomte-Beckers et. al. (Eds.), Julich, 2006, Part 1, pp. 107-119.

[4] J. Hald, B. Nath, in Proc. "*Power-Gen´98*", Milan, Italy, June, 1998.

[5] T. Uehara, A. Toji, S. Komatsubara, T. Fujita: in Proc. Conf. "*Materials for Advanced power Engineering*", Liege, Belgium, September 2002, J. Lecomte-Beckers et. al. (Eds.), Julich, 2002, Part 3, pp. 1311-1320.

[6] T.U. Kern, M. Staubli, K.H. Mayer, B. Donth, G. Zeiler, A. DiGianfrancesco: in Proc. Conf. "*Materials for Advanced power Engineering 2006*", Liege, Belgium, September 2006, J. Lecomte-Beckers et. al. (Eds.), Julich, 2006, Part 2, pp. 843-854.

[7] A. Strang, V. Vodarek: *Materials Science and Technology,* 1996, **12**, pp. 552-556.

[8] F.B. Pickering, in "*microstructural Development and Stability in High Chromium Ferritic Power Plant Steels*", Cambridge June 1996, A. Strang et. al. (Eds.), London, UK, 1997, Number 1, pp. 1-30.

[9] F. Kauffmann, K.H. Mayer, S. Straub, G. Zies, C. Scheu, W. Willer, H. Ruoff, K. Maile, in Proc. Conf. "*Materials for Advanced power Engineering*", Liege, Belgium, September 2006, J. Lecomte-Beckers et. al. (Eds.), Julich, 2006, Part 3, pp. 1177-1180.

[10] J. Hald, L. Korcakova*, ISIJ International*, 2003, **43**, pp. 420-427.

[11] V. Vodarek, A. Strang: in Proc. Conf. "*Materials for Advanced power Engineering*", Liege, Belgium, September 2002, J. Lecomte-Beckers et. al. (Eds.), Julich, 2002, Part 2, 1223-1232.

[12] L. Korcakova, "*Microstructure Evolution in High Strength Steel for Power Plant Apllication: Microscopy and Modelling*" DTU, Kgs. Lyngby, Denmark, 2002.

[13] W. O. Binder: "symposium on sigma-phase", 146; 1950, ASTM.

[14] H. Hughes: *J. Iron Steel Inst.,* 1967, **205**, 775-778.

[15] P. Ettmayer: *Monatsh. Chem.,* 1971, **102**, 858-863.

[16] D. H. Jack, K. H. Jack: *J. Iron Steel Inst.,* 1972, **209**, 790-792.

[17] V. H. Gerlach, E. Schmidtmann: *Archiv fur das Eisenhuttenwesen,* 1968, **39**, 139-149.

[18] T. Sourmail: *Materials Science and Technology,* 2001, **17**, 1-14.

[19] V. N. Gridnev, V. G. Ivanchenko, V. K. Zulzhenko: *Izvestiya Akademii Nauk SSSR, Metally,* 1983, **3**, 209-212.

[20] F. Kurosawa, I. Taguchi, M. Tanino, R. Matsumoto: *J. of the Japan Institute of Metals,* 1981, **45**, 63-67.

[21] H-O. Andren, A. Henjered, L. Karlsson: in "Stainless steel 84", 91-96; 1985, London, The Institute of Metals.

[22] T. Ishitsuka, H. Mimura: in Proc. Conf. "Materials for Advanced power Engineering", Liege, Belgium, September 2002, J. Lecomte-Beckers et. al. (Eds.), Julich, 1998, Part 3, 1321-1333.

[23] E. Schnabel, P. Schwaab, H. Weber: *Stahl und Eisen,* 1987, **107**, 691-696.

[24] A. Strang, V. Vodarek: in "Microstructural Development and Stability in High Chromium Ferritic Power Plant Steels", Cambridge, UK, June 1996, A. Strang et. al. (Eds.) London, UK 1997, Number 1, 31-52.

[25] M. Svoboda, J. Bursik, I. Podstranska, A. Kroupa, V. Sklenicka, K. H. Mayer: in Proc. Conf. "Materials for Advanced power Engineering", Liege, Belgium, September 2002, J. Lecomte-Beckers et. al. (Eds.), Julich, 1998, Part 3, 1521-1530.

[26] D.B. Williams, C.B. Carter, "*Transmission Electron Microscopy I, basics*", Plenum Press, New York, 1996.

[27] P.J. Goodhew, F.J. Humphreys, "*Electron Microscopy and Analysis*", Taylor and Francis, London, 1988.

[28] M. Loretto, "*Electron Beam Analysis of Materials*", Chapman and Hall, New York, 1984.

[29] B. Sundman, B. Jansson, J.-O. Andersson, *Calphad*, **9**, 1985, pp.153-190.

[30] M. Hillert, L-I. Staffansson: *Acta Chem. Scand.*, **24**, 1970, pp. 3618-3626.

[31] B. Sundman, J. Ågren: *J. Phys. Chem. Solids*, **42**, 1981, pp. 297-301.

[32] E. Kozeschnik, "*Thermodynamische Berechnung der phasengleichgewichte und der Ausscheidungskinetik in metallischen Werkstoffen*", PhD thesis, Graz University of Technology, 1997.

[33] E. Kozeschnik, B. Buchmayr, "*Mathematical Modelling of Weld Phenomena 5*," Institute of Materials, London, Book 734 (2001) 349.

[34] L. Onsager, Phys. Rev. I, 37, 1931, p. 405.

[35] L. Onsager, Phys. Rev. II, 38, 1931, p. 2265.

[36] A. Borgenstam, A. Engstrom, L. Hoglund, J. Agren, *Journal of Phase Equilibria*, **21**, 3, 2000, pp. 269-280.

[37] E. Kozeschnik, J. Svoboda, F.D. Fischer: in Proc. Conf "*International Conference on Solid-Solid Phase Transformations in Inorganic Materials 2005*", Arizona, USA, James Howe, David Laughlin, Jong Lee, David Srolovitz, Ulrich Dahmen, Richard Sisson, William Soffa, C. E. Carpenter (Eds.), TMS, Warrendale PA, 2005 , vol. 2 pp. 301-310.

[38] E. Kozeschnik, J. Svoboda, F.D. Fischer: in Proc. Conf "*Modeling, Control and Optimization in Ferrous and Nonferrous Industry Symposium*" Chicago USA, F. Kongoli, B.G. Thomas, and K. Sawamiphakdi (eds), TMS, Warrendale PA, 2003, pp. 429-434.

[39] J. Svoboda, F.D. Fischer, P.Fratzl, E. Kozeschnik: *Materials Science and Engineering A*, **385**, 2004 pp. 166-174.

[40] E. Kozeschnik, J. Svoboda, P.Fratzl, F.D. Fischer: *Materials Science and Engineering A*, **385**, 2004 pp. 157-165.

[41] R. Becker, Die Keimbildung bei der Ausscheidung in metallischen Mischkristallen, *Ann. Phys.*, **32**, 1938, pp. 128-140.

[42] D. Turnbull, "*Impurities and Imperfections*", ASM, Cleveland OH, USA, 1955, pp. 121-143.

Appendix A

Behaviour of Z-phase in 9-12%Cr steels

Behaviour of Z phase in 9–12%Cr steels

H. K. Danielsen* and J. Hald

The literature on the behaviour of modified Z phase Cr(V,Nb)N in creep resistant martensitic 9–12%Cr steels is briefly reviewed. Ten different 9–12%Cr steels were investigated after prolonged exposure at 600–660°C; the modified Z phase was found in all of them. In steels with high Cr content (11–12%), Z phase precipitates much faster than in 9%Cr steels. Precipitation of Z phase is associated with dissolution of MX carbonitrides, and causes a breakdown in long term creep strength in 9–12%Cr steels. High Cr steels show creep instabilities accompanied with Z phase precipitation, whereas low Cr steels show good long term creep stability. A niobium free CrVN variant of the modified Z phase was observed for the first time during the course of this work. The solution temperature of the Cr(V,Nb)N and CrVN modified Z phases was found to be close to 800°C for 11–12%Cr steels, much lower than the 1200–1250°C solution temperature of the unmodified CrNbN Z phase. Above the solution temperature the modified Z phase is replaced by MX particles.

Introduction

Over recent decades the development of new creep resistant martensitic 9%Cr steels grades such as P91 and P92 for steam power plant applications has allowed increases in operating steam temperatures up to 600°C. New alloys are under development in order to increase the temperature further, up to 650°C, for better efficiency. This high temperature calls for improved steam oxidation resistance besides improved creep strength, and the majority of test alloys have thus been based on 11–12%Cr contents. Short term creep tests have indicated improvements, but after longer testing times all the new 11–12%Cr alloys have experienced dramatic breakdowns in microstructure stability, which could not be explained.

In 2001, two superheater tubes in a test installation of a Danish power plant ruptured prematurely. The tubes, made of the 12Cr–2W–VNbN steel T122 (HCM12A), failed owing to creep after <10% of the expected minimum lifetime of the material, according to standardised creep rupture strength values. Microstructure investigations showed extensive presence of large particles of the complex nitride Z phase, Cr(V,Nb)N, and the expected fine V or Nb rich MX carbonitrides were far in between.

The MX carbonitrides, Nb(C,N) or V(C,N), which precipitate as small and densely distributed particles are one of the major contributors to the creep strength of new 9–12%Cr martensitic steels. The Z phase, Cr(V,Nb)N, contains the same elements as the MX carbonitrides, and its precipitation is accompanied by dissolution of the beneficial MX particles. The Z phase precipitates as large particles, which do not contribute to precipitate strengthening, and thus the creep strength of the steel is considerably lowered.

The discovery of massive Z phase precipitation in a standardised 9–12%Cr steel actually used in power plants raised serious questions about the long term stability of other new steels of similar type.

Very little is known about the behaviour of Z phase in 9–12%Cr steels, since it has been observed to precipitate only after long times of exposure in plants or after long term creep testing. In the present paper, previous observations of Z phase in 9–12%Cr steels are reviewed. An investigation of the behaviour of 9–12%Cr steels has been carried out to elucidate the compositional and microstructural factors controlling Z phase precipitation in these alloys.

Previous observations of Z phase

Original Z phase, CrNbN

The Z phase was discovered as early as 1950 by Binder[1] in Nb alloyed creep resistant austenitic steels, where it has since been frequently observed and credited with beneficial strengthening effects. The Z phase precipitated very quickly as small finely distributed rodlike particles, and it was often the first precipitate to appear. Many attempts were made to determine the crystal structure of the Z phase,[2,3] but it was not until 1972 that Jack and Jack[4] identified it as tetragonal CrNbN (see Fig. 1). In addition to the main elements, minor concentrations of Fe, Mo and traces of other elements have also been identified. Sourmail[5] has given a thorough review on the CrNbN Z phase in austenitic steels.

In 1971, Ettmayer[3] investigated the stability of Z phase in the ternary systems: CrTaN, CrNbN and

Materials Technology, Department of Manufacturing Engineering and Management, Technical University of Denmark, DTU, Lyngby, Denmark

*Corresponding author, Hilmar@ipl.dtu.dk
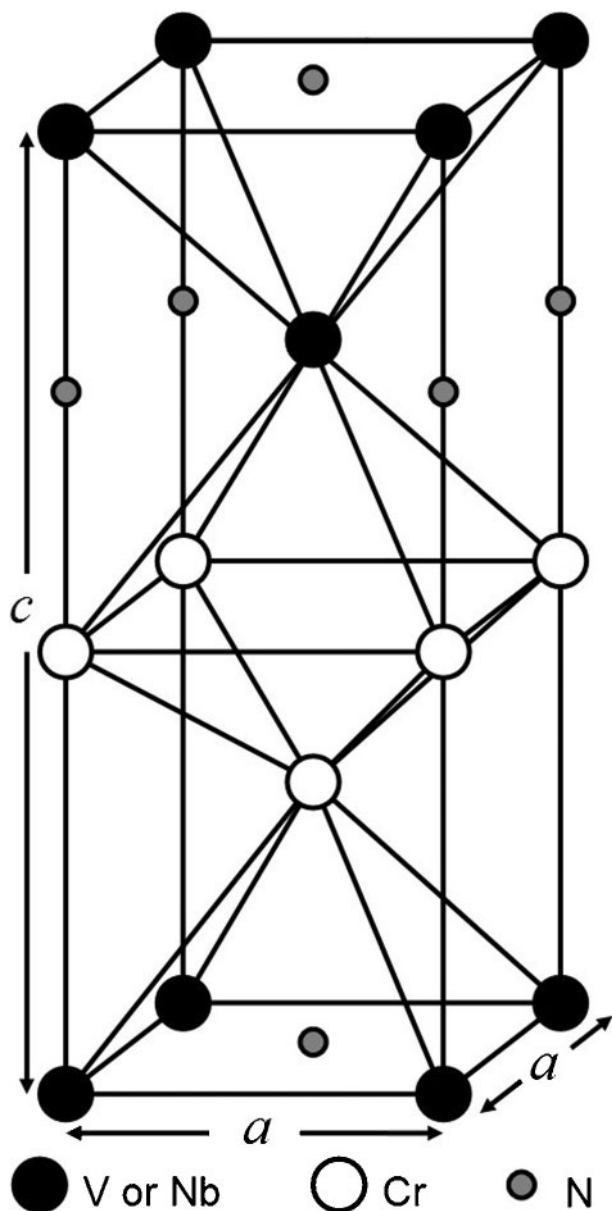
1 **Crystal structure of Z phase:**[4] **lattice parameters of original Z phase, CrNbN, are** *c*=0·739 nm **and** *a*=0·304 nm, **while modified version, Cr(V,Nb)N, has a slightly smaller unit cell, with** *c*=0·739 nm **and** *a*=0·286 nm

2 **Comparison of creep strength of three 10–12%Cr steels at 600°C: Z phase was observed in X19 CrMoVNbN 11 1 by Schnabel** *et al.*[10]

CrVN. He succeeded in making the tantalum and niobium Z phases, but found no vanadium Z phase. Investigations by Gridnev *et al.*[6] in 1983 of phase stability in CrVN systems at 800°C and above showed no presence of a vanadium Z phase.

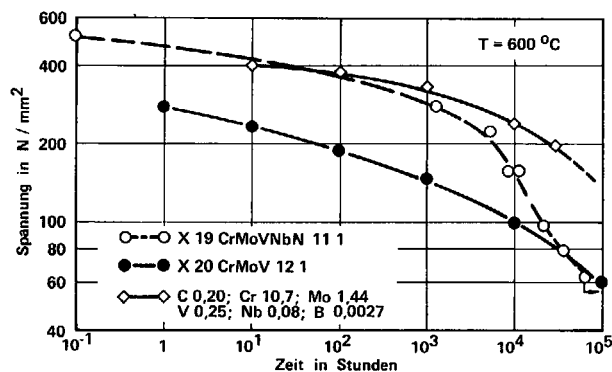In 1981, Kurosawa *et al.*[7] found CrNbN Z phase particles in a ferritic 19Cr–2Mo–NbN steel. Here precipitation occurred rapidly in the temperature range of 700–1000°C, forming very large faceted particles, quite unlike the small particles found in austenitic steels.

Modified Z phase, Cr(V,Nb)N

In 1985, Andren *et al.*[8] found particles with Z phase composition in an 18Cr–12Ni–VNbN austenitic steel after isothermal annealing at 750°C up to 1170 h. Half of the Nb in these particles had been replaced by V, the chemical composition being Cr(V,Nb)N. They were not positively identified as Z phase, because they had an fcc crystal structure. Instead they were assumed to be a metastable precursor to the Z phase. Ishitsuka[9] has recently investigated the possibility of using the Cr(V,Nb)N Z phase as a strengthening agent in vanadium containing austenitic creep resistant steels.

In 1986, Schnabel *et al.*[10] identified a vanadium containing Z phase in a martensitic 11Cr–1Mo–VNbN steel (X19 CrMoVNbN 11 1) which showed a very dramatic drop in creep strength (*see* Fig. 2). However, the authors made no connection between the appearance of the Z phase and this drop in strength.

In 1996, harmful effects of the Z phase on creep strength in martensitic steels were identified by Strang and Vodarek[11,12] who investigated creep samples from a number of 11–12%CrMoVNbN steels that had experienced similar breakdowns in long term creep strength to the X19CrMoVNbN 11 1 grade. They found that precipitation of Z phase as large particles occurred concurrently with the breakdown in strength and proposed that the Z phase was dissolving the beneficial MX particles, which contain the same elements as Z phase. With the dissolution of fine MX particles, the creep strength of the steel would fall off. Investigations of the crystal structure of the precipitated particles led to the introduction of the term modified Z phase. The modified Z phase differs from the original Z phase in containing vanadium, the unit cell formula being $Cr_2(V,Nb)_2N_2$. The crystal structure remains the same, but modified Z phase has a slightly smaller parameter of the unit cell *a*, 0·286 nm compared with 0·304 nm for the original Z phase. The modified Z phase behaved very differently from the original Z phase. It precipitated only after long exposure times, and then only as very few, coarse particles. Based on comparisons of 12CrMoVNbN steels with varying Ni content (0·52–1·15 wt-%), it was concluded that high Ni contents accelerated the Z phase precipitation.[12]

The investigations by Strang and Vodarek were performed on older steels with approximately five times higher niobium content than the modern 9–12%Cr steels, therefore there was little concern that Z phase might affect the stability of newly developed steels. However, a number of experimental 10–12%Cr steels under development for application up to 650°C steam temperature have shown promising creep behaviour in short term tests, but after prolonged exposure times the strength dropped dramatically (*see* Fig. 3).

In 2001, Svoboda *et al.*[14] investigated the 11Cr–3W–3Co–VNbN experimental steel TAF650, which suffered
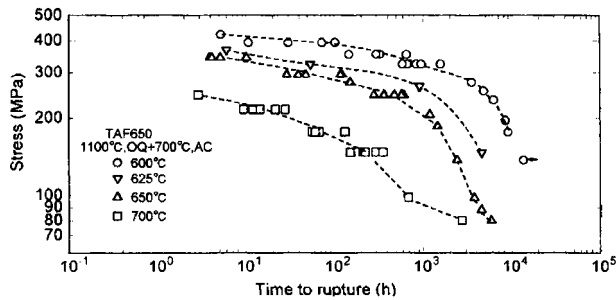
3 High hopes were pinned on steels like TAF650 (11Cr–3W–3Co–VNbN) based on short term creep tests, but as tests reached some 10 000 h their strength dropped dramatically[13]

a severe drop in creep strength after 10 000 h at 650°C. They observed Laves phase (Fe_2W), Z phase and only few of the smaller MX particles, concluding that the Z phase was responsible for the dissolution of the MX particles, and that the combined effect of Laves phase and Z phase precipitation was responsible for the breakdown of the steel.

Observed microstructure instabilities in new 9–12%Cr steels had long been explained by Laves phase (Fe_2W) precipitation, causing a loss of solid solution strengthening, because a number of these steels contain up to 2·5 wt-% tungsten. However, quantitative estimates of particle strengthening from Laves phase and solid solution strengthening from W in such steels have demonstrated that the solid solution strengthening effect is insignificant, and that the particle strengthening effect can be considerable.[15,16]

There have been several other observations of Z phase in 9–12%Cr steels,[17–22] but little is known of what affects its precipitation or how to avoid it. The Z phase is often observed along with decreasing numbers of MX particles, but it is not always accompanied by a dramatic decrease in creep strength. The composition of the observed Z phases, especially the V and Nb content, seems to vary from source to source, but the empirical formula is always Cr(V,Nb)N.

Experimental

The potentially serious implications of the premature failures of two T122 superheater tubes in the Danish power plant referred to above led to further investigations of similar materials. Ten 9–12%Cr steels were acquired and investigated to obtain a more thorough overview of Z phase behaviour in such steels. The steels had experienced long term exposure either in power plants or in creep testing or they were subjected to long term heat treatments in the laboratory (*see* Table 1). After exposure or heat treatment microstructure investigations were made to detect Z phase precipitates.

Most of the investigations were based on TEM observations of carbon extraction replicas. The replicas were prepared by chemically etching with Vilellas etchant (1% picric acid and 5% hydrochloric acid in ethanol) for ~15 s. A carbon film was sputtered onto the samples, and stripped with a mixture of 10% bromium in methanol. The extraction replicas were caught on small copper grids and cleaned with ethanol.

TEM observations were made in a Philips EM 430 with an EDAX PV9760/20 energy dispersive spectroscopy (EDS) and a JEOL 3000F field emission gun transmission electron microscope (FEGTEM) with an Oxford Instruments Inca Link ISIS EDS and a Gatan imaging filter electron energy loss spectroscopy (EELS).

Precipitate compositions were analysed with EDS, which formed the basis of the phase identification of the particles. Because it is not possible to measure the N content with EDS, the Z phase was identified by its metallic composition, ~50 at.-%Cr+Fe and 50 at.-%V+Nb (*see* Fig 4*a*). This was found to be an easy and reliable method to distinguish Z phase from other particles, because no other V or Nb containing particles in the 9–12%Cr steels have such a composition.

Some EELS measurements were made in order to verify N content of the particles. The nitrogen content was measured using the K peak at 401 eV, vanadium using the $L_{2,3}$ peaks starting at 513 eV and chromium using the $L_{2,3}$ peaks starting at 575 eV. The background was fitted using a power law. There were problems

Table 1 Compositions (wt-%) of steels investigated during course of this work and treatment and exposure conditions

	P91	E911	P92	AXM	P122	T122	NF12	FN5	TB12M	X20
Composition										
C	0·10	0·11	0·11	0·11	0·11	0·09	0·085	0·11	0·113	0·19
N	0·053	0·065	0·049	0·05	0·053	0·0609	0·045	0·027	0·055	0·025
Si	0·36	0·18	0·17	0·08	0·02	0·25	0·25	0·06	0·01	0·23
Mn	0·37	0·46	0·43	0·42	0·56	0·60	0·44	0·55	0·51	0·49
Cr	8·30	8·61	9·27	10·48	11·0	12·20	11·60	11·20	11·33	11·5
Mo	0·95	0·92	0·48	1·04	0·42	0·35	0·14	0·26	0·5	0·91
W	–	0·995	1·701	0·99	1·94	1·97	2·68	2·63	1·98	–
Ni	0·15	0·21	0·25	0·77	0·32	0·18	0·17	0·40	0·96	0·66
Nb	0·07	0·089	0·067	0·043	0·05	0·06	0·08	0·065	0·082	–
V	0·21	0·19	0·197	0·18	0·19	0·25	0·20	0·22	0·18	0·31
Cu	–	–	–	0·04	0·87	0·43	0·01	–	0·06	0·054
Al	0·15	0·013	0·005	0·008	0·012	0·004	–	–	0·004	0·016
B	–	–	0·0026	0·0002	0·0011	0·0021	0·0026	0·00100	–	–
Co	–	–	–	–	–	–	2·48	2·66	–	0·021
Condition										
Heat treatment	1050°C/ 1 h 780°C/ 1 h	1060°C/ 1 h 770°C/ 2 h	1060°C/ 1 h 770°C/ 2 h	1070°C/ 17 h 570°C/ 22 h 700°C/ 24 h	1050°C/ 1 h 770°C/ 3 h	1050°C/ 0·2 h 790°C/ 3 h	1100°C/ 0·2 h 760°C/ 1 h	1100°C/ 4 h 570°C/ 8 h 715°C/ 24 h	1080°C/ 2·5 h 775°C/ 2 h	1050°C/ 1 h 750°C/ 2 h
Exposure	8000 h/ 650°C	10 000 h/ 650°C	31 000 h/ 650°C	43 000 h/ 600°C	10 000 h/ 650°C	12 000 h/ 660°C	17 000 h/ 650°C	8000 h/ 650°C	10 000 h/ 650°C	150 000 h/ 600°C
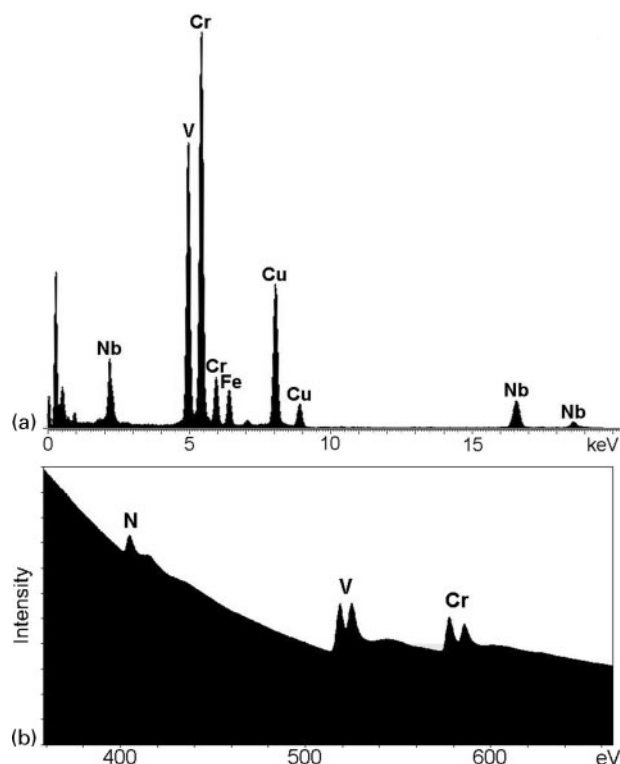
4 *a* **spectrum (EDS) from Z phase, copper signal is from grit and** *b* **spectrum (EELS) from Z phase: both spectrums are taken on carbon extraction replica of T122**

measuring the Cr content as the proximity of the V peaks made it difficult to fit the background. The Nb and Fe contents were not measured, as the peaks were deemed too small for quantitative measurements. Small amount of C in Z phase have previously been reported,[8,23,24] but as present measurements were made on carbon extraction replica, this could not be confirmed.

X-ray powder diffraction investigations of extracted precipitates were made of a number of samples. Precipitates were extracted from the steel by electrolysis using a 95% ethanol and 5%HCl mixture as electrolyte. This dissolved the steel, while leaving all the particles intact. The particles where then fixed on a silicon single crystal and investigated using a Philips PW1820/3711 X-ray diffractometer.

Results

Observations of Z phase
Z phase was found in all the investigated steels, but only after exposure for several thousand hours at 600–660°C.

This indicates that the modified Z phase is a stable phase in all the 9–12%Cr martensitic steels that contain its constituents. There was great variation in the quantity of Z phases found in different steel types, as well as in the time necessary for precipitation to occur (*see* Table 2).

Z phase was clearly identified in the two failed T122 tubes after exposure for 12 000 h at 660°C and 30 000 h at 610°C, and the MX were almost completely dissolved. Investigations of a thick section pipe of the similar steel grade P122 after heat treatment for 10 000 h at 650°C showed much fewer Z phases, and MX still present in numbers. The only major difference between the T122 and P122 steels is the chromium content, and it was speculated that this element could be of major significance to Z phase precipitation.

Other high Cr steels, which had suffered similar breakdowns to T122, were investigated, i.e. the test alloys NF12, FN5 and TB12M. As expected, Z phases were found in high numbers. For steels exposed for >10 000 h, only a few MX particles were observed.

Investigations of three commercial 9%Cr steels were carried out, i.e. P91, E911 and P92, although no drastic breakdowns in strength had been observed. Z phase was found in all these steels, but there were very few, even in the P92 samples exposed for 31 000 h at 650°C. All the samples still contained a considerable amount of MX particles.
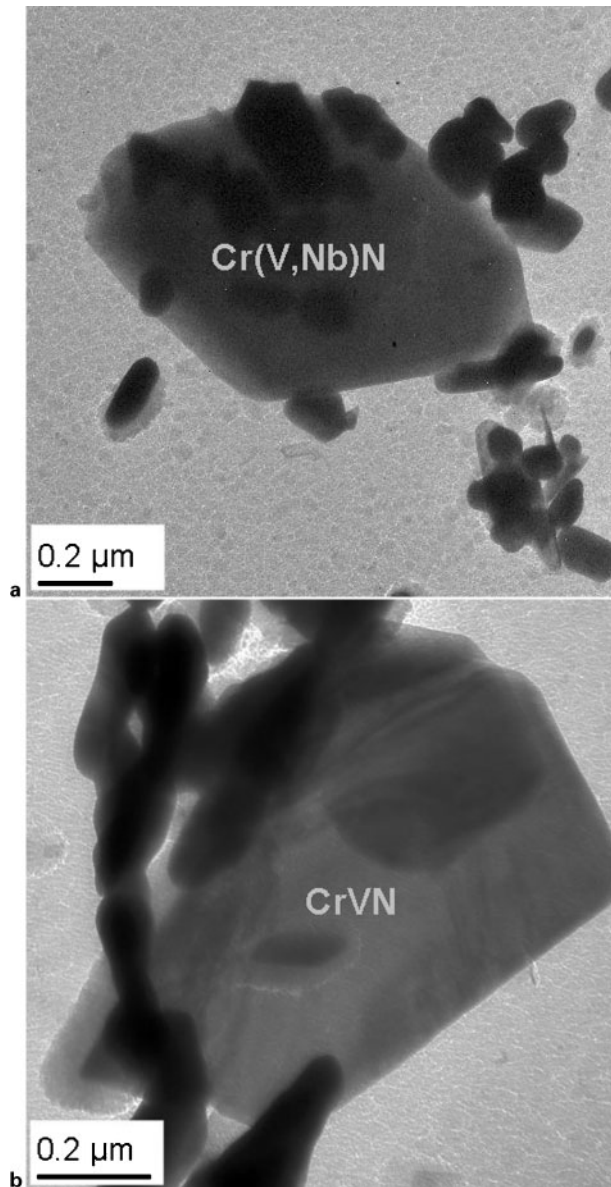
Composition of Z phase
As mentioned above, the identification of the modified Z phase was based on a composition with approximately 50 at.-%Cr + Fe and 50 at.-%V + Nb (*see* Table 3). The Cr/Fe ratio was always very uniform, with around 45 at.-%Cr and 5 at.-%Fe. The V and Nb contents were mostly about 40 at.-%V and 10 at.-%Nb, but there were relatively large variations, both when looking at different particles in the same extraction replica samples, and even within the particles themselves. Generally, it appears that the niobium content in the Z phase is higher in samples which contain few Z phase precipitates, usually 9%Cr steels. Some EELS measurements were made, showing the presence of nitrogen (*see* Fig. 4*b*). Many literature sources indicate small Mo concentrations in the modified Z phase, but this could not be confirmed during the course of the present work.

CrVN
Modified Z phases with very low niobium contents have been observed in martensitic steels, but a niobium free CrVN Z phase variant had never been found. Ettmayer[3]

Table 2   Overview of estimated degree of Z phase precipitation in investigated steels

| Steel type | Cr content, wt-% | Exposure | | Observed Z phase |
		Time, h	Temperature, °C	
P91	8·30	8000	650	Very low
X20	11·5	150 000	600	Low
E911	8·61	10 000	650	Low
P92	8·96	31 000	650	Low
P122	11·0	10 000	650	Medium
AXM	10·48	43 000	600	Medium
FN5	11·20	8000	650	Medium
TB12M	11·33	10 000	650	High
T122	12·20	12 000	660	High
NF12	11·60	17 000	650	High

5   *a* modified Z phase found in NF12 sample exposed at 650°C for 17 000 h and *b* CrVN Z phase found in X20 sample exposed at 600°C for 150 000 h

Table 4 EELS and EDS measurements of Z phase in X20 and T122: calculated compositions are based on EDS and N/V ratio of EELS results, at.-%

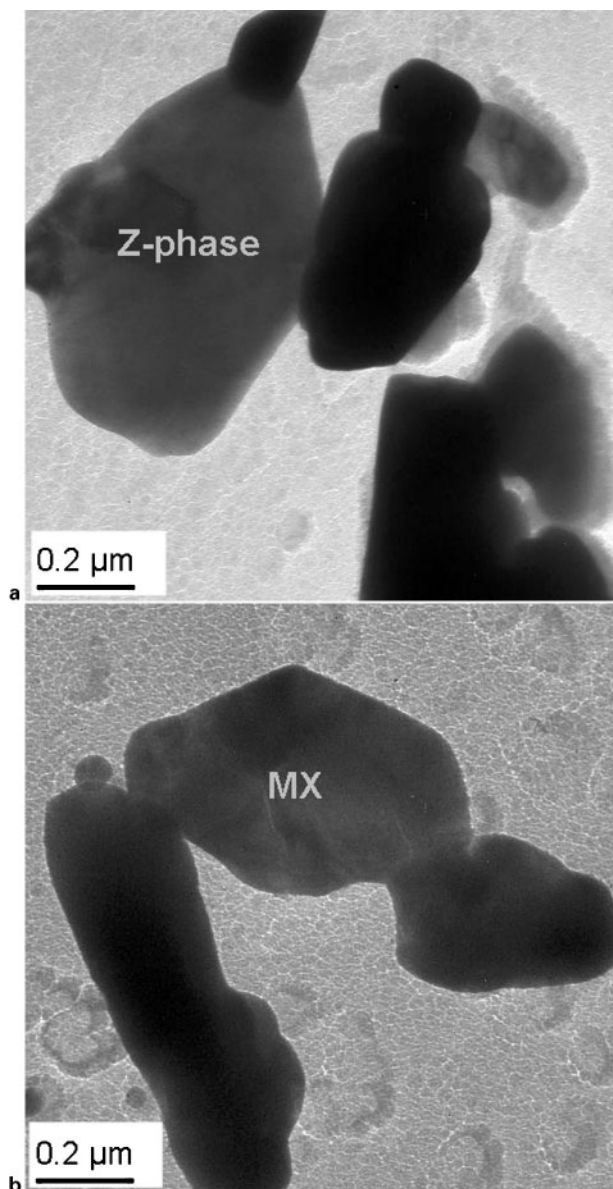|	Cr	Fe	V	Nb	N
EELS X20	29	–	41	–	30
EDS X20	40	6	54	–	–
EDS+N X20	29	4	39	–	28
EELS T122	33	–	37	–	30
EDS T122	47	5	42	6	–
EDS+N T122	35	4	31	5	25

of the Z phase was predicted[25], and consequently a search for it was initiated. Several samples of the 12CrMoV steel X20, which does not contain Nb, were investigated. In one of these samples, exposed at 600°C for 150 000 h, Z phase was found (*see* Fig 5). Even though this sample had a very long exposure time, very few Z phase particles were found, and MX particles were still present. The Z phase identification was based on the metallic composition (*see* Table 3), but EELS measurements confirmed presence of N in amounts indicating Z phase composition (*see* Table 4). The Cr EELS measurements were not reliable as it was difficult to fit a background, so the Z phase composition was calculated using EDS measurements and the N/V ratio obtained in EELS measurements. The calculated N content was somewhat lower than the expected 33 at.-%, for both Cr(V,Nb)N and CrVN.

Because no previous reports of a Nb free modified Z phase were found in the literature, electron diffraction investigations were carried out to verify the crystal structure. These showed a crystal structure similar to that of modified Z phase.[26] Except for what appears to be a very slow precipitation speed, the CrVN phase seems to be identical to the modified Z phase.

Heat treatment experiments

The original Z phase, CrNbN, is known to be stable at temperatures up to 1200–1250°C in austenitic steels. The solution temperature appears to be somewhat dependent on the composition of the steel.[23] CrNbN has also been observed in ferritic steel up to 1000°C,[7] but no information has been found on the solution temperature of the modified Z phase Cr(V,Nb)N.

To investigate the precipitation speed and stability range of the Z phase in 9–12%Cr steels, heat treatments at 700 and 725°C were carried out. It was expected that this would accelerate the precipitation, eliminating the need for long term experiments. Six different steels, in the normalised and tempered condition, including T122 and NF12, were exposed at 700 or 725°C for up to

was successful in making the CrNbN and CrTaN Z phases, but he failed to create a CrVN Z phase. Further investigations of the ternary CrVN system by Gridnev *et al.*[6] showed no Z phase at temperatures of 800°C and above.

During work on development of a thermodynamic model of the Z phase the existence of the CrVN variant

Table 3 Average metallic composition of Z phases found in different steels: Nb/V ratio varied significantly from particle to particle, at.-%

Steel type	Observed Z phase	Cr	Fe	V	Nb
P91	Very low	Not enough particles observed for statistics			
X20	Low	40	6	54	–
E911	Low	46	4	27	23
P92	Low	48	5	33	14
P122	Medium	45	5	33	17
AXM	Medium	43	5	44	8
FN5	Medium	47	6	38	9
TB12M	High	47	5	37	11
T122	High	46	5	42	7
NF12	High	47	5	37	10

6   *a* Z phase particle after heat treatment at 800°C of T122 and *b* large MX particle precipitated after heat treatment at 850°C of T122

7   **Powder diffraction of precipitates from T122 after exposure at 660°C for 12 000 h and further heat treatment at 700–850°C for 100 h: Z phase peak disappears at ∼800°C**

1000 h. However, no Z phase was found in any of these steels, shelving the plans to precipitate Z phases in short term experiments. Instead it was decided to use steels which had already developed Z phase during long term exposure in power plants or test facilities. A short heat treatment at higher temperatures could provide a quick way of determining the solution temperature of the Z phase.

The used materials included T122 exposed at 660°C for 12 000 h and NF12 exposed at 650°C for 17 000 h. Later investigations of the CrVN Z phase were carried out on an X20 sample exposed for 150 000 h at 600°C. The exposed samples were heated to a temperature in the range of 700–850°C and held for 100–150 h, after which the precipitates were investigated. These experiments indicated the solution temperature of the modified Z phase to be between 800 and 850°C in these steels, based on particle composition. Further experiments with T122 narrowed this range to 800–830°C. This is a very large difference in stability compared with the solution

temperature for the original CrNbN Z phase (1200–1250°C).

In the samples where the Z phase had been dissolved, it had been replaced by (or transformed into) large particles consisting mainly of V and Nb (*see* Fig. 6). The composition of the metallic elements was 66 at.-%V, 20 at.-%Nb, 13 at.-%Cr, which suggests these are MX particles. Electron diffraction revealed an fcc structure with lattice parameter of 0·42 nm, which also indicates MX particles. This has been supported by X-ray diffraction of T122 exposed at 660°C for 12 000 h, and then heated to 700–850°C for 100 h (*see* Fig. 7). Only one Z phase peak is visible as most other peaks are overshadowed by carbide[12] or Laves phase peaks. The Z phase peak disappears at ∼800°C, and the MX peaks (fcc 0·416 nm) appear at approximately the same temperature.

In the temperature interval between 800 and 830°C (T122) the newly formed MX particles seemed to coexist with the Z phase, but this could be because of insufficient time to dissolve the Z phase. In the opinion of the authors the modified Z phase has a thermodynamic solution temperature of ∼800°C in martensitic steels.

Nucleation

The present investigation has been carried out on carbon extraction replicas, which makes it easy to identify the Z phases. With this technique it is however not possible to determine the location of the Z phase particles in the microstructure, and consequently, no systematic information on the nucleation sites of Z phase could be gathered. However, some general observations on the nucleation process are presented below.

Quite small Z phase precipitates, below 50 nm in size, were found in samples where most of the MX particles have been replaced by Z phase. Here they seem to coexist with the larger Z phase particles (*see* Fig. 8). The small Z phase particles generally seem to have a higher Nb content than their larger counterparts.

Most large Z phase precipitates were found in the vicinity of carbide rich areas, which may indicate locations near a prior austenite grain boundary. The small precipitates were generally not observed close to other particles, but it would be more difficult to spot a small precipitate in a carbide rich area.
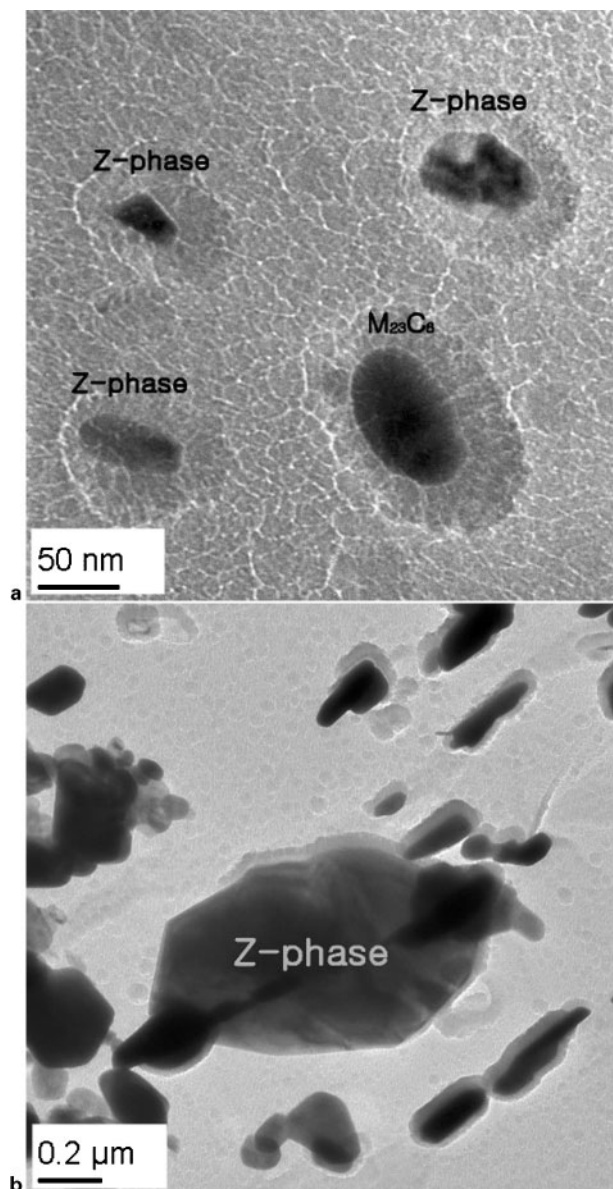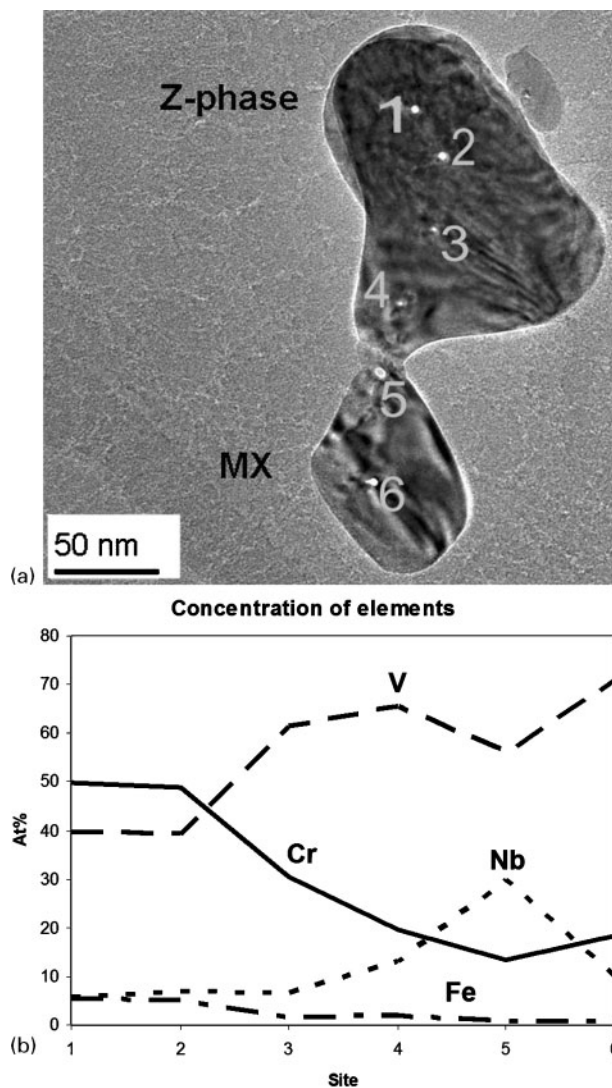
8 Example of *a* small and *b* large Z phases coexisting in same steel (AXM): both pictures taken on same extraction replica

9 *a* Z phase particle in contact with MX particle and *b* concentration profile: notice high Nb content at bottle-neck (site 5); measurements made on T122 after exposure at 660°C for 12 000 h

It is not known whether the Z phase nucleates on its own or on MX particles, or perhaps smaller MX particles transform into Z phase. There are, however, some indications of a connection between MX and Z phase. Figure 9 shows a case where Z phase and MX actually are in direct physical contact.

Discussion

The literature review and investigations of several new 9–12%Cr steels alloyed with V, Nb and N after prolonged exposure to temperatures in the range of 600–660°C have revealed a clear connection between high chromium content and accelerated precipitation of the modified Z phase Cr(V,Nb)N in these steels. Z phase was observed in all the investigated steels, indicating that this is an equilibrium phase. The high Cr (11–12%) steels (T122, NF12, TAF650 and TB12M) showed progressed precipitation after 10 000–17 000 h at 650°C, and the low Cr (9% and below) steels (P91, P92

and E911) were clearly less affected by Z phase precipitation, even after exposure for up to 31 000 h at 650°C.

The high Cr steels all showed premature breakdown in creep strength in the same time and temperature range as the Z phase precipitation, whereas the low Cr steels have demonstrated good long term creep stability up to >50 000 h at 650°C.[27] This clearly demonstrates that accelerated Z phase precipitation has a crucial influence on the premature breakdown in creep strength observed in the high Cr steels.

Because Z phase was found in all the investigated steels, the presence of Z phase in itself does not have a direct influence on the creep strength. Z phase precipitation is always accompanied by dissolution of the beneficial MX carbonitrides, and Z phase has to precipitate in large enough quantities to dissolve an appreciable amount of MX particles in order to affect the creep strength.

The presence of niobium does appear to accelerate Z phase precipitation. In the 12CrMoV steel X20 with high Cr but no Nb, Z phase was found after exposure for 150 000 h at 600°C. Even after such extended

exposure, very few Z phase particles were observed. The empirical chemical composition of these Z phases was CrVN, but their behaviour appeared similar to the Cr(V,Nb)N Z phase, except for a slow precipitation rate. To the best of the authors' knowledge, this is the first observation of Nb free modified Z phase.

The other major Z phase elements, V and N, may also have an effect on the rate of precipitation of Z phase, but this could not be verified in the present work. Vodarek and Strang[28] have suggested that Ni accelerate precipitation of Z phase, but no clear trends supporting this proposition were observed in the present investigation.

As the Z phase nucleates, it will grow at the expense of the MX particles. An understanding of the nucleation process could be crucial for delaying this process in high Cr steels, reducing the amount of precipitated Z phase to the levels in the 9%Cr steels or X20. The presence of Nb could be connected with nucleation of the Z phase, because smaller Z phase particles seem to have a higher Nb content than the larger particles. Some sources[18,28,29] report modified Z phase as being present close to the grain boundaries and the Nb rich MX particles, which further indicates the importance of niobium.

Vodarek and Strang[28] often observed the Z phase in association with NbX particles, which presumably reflects the low diffusion capability of niobium. Because most of the NbX particles are located along prior austenite grain boundaries, the Z phase would also precipitate here. Dissolution of C rich NbX particles leads to precipitation of $M_{23}C_6$ chromium carbides, which are often observed close to Z phase.

Dissolution of the MX particles in the prior austenite grain boundaries would also correspond to the observations by Kimura *et al.*[18] of dislocation recovery in these areas in steel P91. The Z phase was observed near prior austenite grain boundaries, where the NbX particles generally can be found. Their observations of the MX particles show a slow disappearance of Nb rich particles with time. It would seem that the Z phase consumes all the Nb content early in its precipitation in P91. It should be noted that vanadium rich secondary MX particles were still present in the P91 steel.

Erneman[29] studied N enriched V free austenitic steels by SEM, observing large, Nb rich particles with a core/rim structure. The core had the composition of a Nb rich nitride, whereas the rim was a nitride with almost equal concentrations of Cr and Nb. This does at least suggests that either the CrNbN Z phase precipitates on the surface of NbX, or NbX transforms into Z phase. The lattice parameter of CrNbN is slightly different from the Cr(V,Nb)N modified Z phase, but this would indicate a possibility of nucleation on/around NbX or perhaps VN particles.

Andren and co-workers[8,24] have observed particles with Z phase composition in V containing austenitic steels at 750°C. These particles had an fcc structure similar to that of MX with a lattice parameter of 0·419 nm, slightly higher than that of VN. It was suggested this was a precursor to the Z phase.

As seen above, the nucleation process for the modified Z phase remains unclear. There are some indications of a correlation between the nucleation of Z phase and the MX particles, whether Z phase nucleating on MX particles, or a direct transformation. In the present work, some examples of such a correlation have been found (*see* Fig. 9a), but in most cases no MX particles have been observed in the vicinity of the Z phase precipitates. Because there is no conclusive evidence for such a correlation, further work, preferably using thin foils, is necessary to gain more knowledge on the nucleation process.

Conclusion

A thorough investigation into the presence of modified Z phase, Cr(V,Nb)N, in creep resistant martensitic 9–12%Cr steels has been carried out, including a literature survey and experiments.

Ten commercial and experimental steels of varying composition have been investigated, and modified Z phase has been found in all these steel types to some degree. This indicates the Z phase is stable in all 9–12%Cr martensitic steels containing its constituents.

The chromium content in 9–12%Cr martensitic steels has a strong influence on the precipitation of modified Z phase. The higher chromium (11–12%) steels have a much higher rate of Z phase precipitation than steels with ∼9%Cr.

Z phase precipitation causes dissolution of MX carbonitrides, which are beneficial to creep stability, hence progressive Z phase precipitation causes a breakdown in creep strength. The high Cr steels show creep instabilities concurrent with Z phase precipitation, whereas the steels with ∼9%Cr and limited Z phase precipitation show good long term creep stability.

The very slow Z phase precipitation in Nb free 12%CrMoV steel suggests that niobium also has an accelerating effect on Z phase precipitation.

A niobium free CrVN variant of the modified Z phase has been found for the first time. Its precipitation is slower than regular Cr(V,Nb)N, but it appears similar to Cr(V,Nb)N in every other respect.

The solution temperature of the modified Z phases Cr(V,Nb)N and CrVN has been determined to be close to 800°C in 11–12%Cr martensitic steels, which is much lower than the 1200–1250°C solution temperature for CrNbN. Above the solution temperature the modified Z phase is replaced by MX particles.

Acknowledgements

References

1. W. O. Binder: 'Symposium on sigma-phase', 146; 1950, Cleveland, OH, ASTM.
2. H. Hughes: *J. Iron Steel Inst.*, 1967, **205**, 775–778.
3. P. Ettmayer: *Monatsh. Chem.*, 1971, **102**, 858–863.
4. D. H. Jack and K. H. Jack: *J. Iron Steel Inst.*, 1972, **209**, 790–792.
5. T. Sourmail: *Mater. Sci. Technol.*, 2001, **17**, 1–14.

6. V. N. Gridnev, V. G. Ivanchenko and V. K. Zulzhenko: *Izvestiya Akademii Nauk SSSR, Metally,* 1983, **3**, 209–212.

7. F. Kurosawa, I. Taguchi, M. Tanino and R. Matsumoto: *J. Jpn Inst. Met.*, 1981, **45**, 63–67.

8. H. O. Andren, A. Henjered and L. Karlsson: in 'Stainless steel 84', 91–96; 1985, London, The Institute of Metals.

9. T. Ishitsuka and H. Mimura: Proc. Conf. on 'Materials for advanced power engineering', (ed. J. Lecomte-Beckers *et al.*), Part 3, 1321–1333; 2002, Liege, Belgium, Julich.

10. E. Schnabel, P. Schwaab and H. Weber: *Stahl und Eisen,* 1987, **107**, 691–696.

11. A. Strang and V. Vodarek: *Mater. Sci. Technol.*, 1996, **12**, 552–556.

12. A. Strang and V. Vodarek: in 'Microstructural development and stability in high chromium ferritic power plant steels', (ed. A. Strang *et al.*), No. 1, 31–52; 1997, London, The Institute of Materials.

13. T. Uehara, A. Toji, S. Komatsubara and T. Fujita: Proc. Conf. on 'Materials for advanced power engineering', (ed. J. Lecomte-Beckers *et al.*), Part 3, 1311–1320; 2002, Liege, Belgium, Julich.

14. M. Svoboda, J. Bursik, I. Podstranska, A. Kroupa, V. Sklenicka and K. H. Mayer: Proc. Conf. on 'Materials for advanced power engineering', (ed. J. Lecomte-Beckers *et al.*), Part 3, 1521–1530; 2002, Liege, Belgium, Julich.

15. L. Korcakova: 'Microstructure evolution in high strength steel for power plant application: microscopy and modelling' PhD thesis, DTU, Copenhagen, Denmark, 2002.

16. J. Hald: *VGB PowerTech.*, 2004, **12**, 74–79.

17. J. Bursik and N. Merk: in 'Mechanical behaviour of materials at high temperature', (ed. C. M. Branco *et al.*), 299–307; 1996, Netherlands, Kluwer Academic Publisher.

18. K. Kimura, K. Zuzuki, H. Kushima and F. Abe: in 'Creep restistant metallic materials', (ed. Z. Kubon *et al.*), 186–195; 2001, Ostrava, Czech Republic.

19. R. Ishii, Y. Tsuda, M. Yamada and K. Kimura: *J. Iron Steel Inst.*, 2002, **88**, 36–43.

20. G. Zies, K. Maile, K. H. Mayer and S. Straub: Proc. 28th MPA Seminar on 'Phase characterization of advanced 9–12% Cr-steels with different creep behaviour', Stuttgart, October 2002, Staatliche Materialprüfungsanstalt Universität, 52.1–22.

21. K. Suzuki, S. Kumai, H. Kushima, K. Kimura and F. Abe: *J. Iron Steel Inst.*, 2003, **89**, 69–76.

22. I. Letofsky-Papst, P. Warbichler, F. Hofer, E. Letofsky and H. Cerjak: *Z. Metallkd.*, 2004, **95**, 19–21.

23. V. H. Gerlach and E. Schmidtmann: *Archiv fur das Eisenhuttenwesen*, 1968, **39**, 139–149.

24. L. Karlsson, A. Henjered, H. O. Andren and H. Norden: *Mater. Sci. Technol.*, 1985, **1**, 337–343.

25. H. Danielsen and J. Hald: Proc. Conf. on 'Advances in materials technology for fossil power plants', (ed. R. Viswanathan *et al.*), 999–1012; 2005, Hilton Head, USA, ASM international.

26. H. K. Danielsen, J. Hald, F. B. Grumsen and M. A. J. Somers: submitted to *Metall. Mater. Trans.*

27. J. Hald: Proc. 1st Int. Conf. on 'Super-high strength steels'; 2005, Rome, Italy, AIM and CSM.

28. V. Vodarek and A. Strang: Proc. Conf. on 'Materials for advanced power engineering', (ed. J. Lecomte-Beckers *et al.*), Part 2, 1223–1232; 2002, Liege, Belgium, Julich.

29. J. Erneman: 'Evolution of microstructure in two austenitic alloys at high temperature', PhD thesis, Chalmers University of Technology, Gothenburg, Sweden, 2003.

Appendix B

On the Crystal Structure of Z-phase, Cr(V,Nb)N

On the Crystal Structure of Z-Phase Cr(V,Nb)N

HILMAR K. DANIELSEN, JOHN HALD, FLEMMING B. GRUMSEN, and
MARCEL A.J. SOMERS

The Z-phase Cr(V,Nb)N particles in various 9 to 12 pct Cr creep-resistant steels were investigated
with electron diffraction, energy dispersive spectroscopy (EDS), and electron energy loss spectro-
scopy (EELS). In addition to the well-known tetragonal crystal structure for Z phase, a cubic crystal
structure was identified for Cr(V,Nb)N and CrVN particles, but not for CrNbN. The tetragonal and
cubic crystal structures were observed to coexist within the same particles, and the orientation
relationship between the two lattices was determined. Understanding and controlling the nucleation
of Cr(V,Nb)N particles could be of crucial importance to enable improvement of the long-term creep
stability of 9 to 12 pct Cr martensitic steels.

I. INTRODUCTION

MARTENSITIC creep-resistant steels, containing more
than 8 wt pct Cr and small contents of nitrogen and
niobium or vanadium, are known to develop a complex
nitride known as Z phase, Cr(V,Nb)N, upon long-term
exposure to elevated temperatures: 600 °C to 650 °C. In
such steels with more than 11 wt pct Cr, the precipitation of
Z phase is associated with a dramatic reduction of the creep
rupture strength and has led to failure of high-temperature
components.[1]

The first observations of Z phase date back to the 1950s:
Binder[2] observed Z phase to develop in austenitic steel.
Since then, Z-phase particles have been observed frequently
in Nb containing austenitic steels, and they have been
attributed beneficial strengthening effects, since they pre-
cipitate relatively fast and form a fine distribution of small
particles. In 1972, Jack and Jack[3] proposed the crystal
structure of the Z phase for the stoichiometry CrNbN as a
distorted body-centered tetragonal structure (of metal
atoms) with double layers of alternating atoms, and with
lattice parameters $a = 0.304$ nm and $c = 0.739$ nm (Figure
1). Small concentrations of Fe and Mo can be dissolved in
Z phase. It has been suggested that the Fe atoms reside at
the lattice positions of the Cr atoms and that Mo substitutes
Nb. In austenitic steels, the empirical formula is approxi-
mately $(Cr_{0.8}Fe_{0.2})(Nb_{0.9}Mo_{0.1})N$, although the composi-
tion varies with the composition of the steel.

The dissolution temperature of CrNbN in austenitic
steels ranges from 1200 °C to 1250 °C, depending on the
steel composition.[4] Another modification of the Z phase
has been reported for the ternary Cr-Ta-N system.[5] The
stoichiometry was given as $Cr_{1.2}Ta_{0.8}N$. So far, this mod-
ification of Z phase has not been observed in steels, but it is
assumed that it can develop in steels with high tantalum
contents. So far CrVN has not been observed to occur in
ternary systems.[5]

In the 1980s, a new modification of the Z phase was
observed to occur in both martensitic and austenitic
steels.[6,7] Here, niobium atoms had largely been replaced
by vanadium atoms, but the overall stoichiometry remained
intact, Cr(V,Nb)N. In 1996, Strang and Vodarek[8] investi-
gated Cr(V,Nb)N particles in martensitic steels, and deter-
mined their crystal structure as tetragonal, but with a
slightly smaller lattice parameter for the basal plane com-
pared to the original Z phase, $a = 0.286$ nm and $c = 0.739$
nm. Accordingly, the particle was dubbed modified Z
phase, Cr(V,Nb)N. The modified Z phase can contain small
amounts of Fe and the empirical formula $(Cr_{0.9}Fe_{0.1})$
$(V_{0.8}Nb_{0.2})N$ has been proposed for martensitic steels, even
though the V/Nb ratio can vary significantly.[1,9] For mar-
tensitic steels, the dissolution temperature of the modified
Z phase is about 800 °C, which is appreciably lower than
for the original Z phase.[1]

Vodarek and Strang[9] also found that the modified Z
phase in creep-resistant martensitic steels precipitated very
slowly and developed as large, coarse particles (Figure 2).
As the modified Z-phase particles precipitated, the smaller
beneficial MX particles, (Nb,V)(C,N), dissolved in order to
supply the constituents necessary for the growth of Z phase.
The small densely distributed MX particles are of vital
importance for the high-temperature creep strength of the
martensitic microstructure, and hence to the creep strength
in 9 to 12 pct Cr steels. Consequently, the dissolution of
MX particles associated with the precipitation of Z phase is
detrimental for these steels.

Recently, Nb-free Z phase, CrVN, with stoichiometry
$(Cr_{0.9}Fe_{0.1})VN$ was reported to have developed in 11 wt
pct Cr martensitic steels.[1] In the present work, the crystal
structures of mainly CrVN and Cr(V,Nb)N particles are
investigated.

II. EXPERIMENTAL

A. Investigated Materials

Four commercially available steel qualities, three mar-
tensitic and one austenitic, were investigated with compo-
sitions as given in Table I. X20 and T122 were provided by
E2/ELSAM, and 316LN and FV448 were provided by
Professor Vodarek (Vitkovice R and D). The steels were
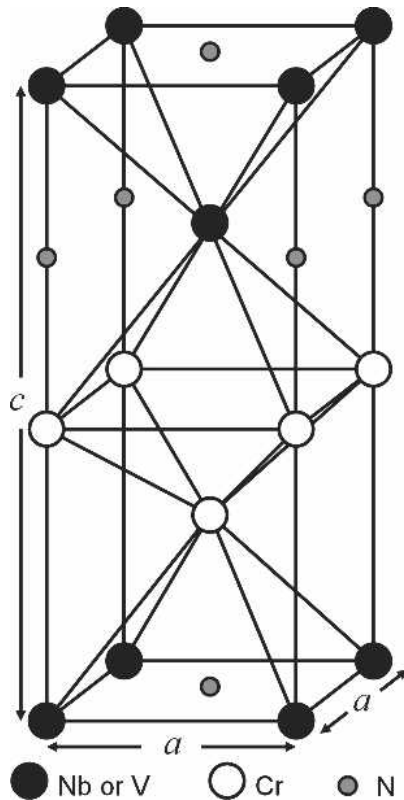subjected to the heat treatment given in Table II.

Fig. 1—The tetragonal Z-phase crystal structure. The lattice parameters of the original Z phase, CrNbN, are $a = 0.304$ nm and $c = 0.739$ nm; the modified Z phase, Cr(V,Nb)N, has slightly smaller a lattice parameters: $a = 0.286$ nm.
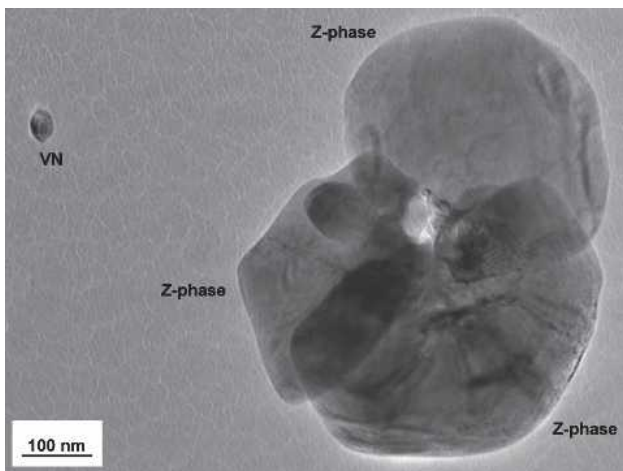

Fig. 2—A VN in the vicinity of three Z phases, showing the difference in size between the precipitates. Taken on a carbon extraction replica of T122.

B. Specimen Preparation

Most investigations were carried out on carbon extraction replicas. Occasionally, thin foils were examined. The carbon extraction replicas were prepared by chemical etch-

ing of polished surfaces in Vilellas etchant (1 pct picric acid and 5 pct concentrated hydrochloric acid in ethanol) for about 15 seconds. Austenitic steels were electrochemically etched in 10 pct oxalic acid applying 3 V. A carbon film was deposited onto the specimens by carbon evaporation, using a Quorum Technologies CC7650. Thereafter, the film was cut into pieces and the sample was dissolved in a mixture of 10 pct bromium in methanol, leaving the carbon extraction replica in the solution. The replicas were cleaned with ethanol and caught on small copper grits.

Thin foils were prepared by electropolishing 100-μm-thick dimple polished samples, using an electrolyte consisting of 6 pct perchloric acid in ethanol in a Struers TenuPol 5 operated at approximately 20 V and -20 °C.

C. Electron Microscopy

All electron microscopic investigations were carried out using a JEOL* 3000F FEG TEM with an Oxford Instruments

---

*JEOL is a trademark of Japan Electron Optics Ltd., Tokyo.

Inca EDS (Oxon, U.K.) and a Gatan Imaging Filter EELS (Pleasanton, CA). A double tilt holder was applied allowing the determination of 10 to 20 diffraction patterns for each particle, so the correct crystal structure could be identified. Generally, convergent beam electron diffraction (CBED) was used, but selected area electron diffraction (SAED) was also performed. Using the Kikuchi lines for orientation, it was possible to obtain diffraction patterns from the exact zone axis.

All of the examined particles were identified as CrVN, Cr(V,Nb)N, or CrNbN using energy dispersive spectroscopy (EDS) in the transmission electron microscope (TEM). Because it was not possible to measure the N content using EDS, the particles were mainly identified by their metallic composition, given by 50 pct Cr + Fe and 50 pct V + Nb + Mo (Figure 3(a)). Occasionally, particles were investigated with electron energy loss spectroscopy (EELS) to assess the nitrogen content. To this end, the N K loss peak at 401 eV, V L$_{2,3}$ peaks starting at 513 eV, and Cr L$_{2,3}$ peaks at 575 eV were chosen. The background to the EELS spectra was fitted using a power law. There were problems assessing the Cr content because the proximity of the V peaks made it difficult to fit the background (Figure 3(b)). The Nb and Fe contents were not determined, as the peak intensities were too low for accurate quantification.

III. RESULTS

A. Identification of a Cubic Crystal Structure

Electron diffraction investigations of CrVN and Cr(V,Nb)N particles showed that the majority of the diffraction patterns were not compatible with the expected tetragonal Z-phase crystal structure. Both CrVN and Cr(V,Nb)N particles had triad axes not present in tetragonal crystal systems (Figure 4). Instead many of the investigated particles showed fcc-like diffraction patterns with a lattice parameter of about 0.405 nm. It is assumed these particles have a crystal structure consisting of an fcc sublattice occupied by metal atoms and N atoms in half the available

Table I. Compositions (Weight Percent) of the Investigated Steels in Which Z-Phase Particles Were Identified

Steel	C	N	Si	Mn	Cr	Mo	W	Ni	Nb	V	Cu	B	Co
T122	0.09	0.0609	0.25	0.60	12.20	0.35	1.97	0.18	0.06	0.25	0.43	0.0021	—
X20	0.19	0.025	0.23	0.49	11.5	0.91	—	0.66	—	0.31	0.054	—	0.021
316LN	0.023	0.161	0.48	1.34	18.1	2.82	—	12.5	0.106	—	—	—	—
FV448	0.14	0.062	0.37	1.00	11.10	0.57	—	0.76	0.32	0.36	—	—	—

Table II. Heat Treatments and Subsequent Thermal Exposure of the Steels

Steel	Heat Treatment	Thermal Exposure
T122	1050 °C/10 min + 790 °C/3 h	12,000 h/660 °C
X20	1050 °C/1 h + 750 °C/2 h	150,000 h/600 °C
316LN	1050 °C	75,000 h/625 °C
FV448	1150 °C + 700 °C/4 h	34,000 h/600 °C

octahedral sites. The same diffraction patterns were obtained in all samples of the investigated steel types containing CrVN and Cr(V,Nb)N. For the CrNbN particles, no fcc-like diffraction patterns have been observed (yet); only the patterns corresponding to the tetragonal Z phase were identified. Thus, the occurrence of a cubic variant of CrNbN could not be confirmed.

The identified fcc-like diffraction patterns for the CrVN and Cr(V,Nb)N particles are similar to those identified for VN, which has a simple cubic (NaCl-type) crystal structure, where the V atoms constitute an fcc Bravais lattice. The lattice parameter of VN, $a = 0.414$ nm (Table III), is only 2 pct larger than that of the observed structure ($a = 0.405$ nm). Nevertheless, confusion between VN and other types of cubic nitrides is excluded, because of large differences in composition, shape, and size of the Z-phase particles as compared to cubic nitrides (Figure 2).

The compositions determined with EDS always showed approximately 50 at. pct Cr + Fe and 50 at. pct V + Nb + Mo. The EELS measurements on thin foils identified the particles as nitrides; no significant content of carbon was found. The boron content was not investigated. The Cr EELS measurements were not reliable because it was difficult to fit a background (Figure 3(b)). Therefore, the Z-phase composition was calculated combining the EDS measurements and the N/V ratio obtained in the EELS measurements (Table IV). The N content was slightly lower than the expected 33 at. pct, both for Cr(V,Nb)N and for CrVN. The obtained nitrogen contents strongly suggest a composition conforming to the stoichiometry M_2N rather than MN. The investigated particles were in the 100- to 500-nm size range, which is significantly larger than the average size of VN (Figure 2).

B. Orientation Relationship between Cubic and Tetragonal Crystal Structures

Further investigations of the crystal structure concern the coexistence of the fcc sublattice of metal atoms and the tetragonal modified Z-phase crystal structures in Cr(V,Nb)N particles. By carefully investigating SAED patterns, it is possible to observe simultaneous diffraction from both crystal structures, since the entire particle contributes to the patterns.

(a)

(b)
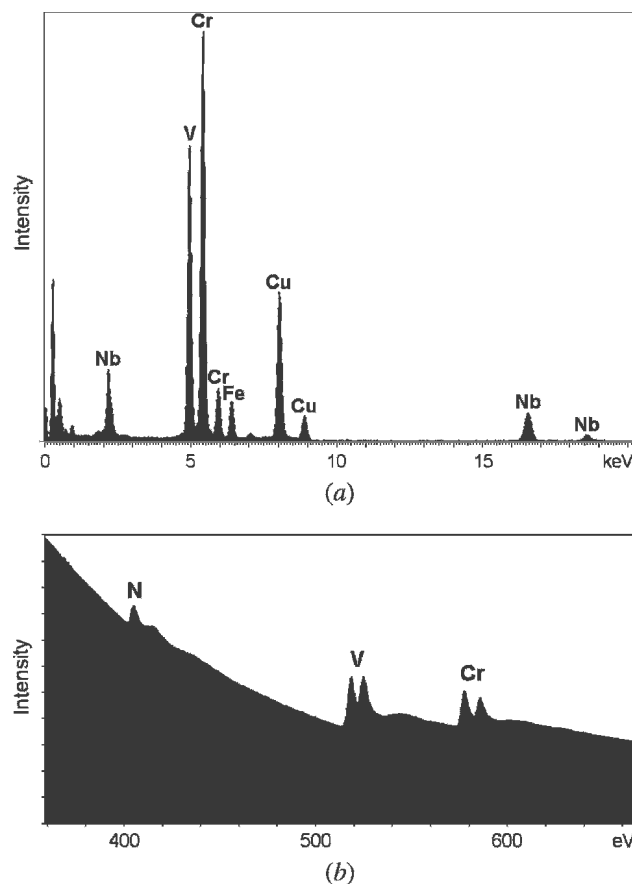
Fig. 3—Measurements of Z phase on carbon extraction replica of T122, using (a) EDS showing the metallic components, Cu signal is from the grit; and (b) EELS showing the main elements, including the nitrogen content.

This can be difficult to observe, as many of the spots from the two crystal structures overlap in the diffraction patterns. In Figure 5, the large brighter spots show an fcc-like pattern, while the spots corresponding to tetragonal Z phase appear as smaller, less intense spots. Generally, the fcc spots partly coincide with some of the tetragonal spots, which can make it difficult to distinguish between the patterns.

Using CBED, only a limited volume of the particle contributes to the diffraction pattern. Therefore, it was possible to observe fluctuations in the relative intensity of cubic and tetragonal spots, depending on the location on the particle. In a few cases, it was possible to get different diffraction patterns at different locations on the same particle and at the same tilt angle (Figure 6).

For the particles that show simultaneous diffraction of both crystal structures for the same tilt angles (Figure 5),
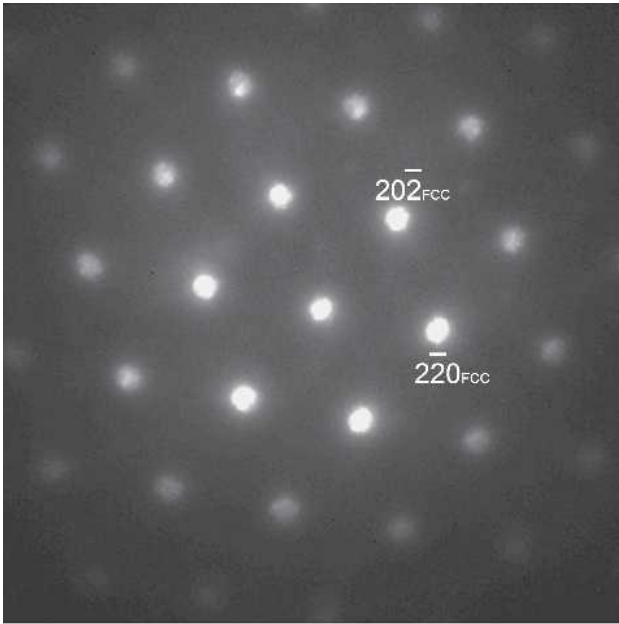
(a)
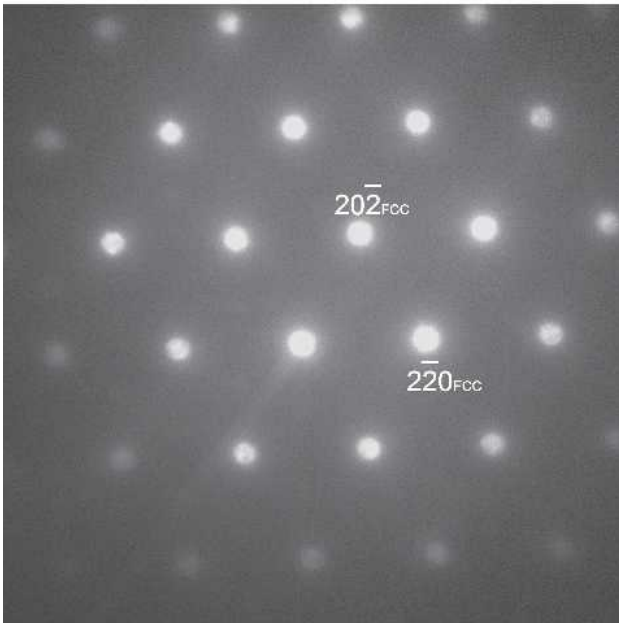
(b)

Fig. 4—Convergent beam electron diffraction patterns of (a) a Cr(V,Nb)N particle taken on a thin foil of T122 and (b) a CrVN particle, taken on an extraction replica of X20. Both patterns show a [111] cubic zone axis.

the following orientation relationship was assessed between the coexisting lattices:

$$(001)_{tetragonal}//(001)_{cubic}$$

$$[010]_{tetragonal}//[110]_{cubic}$$

Based on the orientation relationship and the lattice parameters of both the cubic and the tetragonal structure, the transformation matrix is determined as

Table III. Crystal Structure of Some of the Cr, Nb, and V Nitrides (Cubic and Hexagonal Nitrides Acquired from the JCPDS Database)

Composition	Crystal Structure	Lattice Parameter a	Lattice Parameter c
NbN	cubic	0.439 nm	—
VN	cubic	0.414 nm	—
CrN	cubic	0.414 nm	—
Nb$_2$N	hexagonal	0.306 nm	0.495 nm
V$_2$N	hexagonal	0.492 nm	0.457 nm
Cr$_2$N	hexagonal	0.481 nm	0.448 nm
CrNbN[3]	tetragonal	0.304 nm	0.739 nm
Cr(V,Nb)N[8]	tetragonal	0.286 nm	0.739 nm

Table IV. Results of EELS and EDS Measurements of CrVN in X20 and Cr(V,Nb)N in T122; the EDS + N Compositions are Based upon EDS and the N/V Ratio of the EELS Results (All Contents are Given in Atomic Percent)

Sample	Technique	Cr	Fe	V	Nb	N
X20	EELS	29	—	41	—	30
	EDS	40	6	54	—	—
	EDS + N	29	4	39	—	28
T122	EELS	33	—	37	—	30
	EDS	47	5	42	6	—
	EDS + N	35	4	31	5	25

$$(\text{cubic}\,\mathbf{T}\,\text{tetragonal}) = \begin{pmatrix} 1/2 & 1/2 & 0 \\ -1/2 & 1/2 & 0 \\ 0 & 0 & \dfrac{c}{\sqrt{2}a} \end{pmatrix}$$

Using the results from Vodarek and Strang,[9] where the orientation relationship between the tetragonal modified Z phase and the ferritic matrix is given, it is possible to see that the orientation relationship between the cubic crystal structure and the ferritic matrix would be in agreement with the Baker–Nutting orientation relationship for an fcc particle in a bcc matrix.

IV. DISCUSSION

A. *Distinguishing between Cubic and Tetragonal Z Phase*

Using electron diffraction to identify Cr(V,Nb)N or CrVN particles, it can be difficult to differentiate between the tetragonal modified Z-phase structure and the NaCl-type crystal structure. It is very easy to erroneously identify the cubic diffraction patterns as originating from the tetragonal structure, while the opposite is rarely the case. Many of the cubic diffraction patterns can be interpreted as tetragonal patterns in one way or the other, while the tetragonal Z phase has many more distinct patterns. An example is given in Table V, where the most typical (clearest) fcc-like patterns are listed together with interpretations in terms of a tetragonal structure of the same patterns. Many of these patterns are virtually identical. Only by accurate measurement of the angles, the vectors, and the camera length is it

Fig. 5—(a) SAED pattern showing the simultaneous presence of a cubic [110] zone axis, clear spots, and a tetragonal [010] zone axis, weak spots. Taken on a carbon extraction replica of FV448. (b) Indexing of the SAED pattern.

Fig. 6—(a) The [102] cubic pattern and (b) the corresponding [111] tetragonal pattern. Both CBED patterns were taken at the same tilt angle, at different locations on the same Cr(V,Nb)N particle on a carbon extraction replica of FV448. Note that the cubic spots overlap with the tetragonal spots.

possible to differentiate. In fact, the [001] patterns of both crystal structures are identical.

Using the zone axis from Table V and the transformation matrix from Section III–B, it is straightforwardly obtained that many of the virtually identical diffraction patterns are located at nearly the same tilt angle with respect to the common [001] zone axis. Using the [223] pattern of tetragonal modified Z phase as an example, the corresponding cubic pattern becomes

$$[223]_{tetragonal} \rightarrow [205.5]_{cubic} = [102.75]_{cubic} \approx [103]_{cubic}$$

This means that the [223] zone axis of the tetragonal structure is located close to the position of the [103] zone axis of the cubic structure, which has a virtually identical diffraction pattern. The actual difference between them is calculated to be a tilt angle of only 1.6 deg. Values of the same order of magnitude are obtained for the other zone axes given in Table V, and the results are collected in Table VI. Hence, distinguishing between cubic and tetragonal

crystal structures relies on the investigation of subtle differences.

In certain zone axes, unique spots occur for the diffraction patterns of the tetragonal lattice, which do not occur for the fcc-like patterns. According to kinematic diffraction theory, systematic extinctions occur in fcc lattices when h, k, and l are mixed even and odd; for a tetragonal lattice corresponding to the Z-phase case, systematic extinctions occur only for $hk0$ when $h + k$ is odd.[3] Nevertheless, the present diffraction pattern in Figure 5 shows weak intensity for the 100_Z and -100_Z spots, which can be attributed to deviations from the perfect tetragonal lattice. It is thus possible to distinguish a tetragonal Z-phase structure from a cubic structure by analyzing additional spots in SAED patterns. However, these unique spots are often observed to be

Table V. Some of the Most Common Cubic Zone Axes Can Be Easily Interpreted as Tetragonal, Because the Vectors and the Angle between the Vectors are Nearly Identical

Cubic 0.4045 nm				Tetragonal 0.286 nm			
Zone Axis	1. Vector	2. Vector	Angle	Zone Axis	1. Vector	2. Vector	Angle
[101]	(-1-11) 4.28 nm^{-1}	(-111) 4.28 nm^{-1}	70.5 deg	[221]	(10-2) 4.42 nm^{-1}	(01-2) 4.42 nm^{-1}	68 deg
[215]	(13-1) 8.20 nm^{-1}	(-311) 8.20 nm^{-1}	84.8 deg	[265]	(21-2) 8.27 nm^{-1}	(1-22) 8.27 nm^{-1}	83.9 deg
[103]	(020) 4.94 nm^{-1}	(-311) 8.20 nm^{-1}	72.5 deg	[223]	(1-10) 4.94 nm^{-1}	(21-2) 8.27 nm^{-1}	72.6 deg
[001]	(200) 4.94 nm^{-1}	(020) 4.94 nm^{-1}	90 deg	[001]	(110) 4.94 nm^{-1}	(1-10) 4.94 nm^{-1}	90 deg
[213]	(11-1) 4.28 nm^{-1}	(3-3-1) 10.78 nm^{-1}	82.4 deg	[263]	(0-12) 4.42 nm^{-1}	(-302) 10.83 nm^{-1}	81.2 deg
[112]	(11-1) 4.28 nm^{-1}	(2-20) 6.99 nm^{-1}	90 deg	[021]	(0-12) 4.42 nm^{-1}	(200) 6.99 nm^{-1}	90 deg

Table VI. Calculated Tilt Angles between Zone Axes of the Cubic and Tetragonal Crystal Structures Shown in Table V

Zone Axis, Cubic 0.4045 nm	Zone Axis, Tetragonal 0.286 nm	Difference in Tilt Angle
[101]	[221]	2.6
[215]	[265]	2.0
[103]	[223]	1.6
[001]	[001]	0
[213]	[263]	2.6
[112]	[021]	2.5

very weak as compared to those shared with the fcc-like patterns. The CBED can be useful to identify the additional (tetragonal) spots in the diffraction patterns. The CBED patterns in Figure 6 show which areas of the particle are cubic (no extra spots present, Figure 6(a)) and which are tetragonal (extra spots present, Figure 6(b)).

Preferably, diffraction patterns exclusively belonging to one or the other crystal structure should be investigated. This is more difficult for the cubic patterns than for the tetragonal patterns. To this end, the diffraction pattern of the [111] cubic zone axis was investigated in the present work to positively identify the cubic crystal structure of both Cr(V,Nb)N and CrVN (Figure 4), because it cannot be easily confused with a diffraction pattern of the tetragonal modified Z phase.

In Figure 7, the [111] tetragonal zone axis of Z phase is compared for a partly tetragonal CrVN particle and a presumably fully tetragonal CrNbN particle. The strong (overlapping) spots on the CrVN pattern (Figure 7(a)) show a [102] cubic zone axis, while some extra weak spots indicate its partly tetragonal structure. Some tetragonal spots are still too weak to be observed, *e.g.,* (11-2). On the CrNbN pattern (Figure 7(b)), all tetragonal spots are clearly visible, and the pattern does not indicate the presence of a cubic structure.

There have been previous reports of particles with Z-phase-like composition, and a cubic crystal structure, but they have never been identified as Z phase.
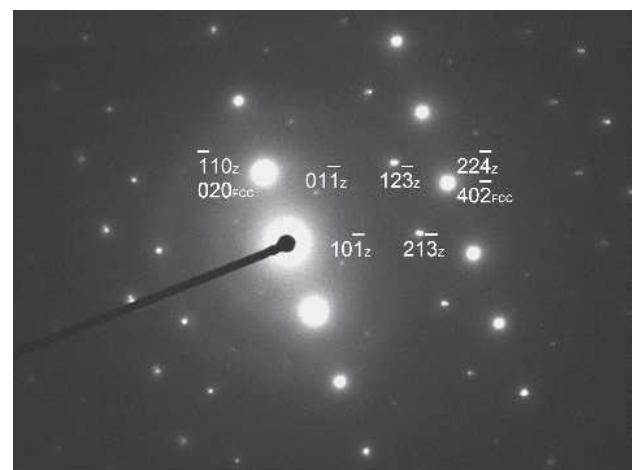
(a)
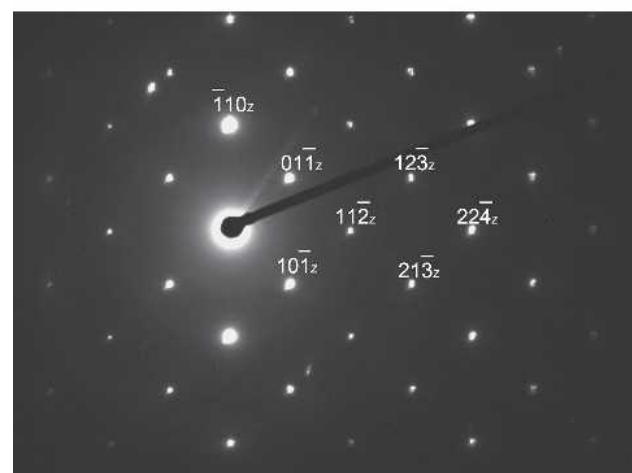
(b)

Fig. 7—(a) A pattern of a [102] cubic zone axis, where some weak spots of the [111] tetragonal zone axis are visible, taken on a CrVN particle on a carbon replica of X20. (b) A [111] tetragonal zone axis taken on a CrNbN particle on a carbon replica of 316LN.

Thorvaldsson and Dunlop[10] have observed vanadium- and chromium-rich particles with an fcc-like diffraction pattern and lattice parameter of 0.406 nm. The metallic composition of these particles was 44 at. pct Cr and 56 at. pct V, which corresponds favorably with the stoichiometry CrVN. However, no measurements of the nitrogen content were presented, and these particles were assumed to be (V,Cr)N particles, *i.e.,* MN stoichiometry.

Cr(V,Nb)N particles have also been identified as having a cubic crystal structure,[11] and were presumed to be a precursor for the Z phase. These particles where observed at 750 °C, which is close to the dissolution temperature, 800 °C. The crystal structure had a larger lattice parameter, 0.419 nm, compared to the one observed at lower temperatures in the present work. Above the dissolution temperature, Cr(V,Nb)N particles are replaced by MX particles with a lattice parameter $a = 0.42$ nm.[1]

B. *Orientation Relationship*

The newly found cubic (presumably NaCl-type) crystal structure and the tetragonal modified Z-phase crystal structure are closely related. The sublattice of metal atoms in the tetragonal Z-phase crystal structure can be described as alternating layers of V/Nb atoms and Cr atom layers (Figure 1). In the V/Nb layers, the metal atoms span an fcc lattice and all octahedral interstices are occupied by N. On the other hand, the Cr layer is compressed in the c direction and deviates therefore from an fcc lattice, and its octahedral interstices are unoccupied. In essence, if the c-axis of the Cr layer was not compressed in the c direction, an fcc lattice would emerge, consisting of the metal atoms (Figure 8(a)), primarily Cr and V in the case of modified Z phase. This fcc sublattice constituted by the metal atoms in the modified Z phase would have a lattice parameter of 0.4045 nm, which is consistent with the experimentally found value of 0.405 nm. The corresponding

cubic crystal structure in the original Z phase, CrNbN, would have a lattice parameter of 0.430 nm, and has not been observed in the present investigation.

The close relation between the tetragonal modified Z phase and the newly found cubic crystal structure can clearly be seen by viewing the two crystal structures along the c-axis (Figure 8(b)). This manifests itself in the two crystal structures having identical [001] diffraction patterns, although the spots are differently indexed, as the unit cells are differently defined, *i.e.,* rotated 45 deg about the c-axis. A transformation from cubic to tetragonal crystal structure should thus be relatively easy, as the crystal only has to be compressed in the c-axis, while the c planes should remain the same (Figure 8(a)). It is anticipated that a transformation between the two crystal structures would involve some ordering/disordering of the atoms, but the exact locations of the metal and interstitial atoms are not known.

C. *Coexistence of the Cubic and Tetragonal Crystal Structures*

No stacking faults or other defects have so far been observed in the Cr(V,Nb)N particles, and beyond the orientation relationship, it is not known how the two structures coexist. Looking at CBED patterns, the structure does not appear to be uniform (Figure 6) and there appears to be variations of the cubic/tetragonal ratio in different areas of the particles.

Generally, the Cr(V,Nb)N particles in FV448 appear to have a higher degree of tetragonal structure than for T122 and X20. This could be associated with the different chemical compositions of the steels or the differences in exposure time and aging temperature. The cubic crystal structure could be a precursor to the more ordered tetragonal modified Z-phase crystal structure in martensitic steels, which could have some significance for the precipitation process of the Cr(V,Nb)N particles. It is not known which
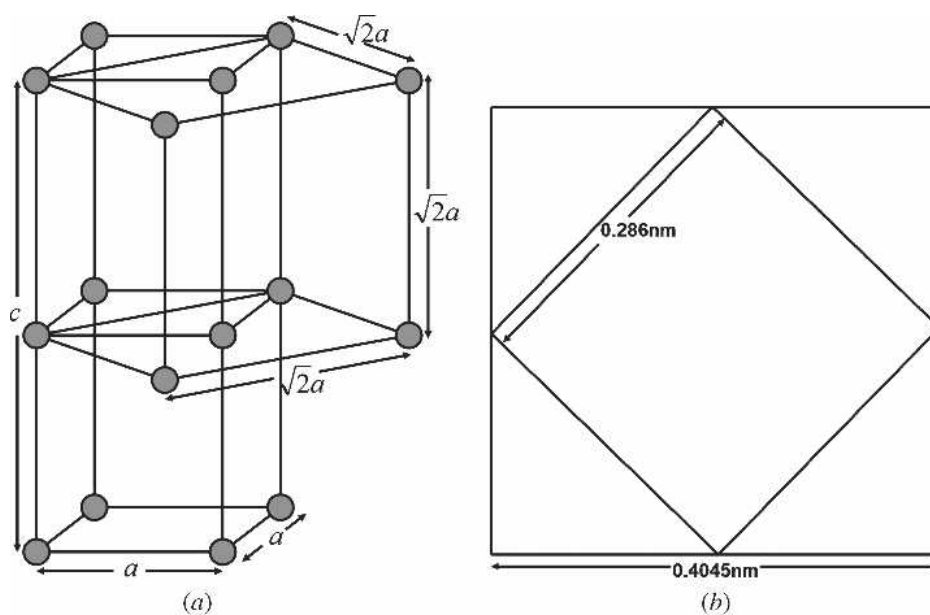

Fig. 8—(*a*) The proposed relation between the tetragonal unit cell of the Z phase and the corresponding cubic unit cell. Some atoms have been left out for clarity. (*b*) The relation seen from the *C*-axis with the corresponding lattice parameters of modified Z phase.

factors would affect the cubic/tetragonal transformation. It is not yet clear whether the size or composition of the particles has an influence on the crystal structure, but the relatively large variation in the vanadium and niobium concentrations, which are frequently observed in these particles, could be related with the crystal structure.

So far no cubic crystal structure was identified in CrNbN. In order to verify whether such particles can exist at all, samples exposed to shorter aging times should be investigated.

V. CONCLUSIONS

Two different crystal structures have been observed to exist in Cr(V,Nb)N particles: the tetragonal modified Z-phase crystal structure and a cubic, presumably NaCl-type, crystal structure. The proposed cubic crystal structure has an fcc sublattice of metal atoms with a lattice parameter of 0.405 nm. It is believed that the fcc sublattice consists primarily of Cr and V atoms and that the N atoms occupy half the available octahedral sites. The cubic crystal structure has a striking similarity with the tetragonal crystal structure of modified Z phase. The two crystal structures appear to coexist in the Cr(V,Nb)N particles, with the orientation relationship

$$(001)_{tetragonal} // (001)_{cubic}$$
$$[010]_{tetragonal} // [110]_{cubic}$$

The recently found CrVN particles in martensitic steels appear to have the same cubic/tetragonal crystal structures as the Cr(V,Nb)N particles. The cubic crystal structure has so far not been identified in CrNbN particles.

REFERENCES

1. H.K. Danielsen and J. Hald: *Energy Mater.*, 2006, vol. 1, pp. 49-57.
2. W.O. Binder: *ASTM*, 1950, STP 110, p. 146–64.
3. D.H. Jack and K.H. Jack: *J. Iron Steel Inst.*, 1972, vol. 209, pp. 790-92.
4. V. H. Gerlach and E. Schmidtmann: *Arch. Eisenhuttenwes.*, 1968, Feb., pp. 139-49.
5. P. Ettmayer: *Monatsh. Chem.*, 1971, vol. 102, pp. 858-63.
6. H.-O. Andren, A. Henjered, and L. Karlson: *Stainless Steel 84*, The Institute of Metals, London, 1985, pp. 91-96.
7. E. Schnabel, P. Schwaab, and H. Weber: *Stahl v. Eisen.*, 1987, vol. 107, pp. 691-96.
8. A. Strang and V. Vodarek: *Mater. Sci. Technol.*, 1996, vol. 12, pp. 552-56.
9. V. Vodarek and A. Strang: *Proc. Conf. on "Materials for Advanced Power Engineering,"* Liege, Sept. 2002, J. Lecomte-Beckers, M. Carton, F. Schubert and P.J. Ennis, eds., Forschungs-Zentrum, Julich GmbH, Julich, 2002, Part 2, pp. 1223-32.
10. T. Thorvaldsson and G.L. Dunlop: *Met. Sci*, 1982, vol. 16, pp. 184-90.
11. L. Karlson, A. Henjered, H.-O. Andren, and H. Norden: *Mater. Sci. Technol.*, 1985, vol. 1, pp. 337-43.

Appendix C

A Thermodynamic model of the Z-phase, Cr(V,Nb)N

A thermodynamic model of the Z-phase Cr(V, Nb)N

Hilmar Kjartansson Danielsen[a,*], John Hald[b]

[a] Department of Manufacturing Engineering and Management, Technical University of Denmark, Kemitorvet building 204, 2800 Kgs. Lyngby, Denmark
[b] DONG Energy/Department of Manufacturing Engineering and Management, Technical University of Denmark, Kemitorvet building 204,
2800 Kgs. Lyngby, Denmark

Abstract

Precipitation of large Z-phase particles, Cr(V, Nb)N, replacing fine MX carbonitrides, Nb(C, N) or V(N, C), has recently been identified as a major cause for premature breakdown in long-term creep strength of a number of new 9%–12% Cr martensitic steels, especially the high Cr variants.

A thermodynamic model of the Z-phase has been developed based on the regular solution model. The model predicts Z-phase to be stable and to fully replace the MX particles in most of the new 9%–12% Cr steels, which is in good agreement with experimental observations.

The rate of precipitation of Z-phase is a crucial factor for the long-term creep stability of these steels. Driving force calculations with the model allow estimates of the influence of the individual alloying elements on the rate of Z-phase precipitation, and can thus contribute useful information for alloy design to delay and retard Z-phase precipitation.

According to these calculations, particularly Cr has a strong accelerating effect on Z-phase precipitation.
© 2007 Elsevier Ltd. All rights reserved.

Keywords: Z-phase; Cr(V, Nb)N; CrVN; CrNbN; Thermo-Calc

1. Introduction

1.1. Background

The recent development of new more creep resistant martensitic 9%–12% Cr steel for steam power plant applications has allowed increased operating steam temperatures up to 600 °C, improving efficiency and reducing environmental impact. In order to increase the temperature further to 650 °C for even better efficiency, steam oxidation has to be considered along with improved creep strength. Thus, a number of experimental steels with 11%–12% Cr are under development. For all of these, short-term creep tests (<10 000 h at 650 °C) have indicated improvements but after longer testing times dramatic breakdowns in microstructure stability have occurred. Recently, the precipitation of the complex nitride Z-phase, Cr(V, Nb)N, has been identified as the root cause of the observed microstructure instabilities in the new steels [1].

The new martensitic 9%–12% Cr steels rely on precipitate particles to obtain good creep properties at high temperatures. One of the major contributors to creep strength are MX carbonitrides, Nb(C, N) or V(N, C), which precipitate as small and densely spaced particles. As the Z-phase contains the same constituents as the MX carbonitrides, its precipitation is accompanied by dissolution of the beneficial MX particles. Z-phase precipitates as relatively large particles, which do not contribute to particle strengthening. Accordingly, the creep strength of steel containing large Z-phase particles is considerably reduced as compared to the same steel containing MX carbonitrides [1].

Thermodynamic equilibrium calculations with computer programs, like Thermo-Calc [2], have been successfully applied to evaluate the phase stability of precipitates and matrix phases of the 9%–12% Cr steels as a function of temperature and chemical composition. Such calculations have led to improved understanding of the influence of precipitate phases (carbides, intermetallic phases and nitrides) on long-term microstructure stability of creep resistant 9%–12% Cr steels [3]. The calculations rely on thermodynamic models of the individual

* Corresponding author. Tel.: +45 45 25 21 92; fax: +45 45 93 62 13.
E-mail addresses: Hilmar@ipl.dtu.dk (H.K. Danielsen), joh@ipl.dtu.dk (J. Hald).

precipitate phases. Hitherto no thermodynamic model of the Z-phase has been incorporated, as the precipitation of this phase in common 9%–12% Cr steels is a recent observation. Reliable prediction of the long-term microstructure stability of 9%–12% Cr steels demands incorporation of a thermodynamic model of the Z-phase. In the present article the development of such a model is described.

1.2. Literature survey

An extensive literature survey was conducted in order to find experimental results for a thermodynamic model of the Z-phase. At least two different kinds of Z-phase have been indicated in the literature. The original version, CrNbN, was discovered in 1950 in an austenitic steel [4]. Since then it has frequently been observed in Nb containing austenitic steels where it precipitated very quickly. In the 1980's a vanadium containing Z-phase, also called modified Z-phase, Cr(V, Nb)N, was observed in both austenitic and martensitic steels [5,6]. In 1996 Strang and Vodarek [7] found that the modified Z-phase precipitated very slowly and developed as large coarse particles in creep resistant martensitic 11%–12% Cr steels. This caused the beneficial MX particles to dissolve, thus lowering the creep resistance considerably.

Information was gathered on composition and dissolution temperature of the Z-phase in a number of austenitic, ferritic and martensitic steels [8–20]. The literature showed distinct differences between the two Z-phase versions. Both the original and modified Z-phases have a tetragonal crystal structure, but there is a slight difference in the *a* lattice parameter (Fig. 1) probably because of the smaller size of V atoms compared to Nb atoms [7,21].

The crystal structure of the Z-phase has recently been found to be more complicated than previously thought, as both cubic and tetragonal crystal structures have been identified [22]. The tetragonal crystal structure is considered to be thermodynamically stable, while the cubic probably represents a metastable transition stage. The tetragonal structure consists of VN/NbN and Cr layers. Analysis of the electron structure using atomistic modelling have shown the VN/NbN layers to have the same character as bulk VN/NbN, while the Cr layers are similar to (metallic) bulk Cr [23].

The empirical formula of the original Z-phase is approximately $(Cr_{0.8}Fe_{0.2})(Nb_{0.9}Mo_{0.1})N$, while for the modified Z-phase it is approximately $(Cr_{0.9}Fe_{0.1})(V_{0.8}Nb_{0.2})N$, varying with the composition of the steels. There were no available sources on the dissolution temperature for the modified Z-phase, but investigations by the authors gave a dissolution temperature of 800 °C [1]. This is significantly lower than that of the original Z-phase, which has been reported to be as high as 1250 °C [12]. The precipitation of modified Z-phase is reported to proceed significantly slower as compared to the original Z-phase.

The only found sources on Z-phase in ternary systems came from Ettmayer [24], who observed the CrNbN and CrTaN Z-phases in their respective ternary systems, but no Z-phase was found in the CrVN system, probably because of high
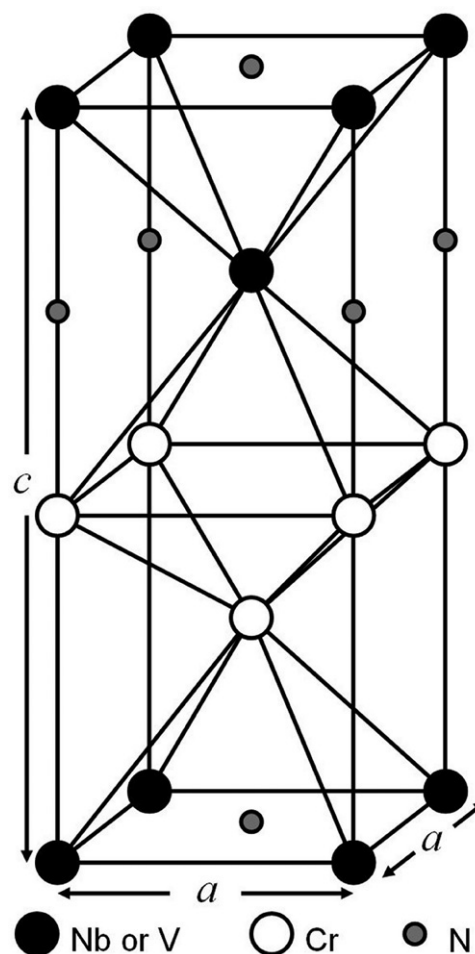

Fig. 1. The crystal structure of the Z-phase. The lattice parameter for CrNbN is $a = 0.304$ nm and $c = 0.739$ nm while for CrVN it is $a = 0.286$ and $c = 0.739$.

experimental temperatures. CrVN had not been observed in ternary systems at 800 °C and above, no information below this temperature was available.

2. The Z-phase model

2.1. The sublattice model

The model of the Z-phase is based on the application of the regular solution model to stoichiometric compounds (the sublattice model) as firstly proposed by Hillert and Staffanson [25] and later extended by Sundman and Ågren [26]. Based on the crystal structure shown in Fig. 1, the Z-phase has stoichiometry ABC and consists of three sublattices on which the A, B and C atoms reside. Sublattice 1 contains A atoms (Cr and Fe), sublattice 2 contains B atoms (V, Nb and Mo), and sublattice 3 contains C atoms (N and vacancies). The empiric formula is thus (Cr, Fe)(V, Nb, Mo)(N, Va).

The Gibbs energy of the Z-phase is calculated according to sublattice model:

$$G_m = \sum y_I^1 y_J^2 y_K^3 \, {}^0G_{I:J:K} + G^{\text{ideal}} + {}^{xs}G \quad (1)$$

where y_c^s is the site fraction of component c on sublattice s. ${}^0G$ corresponds to the Gibbs energy of the mechanical mixture

Table 1
Compositions (wt%, balance Fe), heat treatment and exposure of the 9%–12% Cr steels from own experiments used for fitting

	P91	E911	P92	AXM	HCM12	P122	T122	NF12	FN5	TB12	VM12	X20
C	0.10	0.11	0.11	0.11	0.10	0.11	0.09	0.085	0.11	0.113	0.12	0.19
N	0.053	0.065	0.049	0.05	0.025	0.053	0.0609	0.045	0.027	0.055	0.078	0.025
Si	0.36	0.18	0.17	0.08	0.18	0.02	0.25	0.25	0.06	0.01	0.48	0.23
Mn	0.37	0.46	0.43	0.42	0.51	0.56	0.60	0.44	0.55	0.51	0.37	0.49
Cr	8.30	8.61	9.27	10.48	12.20	11.0	12.20	11.60	11.20	11.33	11.61	11.5
Mo	0.95	0.92	0.48	1.04	1.00	0.42	0.35	0.14	0.26	0.5	0.28	0.91
W	–	0.995	1.701	0.99	0.99	1.94	1.97	2.68	2.63	1.98	1.58	–
Ni	0.15	0.21	0.25	0.77	0.01	0.32	0.18	0.17	0.40	0.96	0.31	0.66
Nb	0.07	0.089	0.067	0.043	0.05	0.05	0.06	0.08	0.065	0.082	0.044	–
V	0.21	0.19	0.197	0.18	0.24	0.19	0.25	0.20	0.22	0.18	0.251	0.31
Cu	–	–	–	0.04	–	0.87	0.43	0.01	–	0.06	0.06	0.054
Al	0.15	0.013	0.005	0.008	–	0.012	0.004	–	–	0.004	–	0.016
B	–	–	0.0026	0.0002	–	0.0011	0.0021	0.0026	0.0010	–	0.0045	–
Co	–	–	–	–	–	–	–	2.48	2.66	–	1.56	0.021
Heat treatment	1050 °C/ 1 h 780 °C/ 1 h	1060 °C/ 1 h 770 °C/ 2 h	1060 °C/ 1 h 770 °C/ 2 h	1070 °C/17 h 570 °C/22 h 700 ° C/24 h	1050 °C/ 1 h 800 °C/ 1 h	1050 °C/ 1 h 770 °C/ 3 h	1050 °C/ 0.2 h 790 °C/ 3 h	1100 °C/ 0.2 h 760 °C/ 1 h	1100 °C/4 h 715 °C/24 h	1080 °C/ 2.5 h 775 °C/ 2 h	1060 °C/ 0.5 h 780 °C/ 2 h	1050 °C/ 1 h 750 °C/ 2 h
Exposure	8 000 h 650 °C	10 000 h 650 °C	31 000 h 650 °C	43 000 h 600 °C	85 000 h 585 °C	10 000 h 650 °C	12 000 h 660 °C	17 000 h 650 °C	8 000 h 650 °C	10 000 h 650 °C	16 000 h 625 °C	150 000 h 600 °C

Table 2
Compositions (wt%, balance Fe), heat treatment and exposure of some austenitic steels from the literature used for fitting

	Ernemann [9]	Hughes [10]	Vodarek [11]	Gerlach [12] S1	Gerlach [12] S2	Uno [13]
C	0.065	0.04	0.021	0.023	0.026	0.040
N	0.020	0.200	0.158	0.213	0.193	0.152
Si	0.40	0.34	0.42	0.51	0.55	0.63
Mn	1.77	1.46	1.11	0.62	0.59	1.18
Cr	17.61	17.70	17.83	16.90	17.05	18.32
Mo	0.17	2.78	2.64	1.95	2.09	–
Ni	11.36	12.00	12.63	17.25	16.85	10.58
Nb	0.78	0.90	0.30	0.77	1.25	0.07
Cu	0.14	–	–	–	–	–
Co	0.13	–	–	–	–	–
B	–	–	–	–	–	0.0002
Heat treatment	1100 °C/3 min	1050 °C/1 h	1300 °C/30 min 1100 °C/90 min	1200 °C/5 h (Varying)	1200 °C/5 h (Varying)	1100 °C/10 min
Exposure	77 782 h 800 °C	–	–	–	–	Varying

of the elements of the phase. ^0G is described by the following equation:

$$^0G_{I:J:K} = {}^0G_I^{\text{SER}} + {}^0G_J^{\text{SER}} + {}^0G_K^{\text{SER}} + C_1 + C_2 T \qquad (2)$$

where $^0G^{\text{SER}}$ is the energy of the standard element reference states, C_1 is the formation energy constant and C_2 is a constant used to describe the temperature dependence. The $^0G^{\text{SER}}$ are known but C_1 and C_2 need to be determined by fitting through experimental data.

G^{ideal} is the entropy of mixing for an ideal solution of the atoms on each of the three sublattices, and can be calculated without fitting:

$$G^{\text{ideal}} = RT \sum y_c^s \ln \left(y_c^s \right) \qquad (3)$$

^{xs}G represents the excess Gibbs energy of mixing, which expresses the deviation from ideal mixing behaviour when a sublattice contains two different elements, e.g. Cr(V, Nb)N instead of CrVN or CrNbN. ^{xs}G can be expressed as:

$$^{xs}G = \sum y_{I_1}^1 y_{I_2}^1 y_J^2 y_K^3 L_{I_1, I_2:J:K} + \sum y_I^1 y_{J_1}^2 y_{J_2}^2 y_K^3 L_{I:J_1, J_2:K} + \sum y_I^1 y_J^2 y_{K_1}^3 y_{K_2}^3 L_{I:J:K_1, K_2} \qquad (4)$$

where L is the first term of a Redlich–Kister series expression and is assumed to be linearly dependent on temperature:

$$L = C_3 + C_4 T \qquad (5)$$

the C_3 and C_4 factors are used as fitting parameters.

In all, 12 pairs of empirical constants (C_1 and C_2, cf. Eq. (2)) need to determined by fitting for the quantitative assessment of ^0G and 24 pairs (C_3 and C_4, cf. Eq. (5)) for L. It was however not necessary to use all of them. The experimental data needed for the fitting of these constants was primarily thermodynamic, e.g. composition and dissolution temperature
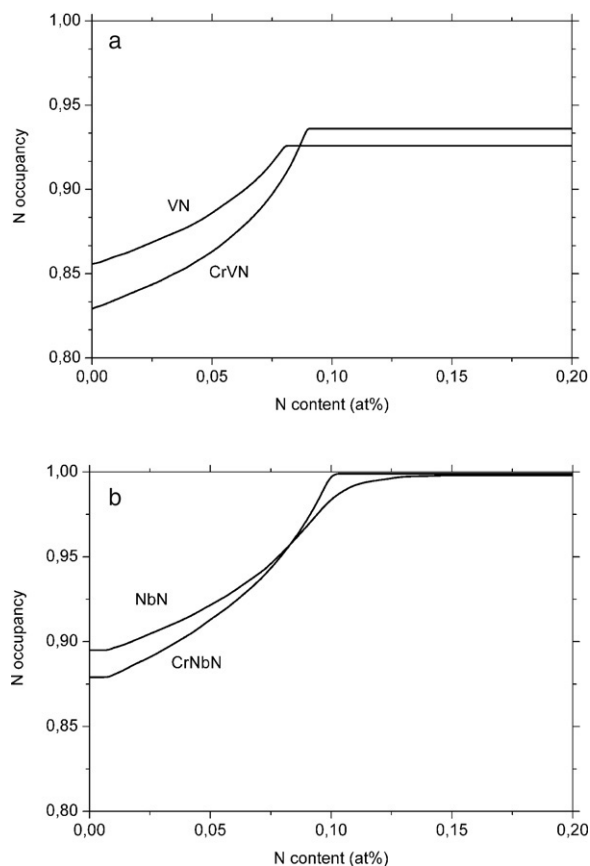
Fig. 2. Comparison of N occupancy for Z-phase and MX as a function of N content in steel at 650 °C. The steels consist of (at.%, balance Fe): (a) 12% Cr and 0.1% V, (b) 12% Cr and 0.1% Nb.
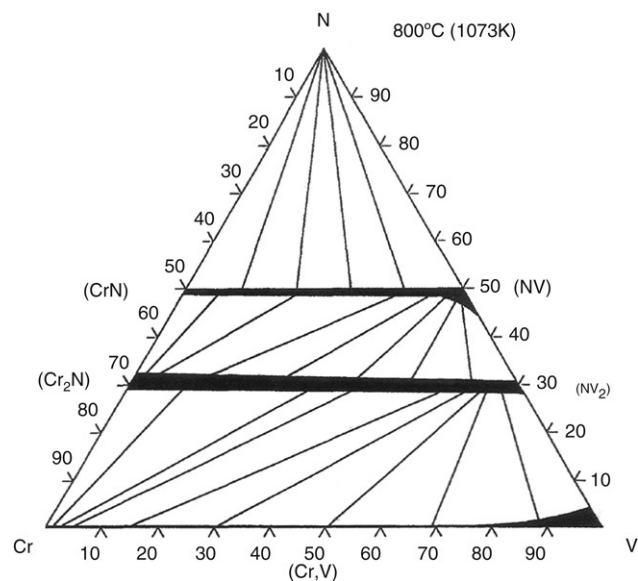

Fig. 3. The CrVN ternary system (at.%) shows full miscibility of Cr and V in matrix and nitrides. Z-phase is not present at 800 °C and above, no information on systems below 800 °C was found [28].

Fig. 4. Calculations in the CrVN ternary system (without Z-phase) along the M_2N and MN lines, with (at.%) (a) 33.3% N and (b) 50% N. There should be full miscibility between the Cr and V nitrides, but this is not the case in either calculation.

used in combination with driving force calculations for fitting of the constants.

2.2. Evaluation of data for fitting

Since there was little experimental information available on ternary systems relevant to the Z-phase, it was decided to model the Z-phase exclusively using data from steels. For martensitic 9%–12% Cr steels, the data used were mainly from own experiments (Table 1) while literature data were used for austenitic steels (Table 2). At first the model was fitted to data for the original Z-phase in Nb-containing (V-free) steels. There was sufficient data available on both the dissolution temperature and Z-phase composition for these steels. All data for the Nb-containing steels was considered to represent systems in (or close to) thermodynamic equilibrium because of the relatively high heat treatment temperatures and fast precipitation of Z-phase in these steels. Thereafter, the model was completed by fitting to data from V-containing steels. Unfortunately, because of the lower heat treatment temperatures and the slow precipitation of the modified Z-phase, the data for these steels does not always represent systems close to thermodynamic equilibrium. Only those systems wherein the MX particles

of Z-phase from systems in equilibrium. Furthermore, the observed rate of precipitation of Z-phase in different steels was

Fig. 7. The driving force for precipitation of Z-phase for several different steels at 650 °C. Compare with Table 6.
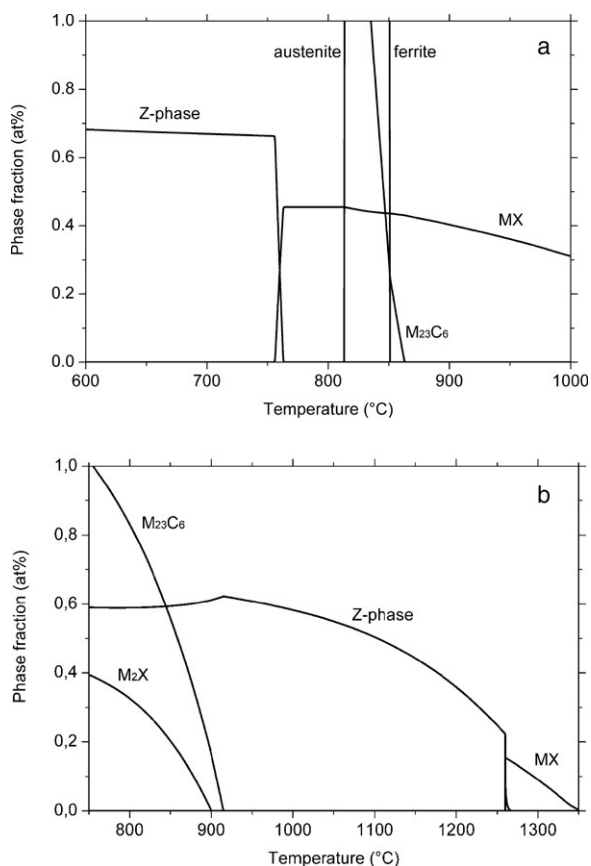

Fig. 5. Thermo-Calc calculations showing the phase quantity as a function of temperature in (a) grade P91 (Table 1) and (b) grade AISI 316 LN (Table 2).
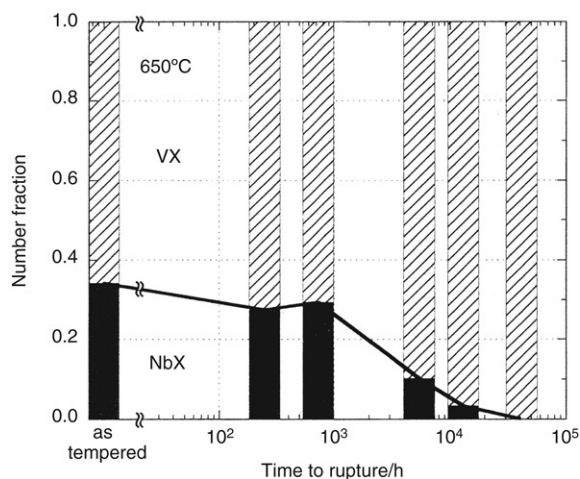

Fig. 6. Changes in the number fraction of primary MX (NbX) and secondary MX (VX) as a function of rupture time at 650 °C in P91 [15].

had almost completely been dissolved by Z-phase development were considered useful for fitting.

The original and modified versions of the Z-phase are considered isomorphous, the Nb and V atoms are fully substitutional on their joint sublattice. Small amounts of Mo and sometimes W have been detected in modified Z-phase [16–20] but this could not be verified by own experiments [1].
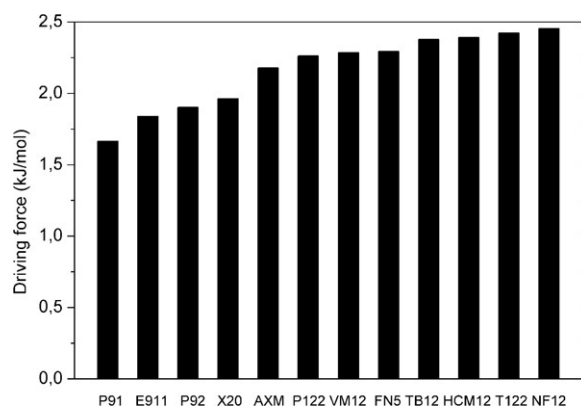
In the model there is only an insignificant amount of Mo in the modified Z-phase, and W is not defined in the Z-phase at all. In the original Z-phase all sources report a relatively high Mo content, which has been included in the model. Tantalum has not been included in the present Z-phase model as information on this element in Z-phase is scarce. A few sources reported small amounts of carbon in Z-phase, but in varying quantity [5,10,12]. Attempts to verify this have been made, but no significant amount of carbon was detected [1]. Therefore, in the current Z-phase model, C was not included.

Vacancies were introduced in the third Z-phase sublattice as to compensate for the possible deviation from stoichiometric composition of the MX particles, e.g. $Nb_1N_{0.9}$ when nitrogen is deficient. Some experiments indicate vacancies being present in Z-phase [1], but little experimental data was available. As atomistic modelling suggest the VN/NbN sublattices to be similar to VN/NbN bulk [23], the fitting imitated the vacancy behaviour of the corresponding MX models, that is VN for CrVN and NbN for CrNbN. The Cr sublattice, being comparable to metallic Cr, was not considered to have any N atoms in its interstitials. Fig. 2 shows an example of this fitting, the shape of the curves depend on both the temperature and the composition of the steel matrix.

The model has primarily been based on data from steels, which have compositions inside the limitations presented in Table 3. The steels had been heat treated within the temperature range 500–1300 °C. Care should be taken when applying the present Z-phase model beyond these limitations, as no verification has been possible.

The model development was performed using the Thermo-Calc software. Since the model is mainly intended for use in steels, the most recent commercially available Thermo-Calc database for iron based alloys, TFCE3 [27], was used.

Calculations of the CrVN ternary system (without Z-phase) with the TCFE3 database showed some inconsistencies with experimental results from the literature. This system contains four phases: gaseous N_2 phase, Cr–V bcc phase, (Cr–V)N NaCl phase (fcc sublattice of Cr–V) and $(Cr–V)_2$ N hexagonal phase (hcp sublattice of Cr–V). According to experimental data the Z-phase is not stable at 800 °C and above (Fig. 3). The TCFE3 database does not handle gas phases, but this has little effect
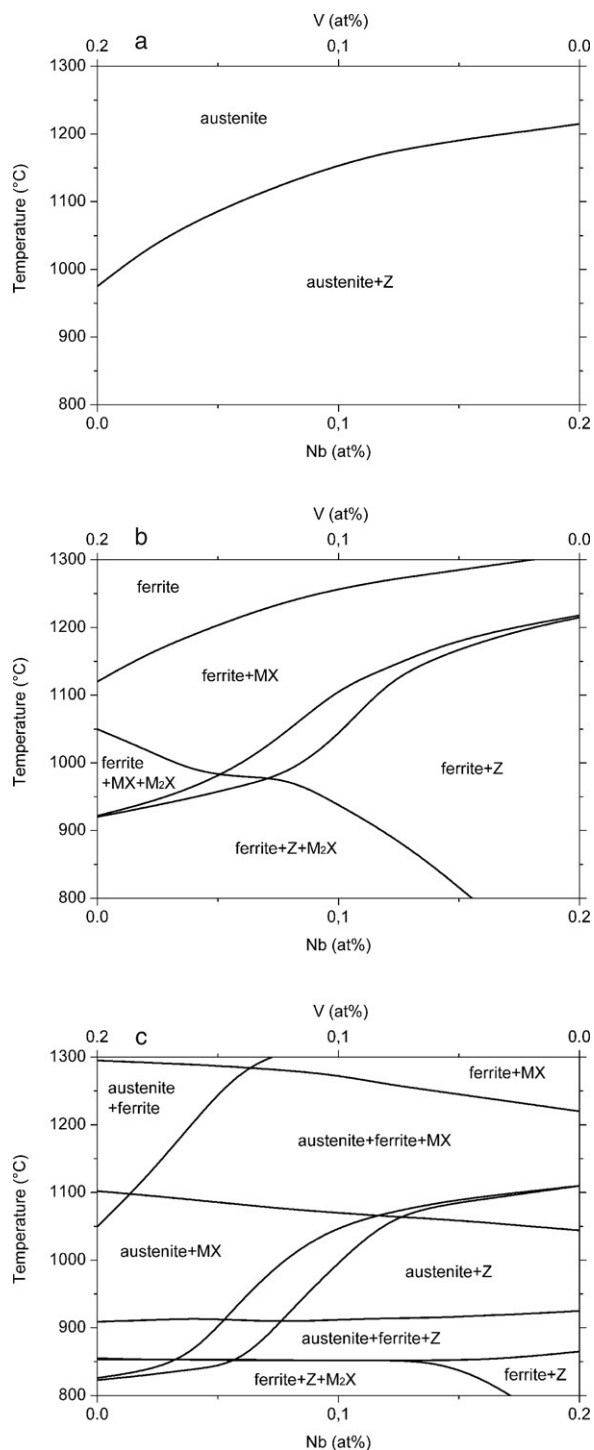
Fig. 8. The effect on Z-phase dissolution temperature when replacing the V content with Nb. Sample (a) austenitic (18Cr 12Ni 0.2N 0.2(Nb+V)), (b) ferritic (20Cr 0.2N 0.2(Nb+V)) and (c) martensitic steels (12Cr 0.2N 0.2(Nb+V)) are used, all numbers in at.%, balance Fe.
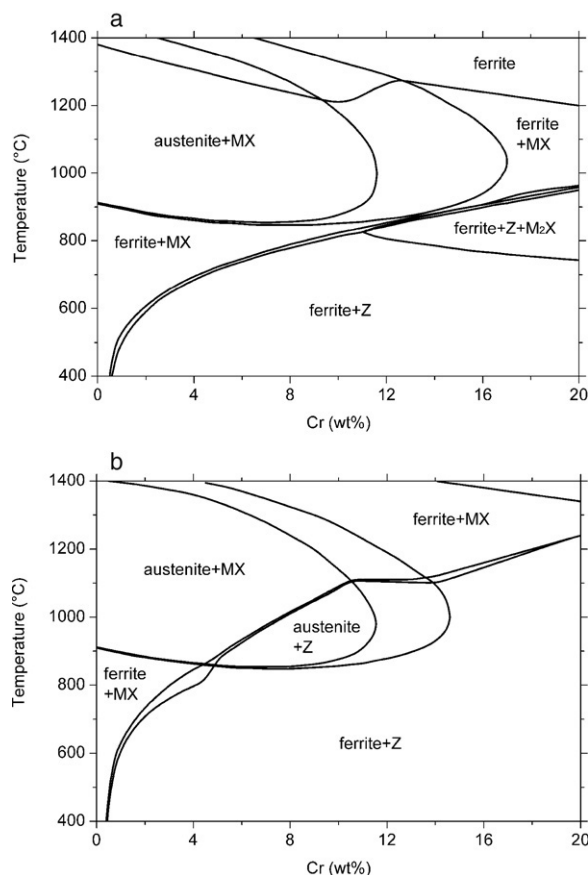

Fig. 9. The behaviour of Z-phase in Fe-Cr diagrams, (a) modified Z-phase in martensitic steel (0.06N 0.06Nb 0.21V) and (b) original Z-phase in martensitic steel (0.06N 0.4Nb), all numbers in wt%, balance Fe.

Table 3
The range of steel compositions (wt%, balance Fe) where Z-phase has been observed in steels

Cr	Ni	C	N	Nb	V	Mo
8–20	0–18	0–0.2	0.015–0.45	0–1.7	0–0.4	0–2.8

on the other phases. Experiments show that Cr and V are fully miscible in the bcc, fcc and hcp (sub)lattices at 800 °C (Fig. 3). This does not appear to be the case in the calculations along the fcc and hcp lines. Contrary to experimental data, calculations of the hcp sublattice indicate that it should become unstable for equal amounts of Cr and V (Fig. 4a). This corresponds to the ideal Z-phase composition, CrVN. Consequently, attempts to fit the Z-phase in this system are futile. In contrast with experimental data, calculations of the fcc sublattice indicate complete immiscibility of Cr and V (Fig. 4b).

On the other hand, in steels the MX and M$_2$X phases appear as VN fcc and Cr$_2$N hcp respectively. Calculations with TCFE3 give a reasonable amount of V solubility in Cr$_2$N, but the amount of Cr in VN is too low as compared to experimental data. Unfortunately, the literature sources for the development of the VN phase descriptions in the TCFE3 database were not available. The Z-phase in the developed model is fitted to be slightly more stable than the other nitride phases. Thus the model relies on the accuracy of the already existing phase description of MX, mainly VN and NbN, and the described inconsistencies in the TCFE3 database might introduce inaccuracies in the developed model. An improvement of the MX phase description was beyond the scope of this work.

Table 4
The fitted thermodynamic parameters of the Z-phase model

$$^0G^{\text{Z-phase}}_{\text{CrNbN}} = {}^0G^{\text{SER}}_{\text{Cr}} + {}^0G^{\text{SER}}_{\text{Nb}} + {}^0G^{\text{SER}}_{\text{N}} - 228\,500 + 85 \cdot T$$

$$^0G^{\text{Z-phase}}_{\text{FeNbN}} = {}^0G^{\text{SER}}_{\text{Fe}} + {}^0G^{\text{SER}}_{\text{Nb}} + {}^0G^{\text{SER}}_{\text{N}} - 88\,000 + 60 \cdot T$$

$$^0G^{\text{Z-phase}}_{\text{CrMoN}} = {}^0G^{\text{SER}}_{\text{Cr}} + {}^0G^{\text{SER}}_{\text{Mo}} + {}^0G^{\text{SER}}_{\text{N}}$$

$$^0G^{\text{Z-phase}}_{\text{FeMoN}} = {}^0G^{\text{SER}}_{\text{Fe}} + {}^0G^{\text{SER}}_{\text{Mo}} + {}^0G^{\text{SER}}_{\text{N}}$$

$$^0G^{\text{Z-phase}}_{\text{CrVN}} = {}^0G^{\text{SER}}_{\text{Cr}} + {}^0G^{\text{SER}}_{\text{V}} + {}^0G^{\text{SER}}_{\text{N}} - 239\,500 + 100 \cdot T$$

$$^0G^{\text{Z-phase}}_{\text{FeVN}} = {}^0G^{\text{SER}}_{\text{Fe}} + {}^0G^{\text{SER}}_{\text{V}} + {}^0G^{\text{SER}}_{N} - 56\,000 + 80 \cdot T$$

$$^0G^{\text{Z-phase}}_{\text{CrNbVa}} = {}^0G^{\text{SER}}_{\text{Cr}} + {}^0G^{\text{SER}}_{\text{Nb}}$$

$$^0G^{\text{Z-phase}}_{\text{FeNbVa}} = {}^0G^{\text{SER}}_{\text{Fe}} + {}^0G^{\text{SER}}_{\text{Nb}}$$

$$^0G^{\text{Z-phase}}_{\text{CrMoVa}} = {}^0G^{\text{SER}}_{\text{Cr}} + {}^0G^{\text{SER}}_{\text{Mo}}$$

$$^0G^{\text{Z-phase}}_{\text{FeMoVa}} = {}^0G^{\text{SER}}_{\text{Fe}} + {}^0G^{\text{SER}}_{\text{Mo}}$$

$$^0G^{\text{Z-phase}}_{\text{CrVVa}} = {}^0G^{\text{SER}}_{\text{Cr}} + {}^0G^{\text{SER}}_{\text{V}}$$

$$^0G^{\text{Z-phase}}_{\text{FeVVa}} = {}^0G^{\text{SER}}_{\text{Fe}} + {}^0G^{\text{SER}}_{\text{V}}$$

$$^0L^{\text{Z-phase}}_{(\text{Cr,Fe})\text{VN}} = -260\,000 + 100 \cdot T$$

$$^0L^{\text{Z-phase}}_{(\text{Cr,Fe})\text{NbN}} = -270\,000 + 100 \cdot T$$

$$^0L^{\text{Z-phase}}_{\text{Cr(Nb,Mo)N}} = -168\,000 + 100 \cdot T$$

$$^0L^{\text{Z-phase}}_{\text{CrNb(N,Va)}} = -64\,000$$

$$^0L^{\text{Z-phase}}_{\text{CrV(N,Va)}} = -87\,000$$

$$^0L^{\text{Z-phase}}_{\text{FeV(N,Va)}} = -87\,000$$

Table 5
Comparison of the calculated and observed dissolution temperatures

	Calculated (°C)	Observed (°C)
X20 [1]	790	800
T122 [1]	835	800
NF12 [1]	840	800
Gerlach [12] S1	1210	1250
Gerlach [12] S2	1240	1250
Uno [13]	1180	1150

The observed values are often not very specific, usually giving intervals of 50 °C or more.

3. Results

3.1. General observations

The thermodynamic parameters of the finished Thermo-Calc model are listed in Table 4. The model predicts the Z-phase to be stable in practically all 9%–12% Cr steels, provided that the main constituents of Z-phase (N and either V or Nb) are present. This corresponds well with experimental observations, as all of the steels investigated by the authors have shown the presence of the Z-phase, provided the thermal ageing process was sufficiently long, i.e. at least a few thousand hours for modified Z-phase at 650 °C [1]. The model also predicts the Z-phase to fully replace MX particles in the temperature range 600–650 °C. This has so far only been observed in some of the 11%–12% Cr steels, causing a severe breakdown in creep strength. Given sufficient exposure time it is expected that this will also occur in the 9%–10% Cr steels, although this could

literally take decades at 650 °C. Thus, it may be impossible to entirely stop the precipitation of Z-phase. It can however be slowed down sufficiently, as not to affect the creep strength within the lifetime of a power plant (as it is seen with grades P91, P92 and X20, Table 1).

3.2. Equilibrium calculations

The equilibrium dissolution temperatures calculated after assessment of all parameters all coincide within 50 °C of experimental values (Table 5). For the martensitic steels (Table 1), the calculated dissolution temperatures are all within the range 750–850 °C, while for the austenitic steels (Table 2) the dissolution temperatures are significantly higher, generally around 1200 °C. The calculated dissolution temperature depends on the steel composition; for steels with a low Cr content it is low (Fig. 5a) and for steels with a low C content it is high (Fig. 5b).

Overall, the model provides good results for the Z-phase compositions, (Tables 6 and 7). As mentioned above, many of the data on V-containing Z-phases include steels which have not reached equilibrium. In 9%–12% Cr steels, the MX particles are usually split up into two populations, the Nb-rich primary MX which precipitates during normalization, and the V-rich secondary MX which precipitates during tempering. When the modified Z-phase precipitates in V- and Nb-containing 9%–12% Cr steels, the Nb-rich MX particles will dissolve before the V rich MX particles (Fig. 6). This is manifested as a relatively high Nb-content of the Z-phase in its early stages of precipitation. Table 6 shows that the Z-phase has a higher Nb-content when it is present in small quantities. In time the Z-phase will dissolve all of the nitrides, giving it an equilibrium composition with a relatively high V-content. As the model calculates thermodynamic equilibrium, the composition calculations are only comparable to steels where the Z-phase has nearly fully replaced the MX particles.

3.3. Driving force calculations

Results in Table 6 show the experimentally estimated quantity of Z-phase in various steels, but care must be taken when making direct comparisons. Taking VM12 and HCM12 as an example, their exposure time and temperature are different, making comparison difficult. In addition the nitrogen content in VM12 is also much greater, allowing it to precipitate a greater quantity of Z-phase and still contain more MX particles compared to HCM12 (as is the case in Table 6).

Driving force calculations can be used for estimating the rate of Z-phase precipitation, predicting which steels are prone to have a rapid Z-phase precipitation, and in which steels Z-phase development is more sluggish. In the case above, of VM12 and HCM12, the driving force would be reflected in the number fraction of MX replaced by Z-phase, not the total amount of Z-phase.

The experimental results have been used for fitting the driving force calculations of the Z-phase model (Fig. 7). The results are in good agreement, as the steels with fast Z-phase
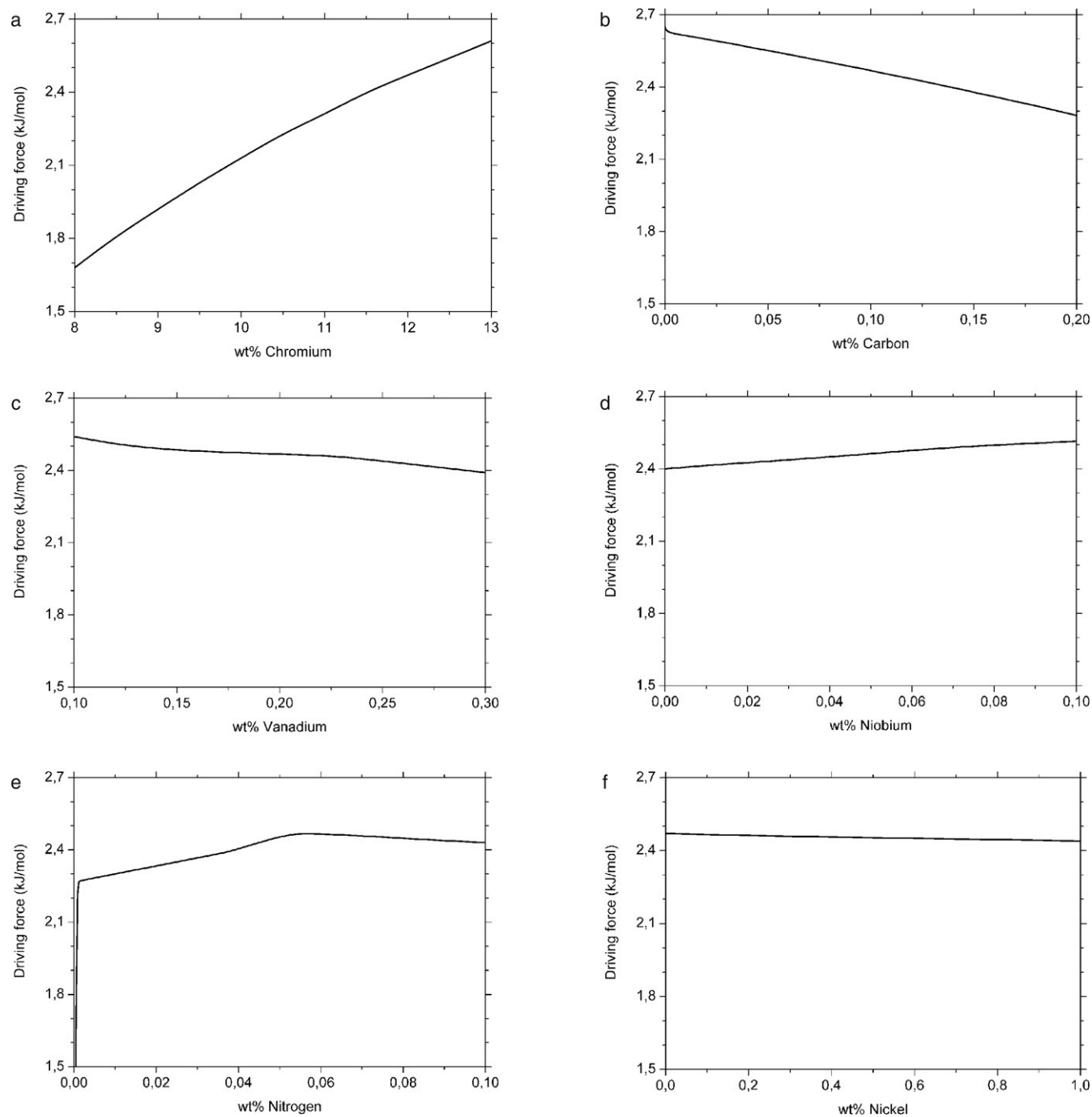
Fig. 10. Driving force for Z-phase precipitation calculated as a function of concentration of certain elements at 650 °C in a conventional 12% Cr steel (wt%, balance Fe): 12% Cr, 0.10% C, 0.21% V, 0.06% Nb, 0.06% N.

precipitation have higher driving forces compared to the steels with slower precipitation speed. However, there are probably other factors, including microstructure and heat treatments, which may influence the kinetics of Z-phase precipitation.

4. Discussion

4.1. Stability of Z-phase variants

As work with the model progressed, the presence of a Nb-free variant of the Z-phase was predicted: CrVN. To the authors' knowledge such a variant has not been observed previously, even though attempts have been made to synthesize it [24]. Attempts to suppress the CrVN phase in the fitting procedure corrupted other results and therefore a search for this phase was initiated. An investigation of a Nb-free 12CrMoV steel X20 which had been exposed for 150 000 h at 600 °C did confirm the occurrence of the CrVN Z-phase [1]. This illustrates the predictive quality of the model.

Observations of austenitic and martensitic steels show a difference in stability (dissolution temperature) of the Z-phase, but they usually contain two different versions of the Z-phase,

Table 6
Calculated metallic compositions compared with measured metallic compositions of modified Z-phase, all numbers in at.%

Steel grade	Exposure	Observed Z-phase quantity	Cr		Fe		V		Nb	
			Obs.	Calc.	Obs.	Calc.	Obs.	Calc.	Obs.	Calc.
P91	8 000 h/650 °C	Very low	Not enough particles observed for statistics							
X20	150 000 h/600 °C	Low	40	45.3	6	4.7	54	50.0	–	–
E911	10 000 h/650 °C	Low	46	44.4	4	5.6	27	39.6	23	10.4
P92	31 000 h/650 °C	Low	48	44.6	5	5.4	33	41.1	14	8.9
P122	10 000 h/650 °C	Medium	45	45.1	5	4.9	33	43.5	17	6.5
AXM	43 000 h/600 °C	Medium	43	45.1	5	4.9	44	44.0	8	6.0
FN5	8 000 h/650 °C	Medium	47	45.1	6	4.9	38	44.5	9	5.5
HCM12	85 000 h/585 °C	Medium	49	44.8	4	5.2	37	42.8	10	7.2
VM12	16 000 h/625 °C	High	48	45.3	5	4.7	40	45.6	7	4.4
TB12	10 000 h/650 °C	High	47	44.6	5	5.4	37	39.6	11	10.4
T122	12 000 h/660 °C	High	46	45.1	5	4.9	42	43.6	7	6.4
NF12	17 000 h/650 °C	High	47	44.7	5	5.3	37	39.6	10	10.4

The V/Nb content varies considerably for samples with low Z-phase content.

Table 7
Calculated metallic compositions compared with measured metallic compositions of original Z-phase, all numbers in at.%

Source	Element							
	Cr		Fe		Nb		Mo	
	Obs.	Calc.	Obs.	Calc.	Obs.	Calc.	Obs.	Calc.
Ernemann [9]	40.4	40.9	9.4	9.1	50.2	50.0	–	–
Hughes [10]	41.8	40.8	8.7	9.2	45.8	46.2	3.7	3.8
Vodarek [11]	37.3	40.8	10.3	9.2	48.5	45.4	3.9	4.6
Gerlach [12] S1	42.0	40.7	8.8	9.3	46.0	46.7	3.2	3.3
Gerlach [12] S2	39.1	41.0	8.5	9.0	49.5	48.2	2.9	1.8

CrNbN and CrVN respectively. Calculations with the model show that generally CrNbN is more stable, also for the same steel compositions. Fig. 8 illustrates the difference in stability for austenitic, ferritic and martensitic steels, when V is replaced with Nb, while Nb+V equals 0.2 at.%. As MX and M₂X are not so stable in austenite (Fig. 8a), the Z-phase is the only stable nitride at the given composition, giving a simple dissolution curve. In the ferritic and martensitic case (Fig. 8b–c) Z-phase and MX can coexist in a certain combination of composition and temperature ranges.

Fig. 9 shows how the Z-phase becomes more stable for higher Cr-contents. Again, the Z-phase is more stable when vanadium is replaced by niobium. Fig. 9a shows how MX is more stable in ferrite as compared to austenite. This is reflected in Fig. 9b, as the Z-phase becomes comparatively more stable inside the austenitic loop. At high Cr contents in Fig. 9a, M_2X appears above 800 °C, while this does not happen in Fig. 9b, even though the nitrogen content is comparatively higher (to the V+Nb content). The difference is mainly caused by the greater affinity of N atoms to CrNbN compared to CrVN (Fig. 2). A similar effect is seen in Fig. 8b; when Nb replaces V, M_2X becomes unstable.

4.2. Alloy design

Driving force calculations with systematic variation of a single element (Fe balance) show the influence of individual alloying elements on the Z-phase precipitation rate. Fig. 10 shows concentration variations of the major Z-phase elements and the resulting effect on the driving force for Z-phase

precipitation at 650 °C in a sample 12% Cr steel with conventional composition. The shape of these curves might vary significantly with the composition of the steel and the temperature.

Cr has the strongest influence in such calculations (Fig. 10a), which corresponds with experimental observations. A higher Cr content in the matrix increases the supersaturation of the Z-phase, and hence the driving force for its precipitation.

The second most influential element is carbon. It is not defined as an element in the Z-phase, but since it precipitates as chromium carbides, it effectively lowers the Cr content in the steel matrix and consequently reduces the amount of Cr available in solid solution for Z-phase precipitation (Fig. 10b).

V, Nb and N are major elements in the Z-phase, but they do not seem to affect the driving force to the same extent as Cr does (Fig. 10c–e). The influences of these elements are more complex and they are correlated. Generally, it can be said that a high N-content compared to the Nb+V content will lead to the formation of Cr_2N, while a low N-content will stabilize V(C, N) and NbC. Fig. 11 shows how the N-content can affect the presence of these particles (VN will not be stable in high Cr containing steels at these temperatures). Comparison with Fig. 10e shows that the driving force for Z-phase flattens out with the appearance of Cr_2N.

Vodarek and Strang [20] have suggested that Ni should have an accelerating effect on the precipitation of Z-phase. The model could not confirm this suggestion (Fig. 10f).

It is suggested that driving force calculations with the present model will be a highly useful tool for alloy design
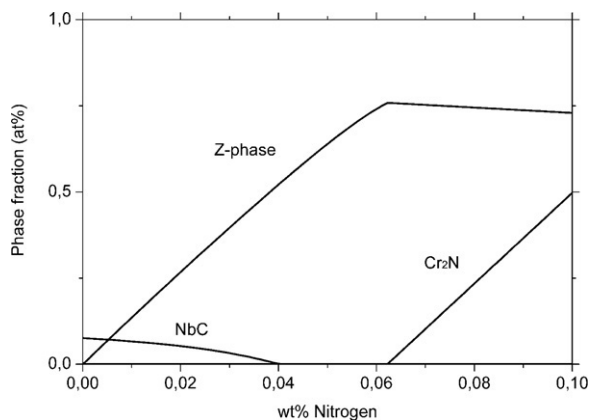
Fig. 11. The phase fraction of MX, M_2X and Z-phase as a function of N concentration at 650 °C. Same composition used as in Fig. 10.

and optimization. Apart from contributing to the design of new alloys to avoid the detrimental effects of Z-phase, minor adjustments of the composition of standardized steels could also be made. For example the composition of a steel Grade could be optimized within the specified composition limits, in order to minimize the driving force and effectively suppress Z-phase precipitation within the useful lifetime of the steel at high temperature.

5. Conclusion

A thermodynamic model of the Z-phase in iron based alloys has been developed using the Thermo-Calc software. The thermodynamic parameters of the model were primarily assessed on the basis of experimental data from austenitic and martensitic steels.

The model predicts Z-phase to be the most stable nitride in basically all 9%–12% Cr steels containing its constituents, and it will eventually fully replace the MX particles in these steels. The rate of Z-phase precipitation can be estimated using driving force calculations from the model. These calculations show that the Cr content has the largest influence on Z-phase precipitation. Such driving force calculations are considered a useful tool for future alloy design and optimisation.

Acknowledgments

References

[1] H.K. Danielsen, J. Hald, Energy Mater. 1 (2006) 49–57.
[2] B. Sundman, B. Jansson, J.-O. Andersson, CALPHAD 9 (1985) 153–190.
[3] J. Hald, VGB PowerTech 12 (2004) 74–79.
[4] W.O. Binder, ASTM STP 110 (1950) 146–164.
[5] H.-O. Andren, A. Henjered, L. Karlsson, Stainless steel 84, The Institute of Metals, London, 1985, pp. 91–96.
[6] E. Schnabel, P. Schwaab, H. Weber, Stahl und Eisen 107 (1987) 691–696.
[7] A. Strang, V. Vodarek, Mater. Sci. Technol. 12 (1996) 552–556.
[8] F. Kurosawa, I. Taguchi, M. Tanino, R. Matsumoto, J. Japan Inst. Metals 45 (1981) 63–67.
[9] J. Erneman, Evolution of Microstructure in Two Austenitic Alloys at High Temperature, Ph.D. Thesis, Chalmers, Gothenburg, 2003.
[10] H. Hughes, J. Iron Steel Inst. 205 (1967) 775–778.
[11] V. Vodarek, Scr. Metall. Mater. 25 (1991) 549–552.
[12] V.H. Gerlach, E. Schmidtmann, Arch. Eisenhuttenwes. 39 (1968) 139–149.
[13] H. Uno, A. Kimura, T. Misawa, Corrosion 48 (1992) 467–474.
[14] K. Kimura, K. Zuzuki, H. Kushima, F. Abe, in: Z. Kubon, M. Filip, V. Foldyna, R. Gladis, A. Jakobova, J. Purmensky, J. Sobotka (Eds.), Creep Restistant Metallic Materials, VITKOVICE-Research and Development, Ostrava, 2001, pp. 186–195.
[15] K. Suzuki, S. Kumai, H. Kushima, K. Kimura, F. Abe, Tetsu-to-Hagane 89 (2003) 69–76.
[16] R. Ishii, Y. Tsuda, M. Yamada, K. Kimura, J. Iron Steel Inst. Japan 88 (2002) 36–43.
[17] J. Bursik, N. Merk, in: C.M. Branco, R. Ritchie, V. Sklenicka (Eds.), Mechanical Behaviour of Materials at High Temperature, Kluwer Academic Publisher, Dordrecht, 1996, pp. 299–307.
[18] G. Zies, K. Maile, K.-H. Mayer, S. Straub, in: E. Roos (Ed.), Modern 9%–12% Cr-Steels for Power Plant Applictaions, Staatliche Materialprüfungsanstalt (MPA) Universität Stuttgart, Stuttgart, 2002, pp. 52.1–52.22.
[19] M. Svoboda, J. Bursik, I. Podstranska, A. Kroupa, V. Sklenicka, K.H. Mayer, in: J. Lecomte-Beckers, M. Carton, F. Schubert, P.J. Ennis (Eds.), Materials for Advanced power Engineering, Forschungszentrum Julich GmbH, Julich, 2002, pp. 1521–1530.
[20] V. Vodarek, A. Strang, in: J. Lecomte-Beckers, M. Carton, F. Schubert, P.J. Ennis (Eds.), Materials for Advanced Power Engineering, Forschungszentrum Julich GmbH, Julich, 2002, pp. 1223–1232.
[21] D.H. Jack, K.H. Jack, J. Iron Steel Inst. 209 (1972) 790–792.
[22] H.K. Danielsen, J. Hald, F.B. Grumsen, M.A.J. Somers, Metall. Mater. Trans. A 37A (2006) 2633–2640.
[23] M. Christensen, G. Wahnström, Chalmers University, Gothenburg, personal communication.
[24] P. Ettmayer, Monatsh. Chem. 102 (1971) 858–863.
[25] M. Hillert, L.-I. Staffansson, Acta Chem. Scand. 24 (1970) 3618–3626.
[26] B. Sundman, J. Ågren, J. Phys. Chem. Solids 42 (1981) 297–301.
[27] Thermo-Calc Software, http://www.thermocalc.se.
[28] P. Villars, A. Prince, H. Okamoto, Handbook of Ternary Alloys Phase Diagrams, ASM International, Materials Park, 1995.

Appendix D

On the Dissolution and Nucleation of Z-phase, Cr(V,Nb)N

In manuscript

On the Dissolution and Nucleation of Z-phase Cr(V,Nb)N

Abstract

Precipitation of large Z-phase, Cr(V,Nb)N, replacing fine MX nitrides, (V,Nb)N, has recently been identified as a major cause for premature breakdown in long-term creep strength of a number of new 9-12%Cr martensitic steels. The Z-phase appears during the service life of these steels, but little is known about its nucleation.

12%Cr steel which contained Z-phase was heat treated in order to investigate the dissolution and reappearance of Z-phase. In both cases it appears that Z-phase and MX phase are in physical contact and have a preferred crystallographic orientation relationship. This could indicate either nucleation of Z-phase on MX (and vice versa) or a chromium diffusion controlled transformation of the precipitates.

1. Introduction

1.1. Background

New creep resistant martensitic 9-12%Cr steels for steam power plant applications have been under development to increase service temperature from 600°C to 650°C. Most of the newest test alloys have relatively high Cr contents of 11-12% for obtaining enhanced oxidation resistance as compared to steel applied at lower temperatures. However, so far attempts to develop applicable steels have been largely unsuccessful, because dramatic breakdowns in long term creep tests occurred. Recently, the precipitation of the complex nitride Z-phase, Cr(V,Nb)N, was identified as the main cause of the microstructure instabilities associated with the long term creep strength [1]. 9-12%Cr martensitic steels rely on precipitation strengthening to obtain good creep properties at relatively high temperatures. The major contributors to the creep strength are MX precipitates, mainly (V,Nb)N, which precipitate as small and densely spaced

particles. The Z-phase contains the same elements as the MX precipitates as well as chromium, so its precipitation is accompanied by the dissolution of the strengthening MX particles. The Z-phase precipitates as large particles, which do not contribute to precipitation strengthening, and thus the creep strength of the steel is considerably lowered.

Investigation of several 9-12%Cr steels and development of a thermodynamic model of the Z-phase have indicated that Z-phase is the most stable nitride in all 9-12%Cr steels, which contain its constituents Cr, V/Nb and N. However, the precipitation rate of Z-phase varies greatly for the various 9-12%Cr steels, depending mainly on the Cr content. Whereas 11-12%Cr steels may develop Z-phase after a few thousand hours exposure at 650°C, a similar appearance of Z-phase in 9%Cr steels may take over 100,000 hours [1-2].

The understanding and control of the Z-phase precipitation reaction (nucleation and growth) is thus crucial to the prediction of long-term stability of the 9-12%Cr steels and to the development of new improved alloys. The growth of Z-phase does not seem to be a limiting factor for the precipitation rate. Both large and small Z-phase particles have been found in all of the investigated steels irrespective of the precipitation rate, the main difference being the number of particles. This indicates that the nucleation of Z-phase may be the controlling factor for the precipitation rate. This paper presents studies of the nucleation of Z-phase in a 12%Cr steel.

It is puzzling why Z-phase does not nucleate along with the MX precipitates, as investigations of 9-12%Cr steels show the Z-phase is thermodynamically the most stable nitride precipitate [1-2]. The only compositional difference between (V,Nb)N and Cr(V,Nb)N is the presence of Cr, which is abundantly present in the matrix. According to the classical nucleation theory, the interfacial energy of Z-phase would have to be relatively high to prevent a nucleation alongside MX. This would make any nucleation impossible after MX has depleted the matrix of

N and V. Thus, the nucleation process of Z-phase does not seem to be similar to other precipitates.

1.2. Crystal structure of Z-phase

The Z-phase version which precipitates in 9-12% Cr steels is primarily V based (empirical formula CrVN), but contains also small quantities of Nb and Fe, and is usually known as the modified Z-phase. The crystal structure of the modified Z-phase has usually been described as tetragonal, lattice parameters a=0.286 nm and c=0.739 nm [3], consisting of alternating layers of VN and Cr, see figure 1a. The Z-phase is usually observed as plate-like particles, with the VN and Cr layers parallel to the plane of the plate.
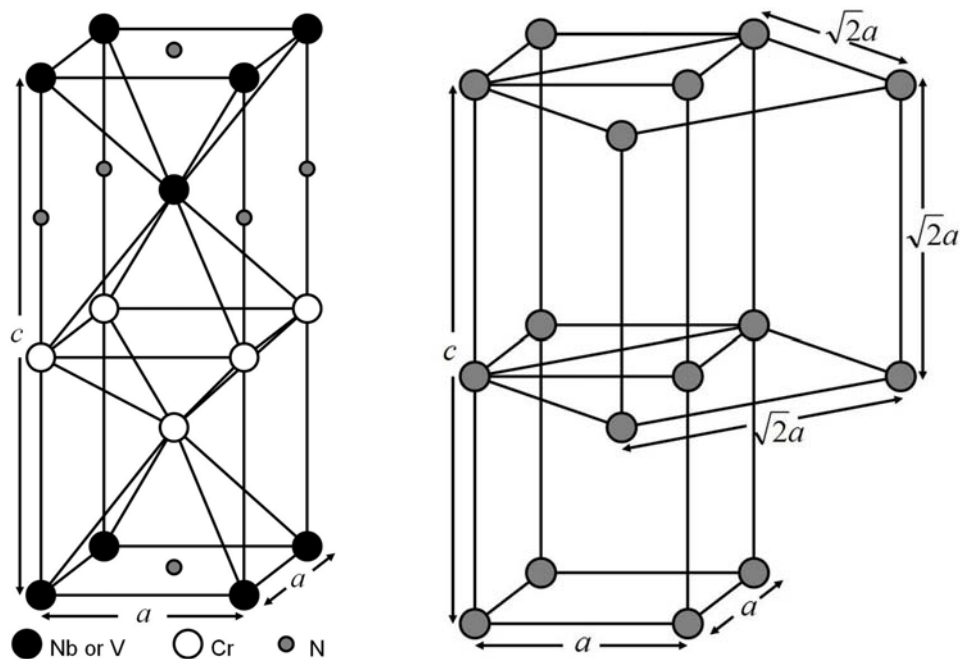
Figure 1: *A) The tetragonal structure usually associated with Z-phase B) The orientation relationship between the cubic and tetragonal structure in Z-phase, some atoms left out for clarity. [4]*

Recent crystallographic investigation of the Z-phase has revealed a more complex crystal structure. Electron diffraction showed the clear presence of cubic fcc diffraction patterns, similar to those found in MX precipitates, though with a

slightly lower lattice parameter, a=0.405nm [4]. This cubic structure was found to coexist with the tetragonal structure in the Z-phase. A clear orientation relationship was assessed between the two structures, see figure 1b, with perfectly matching lattice parameters.

Further investigations showed that the cubic structure was predominant in samples which had been exposed for relatively short times, while the tetragonal diffraction patterns became clearer with longer exposure times[5]. On the basis of this observation it is speculated that the cubic structure is metastable as compared to the tetragonal structure of Z-phase.
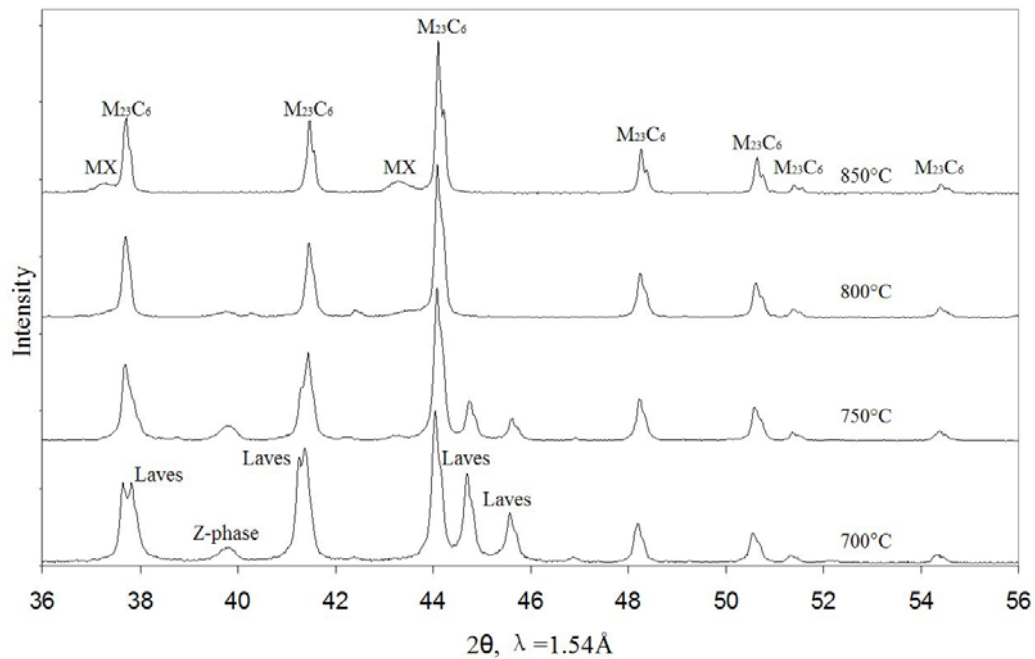
Figure 2: *X-ray powder diffraction of precipitates from a Z-phase containing T122 steel after heat treatments at 700-850°C for 100h; the Z-phase peak disappears at roughly 800°C and is replaced by MX peaks. [1]*

1.3. Solution temperature of Z-phase

The solution temperature of Cr(V,Nb)N Z-phase in 9-12%Cr steels was investigated as input data for a thermodynamic model of Z-phase [1-2]. For this task, various steels where the Z-phase had replaced MX precipitates were

chosen. Short heat treatments at temperatures around 800C° showed that Z-phase was replaced by MX precipitates; the reverse situation of that occurring at 650°C. The X-ray diffraction pattern of the precipitates (without matrix) in Figure 2 shows the Z-phase peaks are replaced by MX peaks (fcc 0.416nm) at around 800°C.
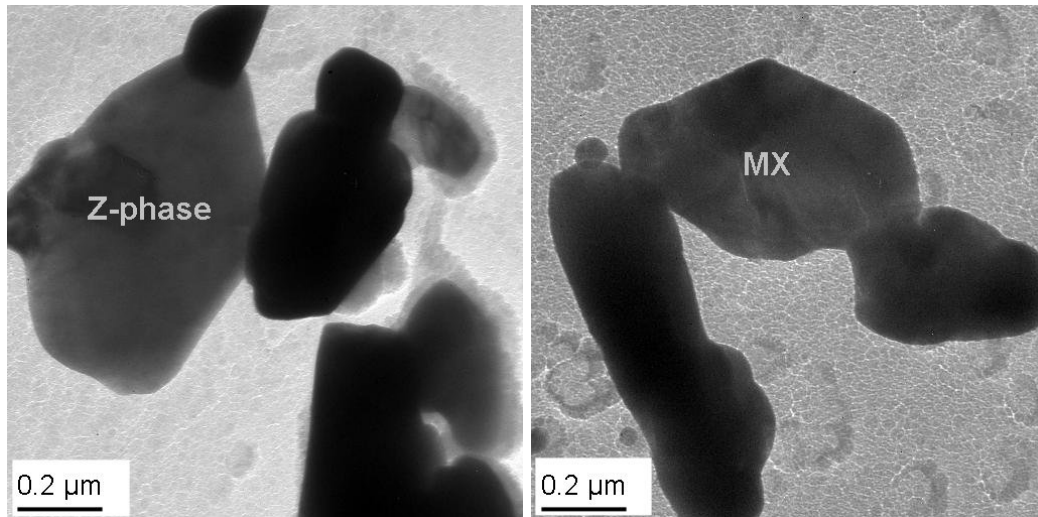

Figure 3: *A) Z-phase particle after heat treatment at 800°C and B) MX particle after heat treatment at 850°C. [1]*

After heat treatment for 100h at 850°C the Z-phase was fully replaced by quite large MX precipitates, usually several 100 nm large, which is much larger than the MX precipitates normally found in 9-12%Cr steels after tempering. These large MX precipitates were largely identical to Z-phase in shape and size (Figure 3). EDS measurements showed that the large MX particles are vanadium rich, and electron diffraction confirmed an fcc crystal structure with lattice parameter about 0.42nm, consistent with X-ray diffraction. At temperatures between 800 and 850°C the Z-phase was observed to coexist with the newly formed large MX precipitates.

2. Experimental

2.1. Heat treatments

Relatively small Z-phase precipitates, >50nm, have been observed in 9-12% Cr steels exposed at 600-650°C [1, 6]. Observations of these small particles does not provide a better understanding of their actual nucleation, as studying them becomes progressively more difficult the smaller they get. Therefore a different approach was pursued in this work, using unconventional heat treatments of a material, which had already developed Z-phase during long-term exposure.

C	N	Si	Mn	Cr	Mo	W	Ni	Nb	V	Cu	Al	B
0.09	0.061	0.25	0.60	12.20	0.35	1.97	0.18	0.06	0.25	0.43	0.004	0.002

Table 1: *Composition of the T122 steel.*

The investigated material, T122 (Table 1), originates from a superheater tube of a test installation in a Danish power plant. The tube ruptured prematurely due to creep after 12,000h at 660°C, i.e. less than 10% of the expected minimum lifetime of the material, according to standardised creep rupture strength values. Microstructure investigations showed the abundant presence of the Z-phase, Cr(V,Nb)N, which had dissolved almost all of the V and Nb rich MX precipitates. Thus it was considered ideal for the investigations in the present work.

In order to examine the Z-phase nucleation, its dissolution above 800°C, where large Z-phases are replaced by large MX precipitates in a relatively short time, was investigated. Samples of T122 were heat treated at 810°C for 100 h, whereupon the Z-phase was partly replaced by MX. Thereafter, samples of T122 were heat treated at 850°C for 100h in order to replace all Z-phase with large MX precipitates. Subsequently, heat treatment was carried out at 650°C for 4000 h as to redevelop Z-phase in an environment of large MX particles, see (Table 2).

	Normalised and tempered	Precipitation of Z-phase	Dissolution of Z-phase	Re-appearance of Z-phase
Heat treatment	1050°C/0.2h 790°C/3h	1050°C/0.2h 790°C/3h 660°C/12,000h	1050°C/0.2h 790°C/3h 660°C/12,000h 810°C/100h	1050°C/0.2h 790°C/3h 660°C/12,000h 850°C/100h 650°C/4,000h
Nitride behaviour	None → Small MX	Small MX → Large Z-phase	Large Z-phase → Large MX	Large MX → Large Z-phase

Table 2: *Heat treatments applied in the present work.*

2.2. Electron microscopy

Examination of precipitates resulting from the various heat treatments was performed with transmission electron microscopy on carbon extraction replicas. The replicas were prepared from polished surfaces, which had subsequently been etched chemically in Vilella's etchant (1% picric acid and 5% conc. hydrochloric acid in ethanol) for about 10-15 seconds. A carbon film was deposited onto the specimens by carbon evaporation, using a Quorum Technologies CC7650. Thereafter the carbon film was cut into pieces and the sample was electrochemically dissolved in a mixture of 5% HCl in ethanol, leaving the carbon extraction replica in the solution. The replicas were caught on small copper grids and cleaned with ethanol prior to electron microscopical investigation.

All electron microscope investigations were carried out using a JEOL 3000F FEG TEM with an Oxford Instruments Inca EDS and a Gatan Imaging Filter EELS. The composition of the precipitates was primarily investigated with EDS, both for identification of the precipitates as well as for determining compositional variations within the precipitates. The crystallography of the precipitates was investigated using both SAED and CBED.
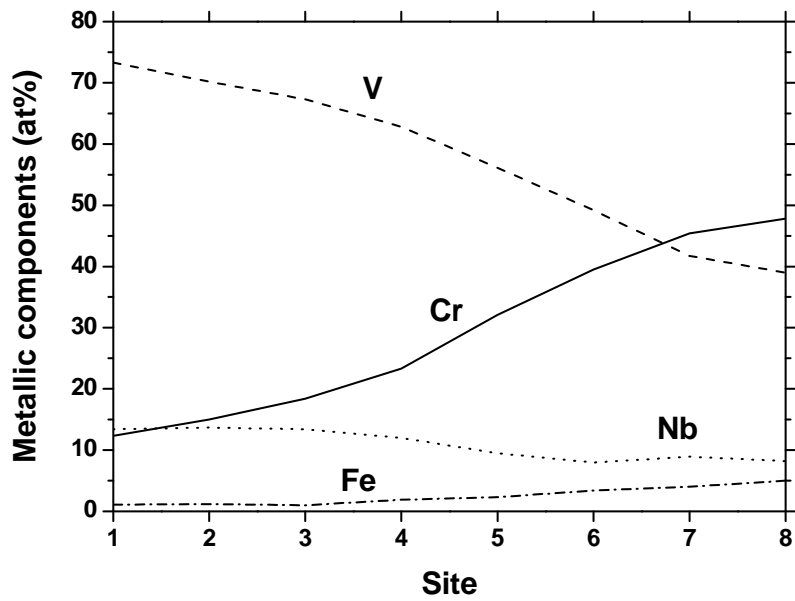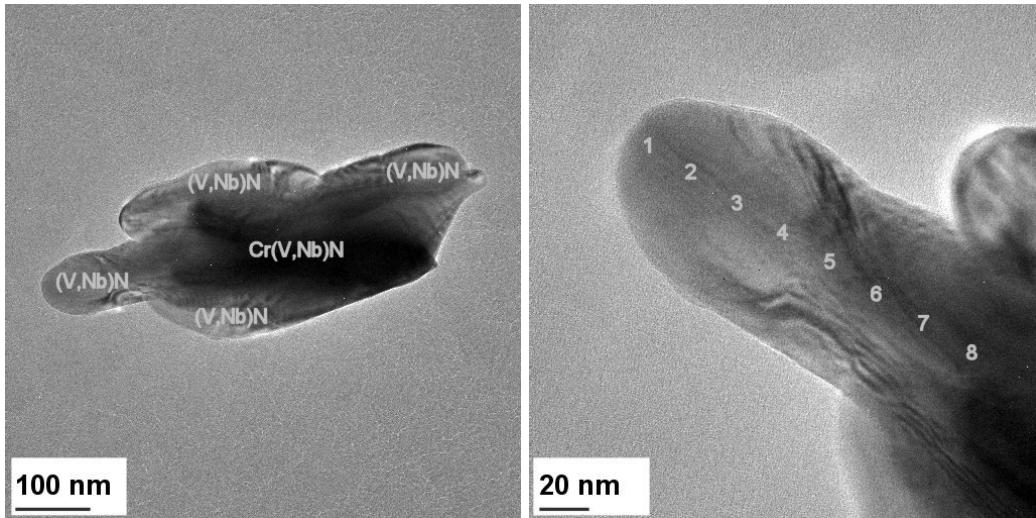
Figure 4: *A) After heat treatment at 810°C/100h, many particles have a core/rim composition. B) No defects in the particles can be observed ([001] zone axis) even though the lattice parameter for fcc unit cells changes from 0.420 nm (site 1) to 0.404 nm (site 8). C) There is a smooth transition in the composition from site 1 to site 8.*

3. Results

3.1. Dissolution of Z-phase; MX replacing Z-phase

The dissolution of Z-phase was investigated in samples exposed at 810°C/100h, where the Z-phase was partly replaced by MX. Both homogeneous Z-phase and homogeneous MX particles were observed after the heat treatment. In addition many irregularly shaped particles were observed with an inhomogeneous (hybrid) composition. Generally, the irregular particles had a composition of Z-phase in the core and a composition resembling MX at the rim. In many cases, composition profiles showed a smooth transition from the Z-phase composition to the MX composition (Figure 4). Electron diffraction indicated a change in lattice parameter (fcc unit cells) from 0.404nm in the core to 0.420nm at the rim, which also is consistent with a change from Z-phase to MX. Generally no defects were observed in the structure that could be associated with an interface or other discontinuities, indicating a smooth transition from one crystal structure to the other.
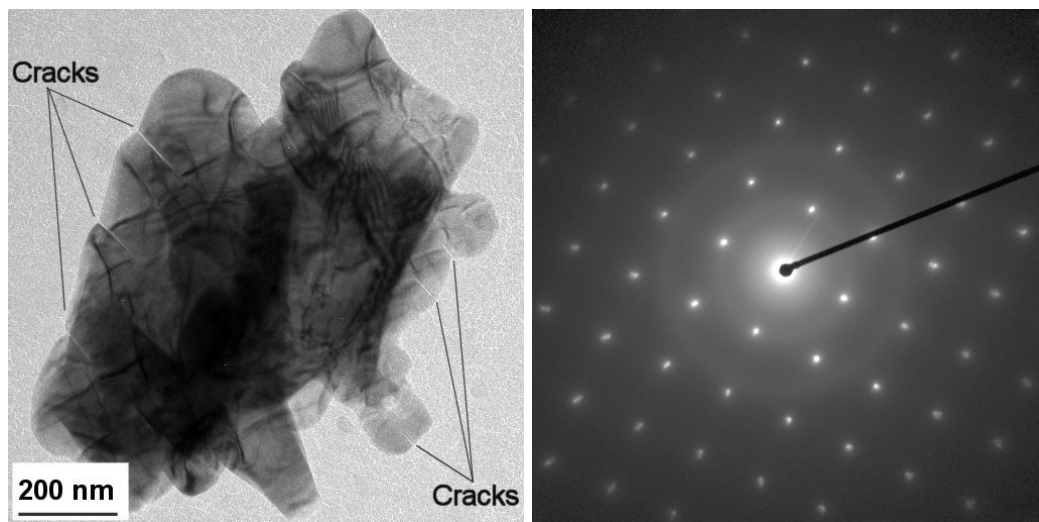

Figure 5: *A) Larger particles with core/rim compositions tend to develop cracks at the rim. B) Electron diffraction shows a [001] cubic pattern where the spots are elongated away from the centre, indicating a change in lattice parameters.*

Large cracks, up to 100nm, were observed at the edges of relatively large particles, suggesting that high tensile stresses were present along the rim of these particles before sample preparation. The cracks appear to have preferred orientations, see figure 5a and 6a, possibly corresponding to the <001> cubic planes.
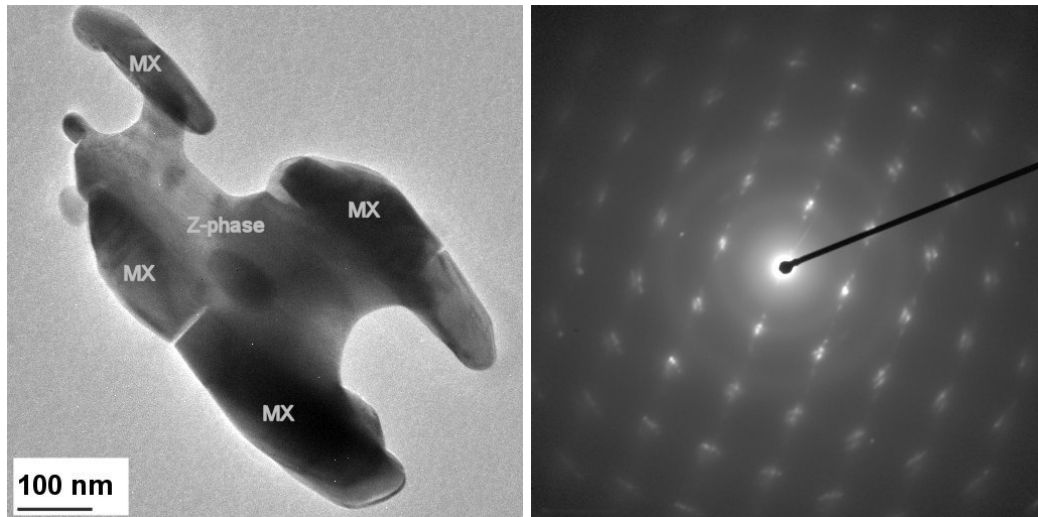

Figure 6: *A) Looking at the side of the plate-like hybrid particles, Z-phase/MX areas seem to be organized into a sandwich structure. B) Electron diffraction shows two [100] cubic patterns with different lattice parameters and a [110] tetragonal pattern in the background.*

The Z-phase is often observed as plate-like forms with the [001] zone axis perpendicular to the plane of the plate. Looking along [001] onto the plate (Figures 4 and 5) a smooth concentration gradient from the rim to the core is observed. Looking from the side of the plate, hybrid particles with sandwich structures are observed with MX at the edges and Z-phase in-between (Figure 6a). The cubic diffraction spots (tetragonal spots only weakly visible) in Figure 6b are sharply divided into MX and Z-phase, whereas the difference in lattice parameter is not very pronounced in figure 5b, indicating that the Z-phase in figure 6 is at a more advanced stage of dissolution. The orientation relationship between MX and Z-phase crystal structures was always in correspondence with that given in Figure 1b.

10

3.2. Re-appearance of Z-phase; MX replacing Z-phase

The samples heat treated at 850°C/100h + 650°C/4000h allowed to examine the re-appearance of Z-phase from large MX particles, which facilitates the actual observation and analysis.

Both Z-phase and MX particles were present in the sample, and they were often observed close to (and in direct contact with) each other. Core/rim structures, similar to those after heat treatment at 810°C, were also observed, albeit with MX at the core and Z-phase at the rim (Figure 7).
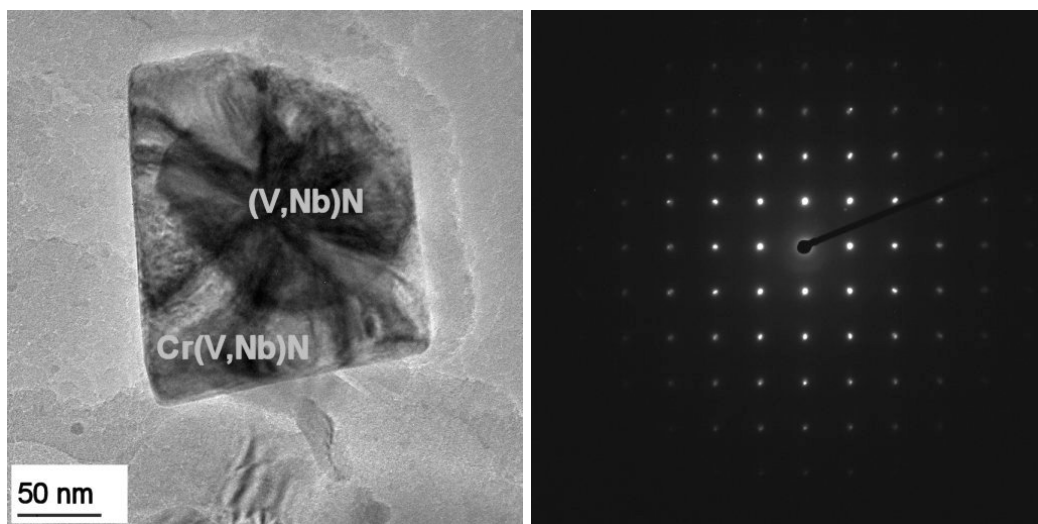

Figure 7: *A) Particles with core MX/rim Z-phase have been observed. B) As in figure 5b, electron diffraction of [001] cubic pattern shows slightly elongated spots. The difference in lattice parameters is very small.*

The compositional transition from the Cr-rich Z-phase to the Cr-poor MX regions appeared to be sharper than for the samples heat treated at 810°C, and sometimes the MX/Z-phase areas could be distinguished in brightfield images (Figure 7a). Sandwich structures were also observed after heat treatment at 650°C, but with MX sandwiched in-between two Z-phase edges (Figure 8). The orientation relationship between the MX and Z-phase crystal structures was again identical to the one in Figure 1b. A slight change in lattice parameters was

11

also observed in these particles, but no cracks, neither in the MX nor in the Z-phase particles were observed after heat treatment at 650°C.
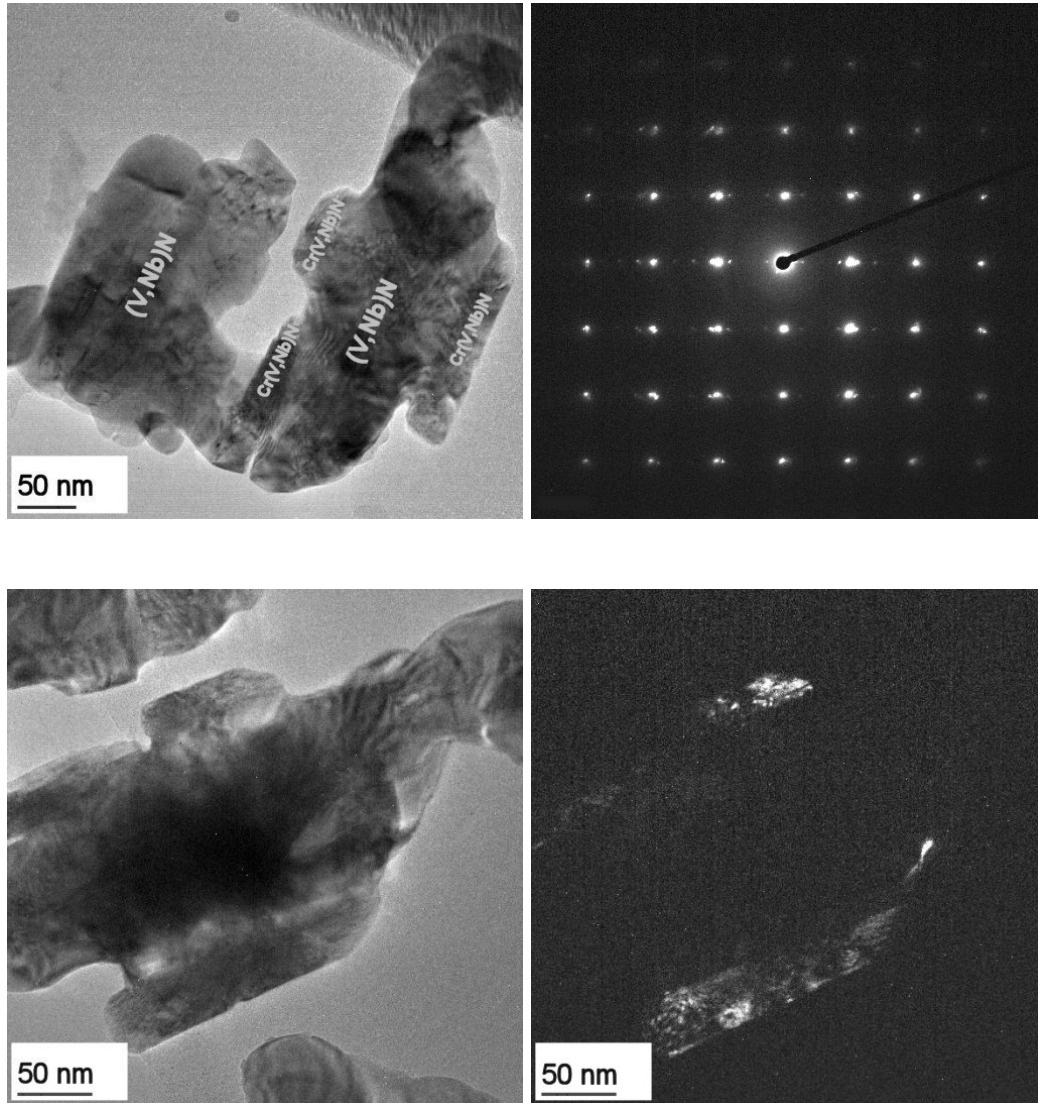

Figure 8: *A) At 650°C sandwich structures also appear, only with MX in the middle. B) The [100] cubic and [110] tetragonal patterns show a clear orientation relationship and slightly different lattice parameters. C) The particle in zone axis and D) a corresponding dark field image, (003) tetragonal spot, showing the tetragonal crystal structure to be located in the Cr-rich areas.*

4. Discussion

The obtained results strongly suggest that the nucleation of Z-phase is closely related with the presence of MX precipitates. This could imply the nucleation of Z-phase on an existing MX precipitate, or a physical transformation of MX into Z-phase by Cr diffusion from the ferrite matrix into MX.

The results at 810°C indicate that Cr diffusion out of the Z-phase is taking place. The large cracks appearing in the MX areas surrounding the Z-phase should not arise from a simple nucleation on Z-phase. If Cr diffusion out of Z-phase occurs, the lattice parameter will increase slightly, as there will be more interstitial N atoms per metal atom. However, the Cr diffusion would cause a massive volume reduction of the particle in question. This reduction would initially take place at the surface of the particle, possibly causing high enough stresses to initiate cracks in larger particles, see figure 5 and 6. In case of a diffusion process taking place at 650°C, there should be no such cracks (none were observed), as Cr would diffuse into a MX precipitate, thus increasing the volume of the particle (while decreasing its lattice parameter slightly).

A physical transformation of MX to Z-phase by Cr diffusion would explain the hybrid crystal structure observed in Z-phase particles after heat treatment at 600-650°C in many 9-12%Cr steels. The MX precipitates have a VN composition and a cubic crystal structure, lattice parameter about 0.416 nm. If Cr diffuses into the particles, the composition changes gradually to CrVN, and the lattice parameter is reduced to the observed 0.405nm, as there would be fewer N atoms in the interstitials sites. Then the atoms would slowly order themselves into VN and Cr layers, i.e. the well known tetragonal crystal structure. Observations of 9-12%Cr steels show both crystal structures to be present in the Z-phase, and indicate such an ordering to take place at 600-650°C [4-5].
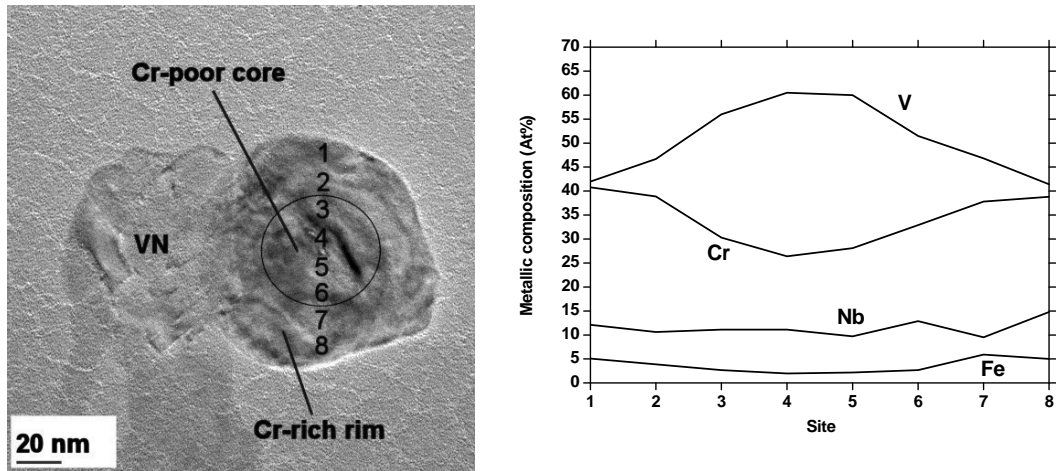
13

Figure 9: *A) A core/rim particle, [001] zone axis, found in T122 after exposure at 660°C/12.000h. B) Concentration profile.*

A physical transformation by Cr diffusion does correspond well with the behaviour seen at 810°C, as smooth compositional transitions are observed in several particles. However, the compositional transition does not seem so smooth at 650°C, where the Z-phase areas are more clearly distinguishable from MX areas. The crucial difference may be in the temperature difference: Z-phase dissolution occurs relatively fast (100h) at 810°C, while its re-appearance at 650°C is much slower (4000h). It is also important to bear in mind that the processes at 650°C and 810°C are not identical, but the opposite of each other, i.e. Z-phase replacing MX and MX replacing Z-phase respectively. The Z-phase could very well nucleate on MX at 650°C, while Cr diffusion out of Z-phase takes place at 810°C. Nevertheless, there are some examples of relatively smooth compositional gradients occurring at lower temperatures when Z-phase replaces MX, see figure 9.

5. Conclusion

The dissolution and nucleation process of Z-phase were investigated, indicating a close relation to the MX precipitates in both cases. The Z-phase and the MX precipitates were shown to be in direct physical contact and have a preferred crystal structure orientation relationship. Two hypotheses for this relation

14

between the precipitates, when Z-phase replaces MX and vice versa, were presented:

Z-phase nucleates on MX (or vice versa) and subsequently dissolves the host precipitate.

Diffusion controlled exchange of Cr atoms between the precipitates and the matrix occurs, which chemically transforms MX into Z (or vice versa) and subsequently transforms the lattice.

Acknowledgements

References

[1] H. K. Danielsen, J. Hald, *Energy Materials*, **1**, 2006, pp. 49-57.

[2] H. K. Danielsen, J. Hald, Paper III, submitted to *CALPHAD*

[3] A. Strang, V. Vodarek, *Materials Science and Technology*, **12**, 1996, pp. 552-556.

[4] H. K. Danielsen, J. Hald, F. B. Grumsen, M. A. J. Somers*, Metallurgical and Materials Transactions A*, **37A**, 2006, pp. 2633-2640.

[5] V. Vodarek, H. K. Danielsen, F. B. Grumsen J. Hald, A. Strang, in: J. Lecomte-Beckers, M. Carton, F. Schubert, P.J. Ennis (Eds.), *Materials for Advanced power Engineering*, Forschungszentrum Julich GmbH, Julich, 2006, pp. 1251-1266.

[6] K. Sawada, H. Kushima, K. Kimura, *ISIJ International*, **46**, 2006, pp. 769-775.

Appendix E

Indexing electron diffraction patterns

Guide

Indexing electron diffraction patterns

This appendix gives a more detailed description of indexing diffraction patterns, including an example with a fcc crystal structure.

V/kV	Wavelength λ/nm
100	0.003702
150	0.002957
200	0.002508
250	0.002199
300	0.001969
350	0.001789
400	0.001644

Table 1: *The wavelengths of the electron beam for different acceleration voltages. The correlation is not linear because of the relativistic approach.*

Picking up where we left at chapter 4.1.6, the Bragg equation is given by:

$$2d \sin \theta = n\lambda \qquad [1]$$

where d is the interplanar spacing in the crystal, λ is the wavelength of the electrons and n is an integer. As the wavelength of the electrons is very small, see table 1, and the interplanar spacing also is very small, commonly less than 0.4nm, the angle θ will also have to be very small, 0.26° for an integer of 1, 0.4nm interplanar spacing and using 100kV. For such small angles we can write sinθ=θ, and when only considering first order diffraction (n=1) Braggs law is simplified to:
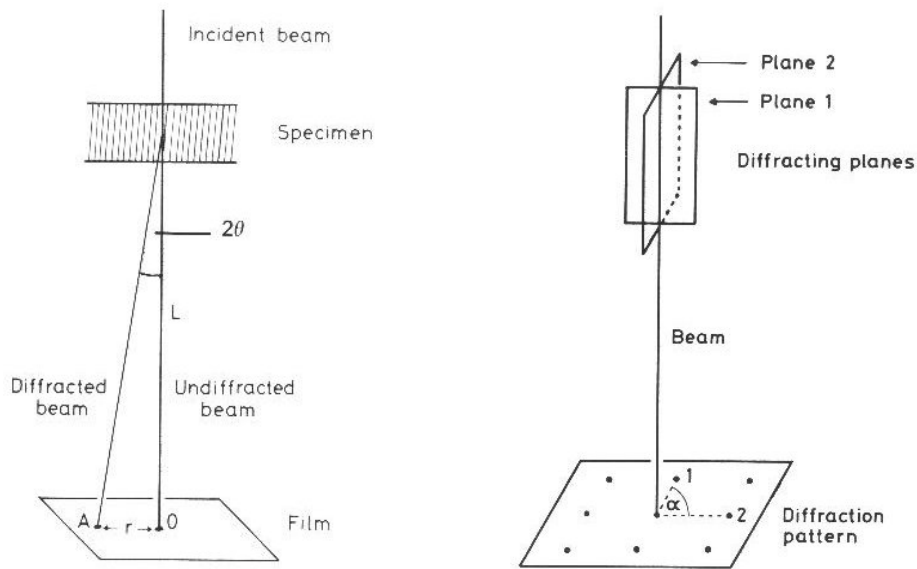
$$2d\theta = \lambda \qquad [2]$$

Figure 1: *Schematic overview over the scattered electrons (left) and the appearance of a diffraction pattern when in zone axis (right). [1]*

Looking at figure 1(left), most elastically scattered electrons will emerge from the crystal at angle 2θ from the incident beam. We can see the relation between the angle θ and the diffraction we observe in a TEM. As the angle θ is very small we can assume sinθ=θ, and get the relation:

$$r = L2\theta \tag{3}$$

where L is the camera length, which depends on the magnification used in the microscope. Combining equation 2 and 3 we get:

$$r = L\lambda / d \tag{4}$$

This is a key equation, which allows us to quantify the interplanar spacing from our diffraction pattern.

The angles in figure 1(left) are clearly exaggerated, and an electron beam will only be strongly diffracted from planes of atoms which are almost parallel to the electron beam. When the beam is almost parallel to two planes of atoms (a zone axis), it will form a diffraction pattern, see figure 1(right).

Crystal system	Unit cell geometry
Cubic	a = b = c α = β = γ = 90°
Tetragonal	a = b ≠ c α = β = γ = 90°
Orthorhombic	a ≠ b ≠ c α = β = γ = 90°
Hexagonal	a = b ≠ c α = β = 90° γ = 120°
Rhombohedral	a = b = c α = β = γ < 120° ≠ 90°
Monoclinic	a ≠ b ≠ c α = γ = 90° ≠ β
Triclinic	a ≠ b ≠ c α ≠ β ≠ γ

Table 2: *The seven crystal systems and their unit cell geometry. [2]*

Crystal structure

The crystal structures can be defined using the standard Miller index notation. We can distinguish between seven different crystal systems, see table 2. This work will only go into detail with the cubic, tetragonal, orthorhombic and hexagonal systems. The interplanar spacings (d) for a certain plane (hkl) for these systems can be calculated if the dimensions of the unit cell (a,b,c) of the crystal structure is known, see following equations.

Cubic:

$$\frac{1}{d^2} = \frac{1}{a^2}(h^2 + k^2 + l^2)$$ [5]

Tetragonal:

$$\frac{1}{d^2} = \frac{1}{a^2}(h^2 + k^2) + \frac{1}{c^2}(l^2)$$ [6]

Orthorhombic:

$$\frac{1}{d^2} = \frac{1}{a^2}(h^2) + \frac{1}{b^2}(k^2) + \frac{1}{c^2}(l^2)$$ [7]

Hexagonal:

$$\frac{1}{d^2} = \frac{4}{3a^2}(h^2 + hk + k^2) + \frac{1}{c^2}(l^2)$$ [8]

The calculations for the other systems are more complex [2]. In order to index a single crystal diffraction pattern, the angle φ between two planes, ($h_1k_1l_1$) and ($h_2k_2l_2$), in a crystal system must be calculated. The following equations can be used.

Cubic:

$$\cos\varphi = \frac{h_1h_2 + k_1k_2 + l_1l_2}{\sqrt{\left((h_1^2 + k_1^2 + l_1^2)(h_2^2 + k_2^2 + l_2^2)\right)}}$$ [9]

Tetragonal:

$$\cos\varphi = \frac{\frac{1}{a^2}(h_1h_2 + k_1k_2) + \frac{1}{c^2}(l_1l_2)}{\sqrt{\left\{\left(\frac{1}{a^2}(h_1^2 + k_1^2) + \frac{1}{c^2}l_1^2\right)\left(\frac{1}{a^2}(h_2^2 + k_2^2) + \frac{1}{c^2}l_2^2\right)\right\}}}$$ [10]

Orthorhombic:

$$\cos\varphi = \frac{\frac{1}{a^2}h_1h_2 + \frac{1}{b^2}k_1k_2 + \frac{1}{c^2}l_1l_2}{\sqrt{\left\{\left(\frac{1}{a^2}h_1^2 + \frac{1}{b^2}k_1^2 + \frac{1}{c^2}l_1^2\right)\left(\frac{1}{a^2}h_2^2 + \frac{1}{b^2}k_2^2 + \frac{1}{c^2}l_2^2\right)\right\}}}$$ [11]

Hexagonal:

$$\cos\varphi = \frac{h_1h_2 + k_1k_2 + \frac{1}{2}(h_1k_2 + k_1h_2) + \frac{3}{4}\frac{a^2}{c^2}l_1l_2}{\sqrt{\left\{\left(h_1^2 + k_1^2 + h_1k_1 + \frac{3}{4}\frac{a^2}{c^2}l_1^2\right)\left(h_{21}^2 + k_2^2 + h_1k_1 + \frac{3}{4}\frac{a^2}{c^2}l_2^2\right)\right\}}}$$ [12]

4

Calculating the angle ρ between two zone axes, [u₁v₁w₁] and [u₂v₂w₂], can be done in order to verify the positions of the diffraction patterns, using the following equations.

Cubic:

$$\cos\rho = \frac{u_1 u_2 + v_1 v_2 + w_1 w_2}{\sqrt{\left((u_1^2 + v_1^2 + w_1^2)(u_2^2 + v_2^2 + w_2^2)\right)}} \qquad [13]$$

Tetragonal:

$$\cos\rho = \frac{a^2(u_1 u_2 + v_1 v_2) + c^2(w_1 w_2)}{\sqrt{\left\{\left(a^2(u_1^2 + v_1^2) + c^2 w_1^2\right)\left(a^2(u_2^2 + v_2^2) + c^2 w_2^2\right)\right\}}} \qquad [14]$$

Orthorhombic:

$$\cos\rho = \frac{a^2 u_1 u_2 + b^2 v_1 v_2 + c^2 w_1 w_2}{\sqrt{\left\{\left(a^2 u_1^2 + b^2 v_1^2 + c^2 w_1^2\right)\left(a^2 u_2^2 + b^2 v_2^2 + c^2 w_2^2\right)\right\}}} \qquad [15]$$

Hexagonal:

$$\cos\rho = \frac{u_1 u_2 + v_1 v_2 - \tfrac{1}{2}(u_1 v_2 + v_1 u_2) + \dfrac{a^2}{c^2} w_1 w_2}{\sqrt{\left\{\left(u_1^2 + v_1^2 - u_1 v_1 + \dfrac{a^2}{c^2} w_1^2\right)\left(u_{21}^2 + v_2^2 + u_1 v_1 + \dfrac{a^2}{c^2} w_2^2\right)\right\}}} \qquad [16]$$

Not all planes in a crystal will cause diffraction, as there can be interference of radiation scattered by different atoms in the unit cell, which can cancel the diffracted rays out. The diffracted ntensity of a particular family of lattice planes depends on the crystal structure, and is also known as the structure factor, F, and can be calculated by the following equation[3]:

$$F_{hkl} = \sum_j f_j e^{2\pi i(hx_j + ky_j + lz_j)} \qquad [17]$$

where F_{hkl} is the intensity of a specific diffraction spot , f_j is the scattering amplitude of the element at position j, hkl are the millers indices and $x_j y_j z_j$ is a vector defining the position j of each atom within the unit cell. This equation is completely general, it applies to all crystal lattices. Using a calculation with a normal fcc structure for an example, four atoms must be included. Setting the

origin on one lattice point at (0,0,0), the others will be located at (½,½,0),(½,0,½) and (0,½,½). Inserting into equation [17] yields:

$$F = f\left(1 + e^{\pi i(k+h)} + e^{\pi i(h+l)} + e^{\pi i(k+l)}\right)$$ [18]

Considering all possible integers for hkl, if all three are either odd or even, all of the exponential terms will be $e^{n2\pi i}$, n being an integer, the exponential terms will be equal to 1. Inserting this into equation 18, the sum would be 4f. If one of the hkl indices is odd and the other two even, or vice versa, the exponential terms will be $e^{n\pi i}$, where n is an odd integer in two of the cases (term equal to -1) and an even integer in one case (term equal to -1). Inserting this into equation 18, the total sum will be 0. Thus if hkl are all even or odd *F=4f*, and if they are mixed *F=0*. This effectively means that half of the indices of fcc diffraction patterns are kinematically forbidden.

Precipitate	Crystal system
$M_{23}C_6$ ($Cr_{23}C_6$)	Cubic
Primary MX (NbC)	Cubic
Secondary MX (VN)	Cubic
Laves phase (Fe_2W)	Hexagonal
Z-phase (CrVN)	Tetragonal/Cubic
M_2X (Cr_2N)	Hexagonal

Table 3: *Precipitates found in the 9-12%Cr steels.*

All of the precipitates usually found in the investigated 9-12%Cr steels have certain crystalline structures, see table 3. Care must be taken when such structures are investigated with TEM, as light elements such as C and N have much smaller atomic scattering amplitudes compared to heavier atoms like Fe or Cr. For example, in the VN precipitate, the V and N atoms reside on separate interpenetrating fcc lattices with the same lattice parameters (NaCl type structure), so if there was no difference between the V and N atoms, it would be a simple cubic lattice (with half the lattice parameter). If the atoms had the same atomic scattering amplitudes we would expect a simple cubic diffraction pattern,

but since it is much higher for V compared to N, it will result in fcc diffraction patterns, where half of the spots are slightly (not visibly) weaker than the other half. That is for hkl all even $F=4(f_V+f_N)$, hkl all odd $F=4(f_V-f_N)$ and hkl mixed $F=0$, where $f_V>>f_N$. When investigating particles in steels, the matrix is ferritic or martensitic. Martensite is a slightly distorted tetragonal version of the ferritic bcc crystal structure.
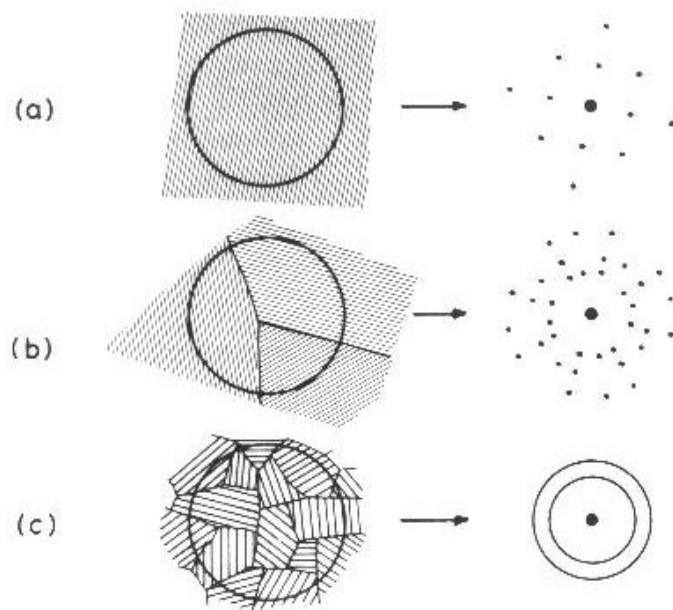

Figure 2: *The difference between SAD patterns from single and polycrystalline materials. [1]*

Polycrystalline materials

In polycrystalline materials, the obtained diffraction pattern will get contributions from many small crystals. If these small crystals are randomly oriented, the pattern will get contribution from all the zone axes, and will be independent of the tilt angle. The pattern will appear as rings because of the random contributions, see figure 2. Such patterns contain information on the lattice spacing of the crystal. The radius of the rings will be inversely proportional to the interplanar spacings, d, in the crystal, given by equation 4, in which case r would be the ring radius.

When the interplanar spacings are known, the material can often be identified using reference tables. If the structure is known, the theoretical interplanar spacings can be calculated, see equations 5-8.

If the camera length is unknown, a pattern should be obtained where the interplanar spacing is known, for example the interplanar spacing of gold. The camera length can then be calculated using equation 4.

If we take a look at the rings of a cubic structure, the innermost ring would be 100, the second one would be 110, then 111, 200, 210, 211, 220, 311 and so on, see equation 5. If this cubic structure would be an fcc structure, only the rings which have all even or odd indices would be visible (see above), e.g. 111, 200, 220, 311, etc. The 100, 110, 210 and 211 rings would be extinct, due to the structure factor. Thus an fcc pattern can be identified on the radius of the rings, as they always have the same ratio, e.g. r_{111}/r_{200} is always a certain constant and so on, see equation 5. Similar methods can be used on other crystal structures.
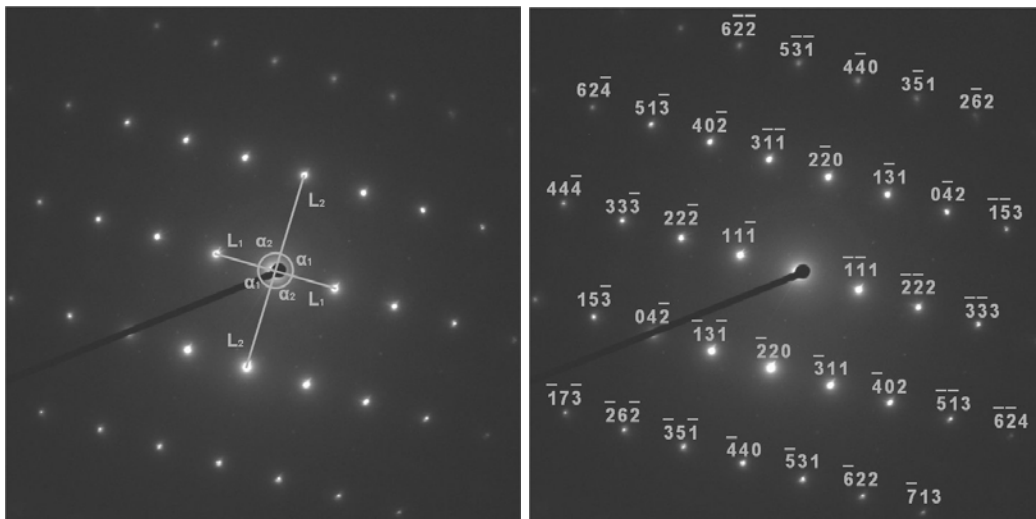

Figure 3: *A diffraction pattern from an fcc [112] zone axis being measured and indexed.*

Single crystal materials

An electron diffraction pattern will appear when the electron beam is almost parallel to two planes of atoms (a zone axis). To reach a zone axis, the specimen

8

must usually be tilted. A zone axis can be found where two or more Kikuchi lines cross each other, see chapter 4.1.8. As the position of the Kikuchi lines is very sensitive to the tilting of the specimen, they are useful to accurately find the exact zone axis. The diffraction pattern should ideally be symmetric around the 0 spot, see figure 3, but if it is not exactly in zone axis, some of the spots might be weaker or stronger than they are supposed to be.

When analysing a diffraction pattern, the length of the vectors from the zero spot to the two nearest spots is measured, see figure 3(left). The length of the vectors will be inversely proportional to the interplanar spacings in the crystal, given by equation 4, where r is the vector length.

As with the polycrystalline materials, it is possible to find the general indices of the planes in question from the interplanar spacing, if the crystal structure is known, see above.

A pattern has been obtained using a digital camera with 300 kV. The pattern is suspected to belong to an fcc pattern with a lattice parameter of 0.404nm. The camera length has previously been found to correspond to 55000 pixels using a gold sample (utilising digital imaging, real camera length of 600mm used in this case). Note the digital images must be of same resolution in order to use the same camera length (4096x4096 in this case).

The two shortest vectors from the centre spot, l_1 and l_2, have been measured to 466 and 754 pixels. The interplanar spacings are found to be 0.232nm and 0.144nm using equation 4. Using equation 5, the theoretical interplanar spacings of plane 111 is found to be 0.233nm and plane 220 to be 0.143nm, a close enough match.

The smallest angle α between the two shortest vectors should then be measured, in this case $\alpha_1 = \alpha_2 = 90°$, see figure 3(left). This angle will be equal to the angle between the two planes of atoms in the zone axis, see figure 1(right).

The specific indexing of the spots can be done using the general indices of the planes. If we have found the nearest spot to belong to a certain plane, for example 220, this spot can indexed as 220, -220, 202, 20-2, 022 etc. because of

the cubic symmetry. We have the freedom to choose the particular indices of <u>one</u> spot, for example 2-20. In order to find the particular indices of the spots belonging to the other plane, calculate the angle between the 2-20 spot and the candidates for the other spot (111, 11-1, 1-1-1 etc.) using equation 9 and then compare with the measured angle. The angle between 1-1-1 and 2-20 is calculated to be 35.2°, far from the measured 90°. The angle between -1-11 and 2-20 is found to be 90°, a perfect match (there are several correct answer because of the symmetry). All of the spots can now be indexed, see figure 3(right). The zone axis of the pattern is the dot product, see figure 1(right), of -1-11 and 2-20, calculating it gives [112]. Because of the cubic symmetry of the fcc structure, the pattern could belong to any of the <211> zone axes, depending on the chosen spot indices.

Positions of zone axes

When obtaining diffraction patterns from a crystal, the tilt position of the patterns should be noted in order to verify the structure. For example, two patterns have been obtained and identified as fcc [112] and [122], and the tilt positions are found to be 22°x, 18°x and 6°x, 9°y. The angle ρ between the two tilt angles in a normal double tilt specimen holder can be calculated by using polar coordinates:

$$\cos(\rho) = \cos(x_1)\cos(x_2)\cos(y_1 - y_2) + \sin(x_1)\sin(x_2) \qquad [19]$$

If we calculate angle between the tilt angles we get 18.2°. Calculating the theoretical angle between the zone axes using equation 13, we get 17.7°, which shows a good correspondence between observed and theoretical values. The tilt positions can also be plotted using the x and y tilt angles, in order to obtain a map, which in case for fcc should be similar to the Kikuchi map shown in chapter 4.1.8.

References

[1] P.J. Goodhew, F.J. Humphreys, "*Electron Microscopy and Analysis*", Taylor and Francis, London 1988.

[2] K.W. Andrews, D.J. Dyson, S.R. Keown, "*Interpretation of Electron Diffraction Patterns*", Adam Hilger Ltd, London 1971.

[3] D.B. Williams, C.B. Carter, "*Transmission Electron Microscopy II, diffraction*", II Diffraction, Plenum Press, New York, 1996.